Article:
Swanner, ED, Lambrecht, N, Wittkop, C et al. (4 more authors) (2020) The biogeochemistry of ferruginous lakes and past ferruginous oceans. Earth-Science Reviews, 211. 103430. ISSN 0012-8252

https://doi.org/10.1016/j.earscirev.2020.103430

Title: The biogeochemistry of ferruginous lakes and past ferruginous oceans

Authors: Elizabeth D. Swanner[1], Nick Lambrecht[1,2], Chad Wittkop[3], Chris Harding[1], Sergei Katsev[4], Joshua Torgeson[5], Simon W. Poulton[6]

Affiliations: [1]Department of Geological and Atmospheric Sciences, Iowa State University, Ames, IA, USA; [2]Department of Genetics, Cell Biology and Development, University of Minnesota, Minneapolis, MN, USA; [3]Department of Biochemistry, Chemistry, and Geology, Minnesota State University; [4]Large Lakes Observatory, University of Minnesota, Duluth, MN, USA; [5]Department of Earth and Environmental Sciences, University of Minnesota, Minneapolis, MN, USA; [6]School of Earth and Environment, University of Leeds, Leeds LS2 9JT, UK

Abstract

Anoxic and iron-rich (ferruginous) conditions prevailed in the ocean under the low-oxygen atmosphere that occurred through most of the Archean Eon. While euxinic conditions (i.e. anoxic and hydrogen sulfide-rich waters) became more common in the Proterozoic, ferruginous conditions persisted in deep waters. Ferruginous ocean regions would have been a major biosphere and Earth surface reservoir through which elements passed through as part of their global biogeochemical cycles. Understanding key biological events, such as the rise of oxygen in the atmosphere, or even the transitions from ferruginous to euxinic or oxic conditions, requires understanding the biogeochemical processes occurring within ferruginous oceans, and their indicators in the rock record. Important analogs for transitions between ferruginous and oxic or

euxinic conditions are paleoferruginous lakes; their sediments commonly host siderite and Ca-carbonates, which are important Precambrian records of the carbon cycling. Lakes that were ferruginous in the past, or euxinic lakes with cryptic iron cycling may also help understand transitions between ferruginous and euxinic conditions in shallow and mid-depth oceanic waters during the Proterozoic. Modern ferruginous meromictic lakes, which host diverse anaerobic microbial communities, are increasingly utilized as biogeochemical analogues for ancient ferruginous oceans. Such lakes are believed to be rare, but regional and geological factors indicate they may be more common than previously thought. While physical mixing processes in lakes and oceans are notably different, many chemical and biological processes are similar. The diversity of sizes, stratifications, and water chemistries in ferruginous lakes thus can be leveraged to explore biogeochemical controls in a range of marine systems: near-shore, off-shore, silled basins, or those dominated by terrestrial or hydrothermal element sources. Ferruginous systems, both extant and extinct, lacustrine and marine, host a continuum of biogeochemical processes that highlight the important role of iron in the evolution of Earth's surface environment.

Keywords

Ferruginous; meromictic; iron speciation; iron formation (IF); siderite; (an)oxygenic photosynthesis

Highlights

- Precambrian marine sediments indicate frequent ferruginous conditions with euxinic intervals
- Siderite from ferruginous lakes informs formation pathways in ferruginous oceans
- Ferruginous meromictic lakes are an expected feature of postglacial landscapes
- Ferruginous lakes can be biogeochemical analogues of ferruginous oceans

1. Introduction

The paucity of iron in the modern ocean (average 540 pmol kg^{-1}) belies that abundant dissolved iron was once a persistent feature of the oceans. The deposition of massive amounts of iron from the ocean in iron formations (IF)—marine chemical precipitates with more than 15 wt % iron—throughout the Archean (4.0 to 2.5 billion years ago; Ga) and in the Paleoproterozoic (2.5-1.6 Ga), and again in the Neoproterozoic (1.0 Ga to 541 million years ago; Ma), speaks to long periods characterized by iron-rich (i.e. ferruginous) oceans (Bekker et al., 2010; Konhauser et al., 2017). The continual discovery of additional mid-Proterozoic, Neoproterozoic, and even Phanerozoic IF signals that ferruginous conditions prevailed throughout key intervals of Earth's history (e,g. Canfield et al., 2018; Z.-Q. Li et al., 2018). Additionally, the application of paleoredox proxies (i.e. iron speciation and trace element enrichments and isotopic compositions) for clastic and carbonate marine sediments (Raiswell et al., 2018; Robbins et al., 2016; Tostevin and Mills, 2020; Wasylenki, 2012) has resulted in an emerging picture that anoxic and iron-rich (i.e. "ferruginous") conditions in the deep ocean were spatially extensive and temporally pervasive, and continued through periods of Earth's history not typified by IF deposition (e.g. Canfield et al., 2008; Clarkson et al., 2016; Johnson

64 and Molnar, 2019; Johnston et al., 2010; März et al., 2008; Planavsky et al., 2011; Poulton et al.,
65 2015; Poulton and Canfield, 2011). However, the very low concentrations of iron in the current
66 ocean point to fundamentally different redox conditions in the modern (oxic) as compared to
67 past (anoxic) oceans. The lack of ferruginous conditions in the modern oceans thus poses a
68 challenge to scientists who endeavor to piece together the workings of the biogeochemistry of
69 past ferruginous oceans.

70 The fundamental shift in redox state of the ocean from ferruginous to oxic resulted from
71 the behavior of iron in response to increasing concentrations of oxygen (O) and sulfur (S)
72 through time. The maintenance of iron in solution is thermodynamically favored either at acidic
73 pH or under anoxic conditions, where both oxidized (Fe^{3+}; ferric) and reduced (Fe^{2+}; ferrous)
74 iron are orders of magnitude more soluble than ferric iron at circumneutral pH or in the
75 presence of oxygen, respectively. Ocean pH was likely circumneutral (i.e. 6-8) throughout
76 Earth's history (Krissansen-Totton et al., 2018), indicating that the primary mechanism for
77 maintenance of iron in ferruginous oceans was through pervasive anoxia. This also implies that
78 ferrous iron was the predominant form of dissolved iron in water. Even under anoxic
79 conditions, iron will precipitate when the solubilities of iron-bearing minerals that form with
80 anions such as oxide (O^{2-}), hydroxide (OH^-), carbonate (CO_3^{2-}), phosphate (PO_4^{3-}), mono- or
81 disulfide (S^{2-} or S^-), or silicate (SiO_4^{4-}) are exceeded. Precipitation of amorphous phases such as
82 ferrihydrite [$Fe(OH)_3$], and minerals such as magnetite (Fe_3O_4), siderite ($FeCO_3$), vivianite
83 ($FePO_4$), or greenalite [$(Fe^{2+},Fe^{3+})_{2-3}Si_2O_5OH_4$] from solutions exceeding the saturation of these
84 minerals, are thought to have resulted in the deposition of IF (Derry, 2015; Kaufman et al.,
85 1990; Konhauser et al., 2017; Tosca et al., 2016). Pyrite (FeS_2) is thought to buffer dissolved iron

86 in organic-rich clastic sediments (Canfield, 1989). The record of these minerals, or products of
87 their diagenetic transformation, leave an imprint in the geological record of the spatial and
88 temporal extent of ferruginous conditions in the waters from which they precipitated.
89 The most enigmatic and volumetrically significant ferruginous sediments are Superior-
90 type IF, which were precipitated from seawater along laterally extensive passive margins
91 (reviewed in Bekker et al., 2010; Konhauser et al., 2017). The deposition of IF has often been
92 linked to the appearance of oxygen in the atmosphere and in the oceans, which was
93 hypothesized to have oxidized dissolved ferrous iron, decreasing its solubility and precipitating
94 it as Fe^{3+} (oxyhydr)oxide minerals (Cloud Jr., 1968). A more nuanced understanding of ocean
95 oxygenation envisions this occurring at a redox interface between a ferruginous deep ocean
96 and oxygen-bearing surface waters (e.g. Konhauser et al., 2017). Alternately, or simultaneously,
97 the disappearance of dissolved iron from the ocean has been linked to the increase of sulfate
98 (SO_4^{2-}) in the oceans, causing Fe^{2+} to precipitate with hydrogen sulfide (H_2S), produced after
99 microbial sulfate reduction, and ultimately buried as pyrite (Canfield, 1998). These
100 interpretations are based upon the nature of the marine sediments we are left to interpret, but
101 their interpretation necessitates an understanding of how iron behaves under varying redox
102 conditions, in the presence of different chemical species, in response to biological activity, and
103 during subsequent diagenesis or metamorphism. The basis for interpretation can be built
104 through reductive experiments, or through observation of the sediments themselves, but
105 investigation of the underlying phenomena in a complex natural setting with analogy to the
106 original chemical environment can help to fill the gaps left between the reductionist and
107 observational approaches.

As the modern oceans are predominantly oxic, they are not well-suited to help scientists understand the microbial, biogeochemical, and mineralogical processes that would have been occurring in ferruginous oceans. Exceptions include oxygen minimum zones (OMZ; Scholz, 2018) or anoxic basins, such as the Cariaco Basin or Black Sea. However, the high levels of sulfate (28 mM in average ocean water) commonly tip these systems toward euxinic conditions (anoxic and containing free H_2S) when oxygen becomes depleted. Marine sulfate concentrations may have been as low as 2.5 µM, or as high as ~200 µM in the Archean Eon (Crowe et al., 2014b; Habicht et al., 2002). While sulfate concentrations likely increased into the Proterozoic Eon, estimates vary from as low as 100 µM (Fakhraee et al., 2019) to as high as 1.5-4.5 mM (Kah et al., 2004). Considering estimates for dissolved iron concentrations in ferruginous oceans (sec. 2) and that abundant organic carbon (C) needed to drive sulfate reduction would have occurred near-shore, euxinic conditions likely developed only locally during the Archean and Proterozoic Eons (Johnston et al., 2010; Li et al., 2010; Poulton et al., 2010).

Modern lakes with vertical zonation in the availability of terminal electron acceptors for mineralization of organic matter and their reduced products (e.g. O_2/H_2O, NO_3^-/NO_2^-, Fe^{3+}/Fe^{2+}, $Mn^{3+/4+}/Mn^{2+}$, SO_4^{2-}/H_2S, CO_2/CH_4) have been long invoked as useful sites for investigating conditions under which past marine sediments that record anoxia or anoxic intervals might have been deposited (Degens and Stoffers, 1976). In order to use lakes as analogues, it is important to recognize the limitations of the analogy by understanding the similarities and differences in physical, chemical, and biological aspects of both systems. Redox stratification can occur in the water column of both lakes and oceans, driven in part by common biological

processes, but the physical processes that govern mixing and ultimately control where and how stratification occurs are distinct in lakes and ocean. Lakes generally mix as a result of wind action and seasonally variable temperature structures. Ocean circulation is ultimately driven by strong salinity and temperature shifts occurring in surface waters at discrete points on the globe, as a result of complex interactions between Earth's rotation and atmospheric circulation.

The oceans are large, and the impact of terrestrial runoff for the supply of non-conservative, redox-active elements such as iron is localized to near shore settings (Boyle et al., 1977; Hawkings et al., 2014), whereas atmospheric and seafloor processes can dominate the iron inputs to the open ocean (Mahowald et al., 2005; Tagliabue et al., 2010). Most lakes in the world are <0.1 km^2 (Verpoorter et al., 2014), and so have more direct interaction with terrestrially derived iron supplied in dissolved or particulate form from runoff, from atmospheric deposition, or from groundwater (Dean et al., 2006; Urban et al., 1987). Partly for this reason, iron is more abundant in freshwaters than in oceans, yet its residence time is generally much shorter (Klein, 1975). Lakes generally have much lower sulfate concentrations than oceans (Klein, 1975) due to the shorter water residence time and behavior of sulfate as a conservative ion under oxic conditions. Thus, many lakes have a sulfate concentration more similar to the ranges inferred for past oceans (Crowe et al., 2014b; Fakhraee et al., 2019; Habicht et al., 2002; Kah et al., 2004). These differences notwithstanding, in the absence of ferruginous oceans today, ferruginous lakes have enormous value for testing hypotheses about how biogeochemical cycles functioned in ancient ferruginous oceans. Oceans are chemically and biologically variable in both time and space and investigating freshwaters that encompass a

range of biogeochemical conditions can be useful for interpreting process that happened in the variable settings recorded by the sedimentary record through Earth's history.

Ferruginous meromictic lakes (i.e. those with permanently anoxic and iron-rich bottom waters), have a long history as interesting but esoteric limnological footnotes (Kjensmo, 1967; Smith Jr., 1940; Yoshimura, 1936), probably in part due to their perceived rarity. Iron-rich varved sediments from ferruginous meromictic lakes, or those that have been ferruginous in the past, have long been recognized for their paleoclimate utility, particularly in the Holocene (Dean et al., 1984). However, with the expanding study of a range of ferruginous sediments beyond IF and beyond the Precambrian in the last one to two decades (Canfield et al., 2008; Poulton et al., 2015, 2004a), and an emerging interest in testing hypothesis regarding biogeochemical hypotheses in ferruginous lakes (Busigny et al., 2014; Crowe et al., 2008a; Walter et al., 2014), a detailed discussion of the utility and limitations of the analogy is warranted. Part of this process involves addressing where these lakes are, how common they are, and why they are there. Through this analysis we can also better understand the full story of iron's importance to life on Earth, and how ferruginous conditions continue to play a role in modern global biogeochemical cycles.

In this contribution, the literature that documents evidence for the extent and nature of past ferruginous oceans is reviewed (sec. 2). Mineral archives and their proxy implications are then discussed, as well as evidence for biological activity and biogeochemical cycles occurring within ferruginous oceans (sec. 3). Evidence for the interpretation of paleoferruginous conditions in lakes based on sedimentary minerals and geochemistry is presented, and their utility to interpreting the sedimentary record of ferruginous oceans is highlighted (sec. 4). The

characteristics of modern ferruginous meromictic lakes are then introduced, with a case study on conditions associated with their occurrence (sec. 5). Then, current research on biogeochemical processes occurring in ferruginous meromictic lakes is reviewed (sec. 6).

Defining ferruginous

The presence of ferruginous conditions in circumneutral pH lakes and oceans is intimately tied to the absence of oxygen in water, as well as the supply of iron and prominence of Fe^{3+} (oxyhdr)oxide minerals as terminal electron acceptors for microbial respiration. In the aquatic sciences, many terms are applied to distinguish waters that are in equilibrium with oxygen in the modern atmosphere (saturated), those where oxygen is low (e.g. hypoxic: less than about 50 µM, which limit the activity of many higher organisms), those with trace amounts of oxygen (suboxic: less than 4.5 µM), or those where oxygen is absent (anoxic). However, the range of actual oxygen concentrations that correspond to these terms is ill-defined, and instruments able to measure truly trace levels of oxygen (e.g. nM) are not in widespread use.

Redox zones are determined by the most abundant redox-active species, which in turn reflect the dominant electron accepting processes supporting microbial organic carbon oxidation (e.g. $CH_2O \rightarrow CO_2 + H_2O + 4H^+ + 4e^-$), and follow the general sequence: oxic ($O_2 + 4H^+ + 4e^- \rightarrow H_2O$), nitrogenous ($2NO_3^- + 4e^- + 4H^+ \rightarrow 2NO_2^- + 2H_2O$), manganous ($2MnO_2 + 4H^+ + 4e^- \rightarrow 2Mn^{2+} + 2H_2O$), ferruginous ($4Fe^{3+} + 4e^- \rightarrow 4Fe^{2+}$), sulfidic or euxinic ($0.5SO_4^{2-} + 4H^+ + 4e^- \rightarrow 0.5H_2S + 2H_2O$), and methanic ($CO_2 + 4H^+ + 4e^- \rightarrow CH_4$) (Canfield and Thamdrup, 2009; Tostevin and Poulton, 2019). The order of this sequence reflects the thermodynamics, specifically a decreasing amount of free energy available to microbes by coupling each electron accepting

reaction to organic carbon oxidation (Froelich et al., 1979). This thermodynamic ordering can vary depending on the environmental activity of species in the redox couple, pH, and temperature. Kinetics can also control which process predominates. Sulfidic is often used synonymously with euxinic, although some authors distinguish these terms further, using sulfidic within sediments and euxinic when referring to free sulfide in the water column.

The use of the term ferruginous in reference to the anoxic and Fe^{2+}-bearing conditions of lakes, oceans, and their sedimentary porewaters appears in the GeoRef database only since 2008 (Canfield et al., 2008). The term has historically been applied to rocks and minerals containing visibly oxidized iron in the geological literature. The earliest entry (1656) in the Oxford English dictionary notes the Latin origins of the word, referred to "of the colour of rusty iron". Entries in the GeoRef database that contain the word "ferruginous" begin to accumulate in the late 1800s, as ferruginous came into fashion as a geological term relating to the presence of iron or iron staining (e.g. rust) in rocks. There has been a shift, however, in its application to aqueous systems, both freshwater and marine, which have the capacity to maintain and transport a reservoir of dissolved, generally ferrous, iron. This shift seems to have started in 2008, as there are no earlier occurrences of the phrases "ferruginous conditions", "ferruginous ocean", "ferruginous water", or "ferruginous lake" before this date. The Oxford English Dictionary lists numerous examples of its usage dating from the 1600s relating to rusty, iron-bearing water or springs, in addition to its fairly common usage to the names of plants and animals, but also rarely minerals (1847: ferruginous opal). Ferruginous, therefore, seems to relate to anything that has a rusty color, or contains iron. From this historical analysis the usage of the word in relation to water predates its usage in relation to minerals or rocks, supporting

its recent application to the ferruginous redox zone found in the water column of some lakes and within past oceans, but its reference to ferrous iron seems more recent.

2. Ferruginous oceans

Iron Formations evidence ferruginous conditions

Banded iron formations (BIF) have the longest history of study of the marine sediments used in interpreting the redox geochemistry of the Precambrian ocean, particularly in the Archean, Paleoproterozoic and Neoproterozoic (Bekker et al., 2010; for reviews see Klein, 2005; Konhauser et al., 2017). The "banded" here refers to visibly laminated chemical sediments, often alternating between iron- or silica-rich, whereas IF is a more general term for chemically precipitated (i.e. non-detrital) sediments with >15-20 wt % iron (James, 1954; Klein, 2005), regardless of the presence of laminations. The most extensive IF deposition occurred from 2.7 to 2.4 Ga, with a spike again at 1.9 to 1.8 Ga **(Figure 1**; Bekker et al., 2010). However, when bias is removed by scaling iron content with crustal preservation, a recent analysis suggested that IF deposition likely persisted at near constant rate from 3.8 to 1.8 Ga (Johnson and Molnar, 2019).

Fewer IF have been identified in the mid-Proterozoic, which in combination with increasing oceanic sulfate through the Proterozoic have been taken as indicating a shift from ferruginous to sulfidic deep ocean redox chemistry during this interval (Canfield, 1998). Higher sulfate concentrations, microbial sulfate reduction, and pyrite formation has been proposed to have titrated iron from seawater (Canfield, 1998; Poulton et al., 2010, 2004a; Rouxel et al., 2005). Yet recent work has described a small 1.4 Ga IF from northern China with comparable iron content to many Archean and Paleoproterozoic IF (Canfield et al., 2018). The ~1.3 Ga

Jingtieshan BIF was recently described from central China (Yang et al., 2015). A 1.0-0.8 Ga iron ore deposit in South China was recently argued to have been deposited as IF based on Fe isotopes, and potentially formed in a similar tectonic setting and same basin to other IF of the same age previously described in Canada (Sun et al., 2018). The youngest IF was recently identified in Western China at 527 Ma (Z.-Q. Li et al., 2018). These findings support the conclusion from many studies, reviewed below, that deep water ferruginous conditions persisted despite rising sulfate levels in the Proterozoic.

Interpreting the relationship between sedimentary iron enrichments and the redox conditions of an overlying water column requires nuance, especially considering that iron enrichments can also be generated during later fluid alteration, or during high-grade metamorphism (Morris, 2012). The deposition of chemically precipitated IF is evidence for the presence of iron at saturation with numerous iron-bearing minerals in the oceans throughout key Precambrian intervals. The equilibrium conditions indicated by some of these minerals, or their interpreted precursors have been used to estimate the Fe^{2+} concentrations of ferruginous seawater (**Table 1**). These minerals or their mineral precursors generally fall into three categories: carbonates, (oxyhydr)oxides, and silicates. Considering the equilibrium of multiple Fe^{2+}-bearing minerals and the iron supply needed to deposit IF, early estimates for Fe^{2+} in Archean-aged ocean basins ranged from 10-100 µM (Eugster and Chou, 1973), 380 µM (Ewers, 1980), 100 µM (Ewers, 1983), and 1800 to 7000 µM (Mel'nik, 1973). Estimates from the solubility of Fe^{2+} in equilibrium with siderite ($FeCO_3$) yielded values of 10-120 µM (Canfield, 2005; Holland, 2007). Newer experimental constraints on the precipitation and saturation of greenalite (an Fe^{2+}-bearing silicate), and slow kinetics of siderite precipitation yielded higher

equilibrium Fe^{2+} concentrations, ~100-1,600 µmolal (Jiang and Tosca, 2019; Tosca et al., 2016). Estimates based on equilibrium with green rust, a mixed Fe^{2+}-Fe^{3+} salt, are 1-10 µM Fe^{2+} in the deep ocean to <1 nM in the surface ocean (Halevy et al., 2017). Estimates based on equilibrium with iron mineral precipitation and iron-binding ligands indicate Fe^{2+} was >50 µM Fe^{2+} during major Archean and Proterozoic BIF deposition and >4 nM during deposition of Ediacaran and Phanerozoic marine red beds (MRB; Song et al., 2017).

Table 1. Estimated Precambrian ocean iron concentrations.

Timeframe	Proxy	Iron	Depth and/or setting	Reference
Precambrian	greenalite, siderite, $Fe(OH)_2$ equilibrium	10-100 µM	banded iron formations	Eugster and Chou, 1973
Precambrian	$Fe(OH)_3$ and siderite equilibrium	100 µM	banded iron formations	Ewers, 1983
Precambrian	$Fe(OH)_3$ and siderite equilibrium; mass accumulation estimates	380 µM	banded iron formations	Ewers 1980
Precambrian	siderite, iron hydroxide, iron sulfide equilibrium at pH 6	1800-7000 µM	banded iron formations	Mel'nik, 1973
Archean and early Proterozoic	siderite equilibrium	10-120 µM	deep ocean; banded iron formations	Canfield 2005; Holland 2007
Precambrian	greenalite equilibrium; siderite kinetics	~100-1,600 µmolal	deep ocean; iron formations	Jiang and Tosca, 2019; Tosca et al., 2016
Precambrian	green rust equilibrium	1-10 µM	deep ocean; iron formations	Halevy et al., 2017
Precambrian	green rust equilibrium	<1 nM	surface ocean; iron formations	Halevy et al., 2017
Archean and Proterozoic	iron-binding ligand equilibrium	>50 µM	deep ocean; banded iron formations	Song et al., 2017
Ediacaran and Phanerozoic	iron-binding ligand equilibrium	>4 nM	deep ocean; marine red beds	Song et al., 2017
late Archean	Fe^{2+} inhibition of calcite	>20 µM	shallow shelf; carbonate platform	Sumner and Grotzinger, 1996
late Archean	Fe^{2+} inhibition of calcite	<80 µM	shelf and slope; carbonate platform	Sumner, 1997
late Archean	iron isotope distillation	30-310 µM	shallow shelf; carbonate platform	Eroglu et al., 2018
late Archean	iron isotope distillation	61-928 µM	shelf and slope; carbonate platform	Eroglu et al., 2018

While the persistence of IF implied a large marine reservoir of iron, the source(s) of iron confounded researchers for decades (Holland, 1973). The contention came from the observation that a terrestrial supply of iron, in the dissolved load of rivers, was insufficient to

account for the concentration of iron that should be at saturation with IF minerals or their precursors. To sustain an iron reservoir given reasonable constraints on mass deposition rates for iron from some major IF, weathering rates and river discharge would have needed to be absurdly high, or an unrealistic amount of volcanism would have been required (Holland, 1973). The discovery of hydrothermal vents on the ocean floor in the 1970s provided a source of iron from the oceans themselves, via alteration of seafloor crust by circulating ocean water, solubilizing iron and emitting it at vents. In an anoxic ocean, this soluble iron source would be buffered locally by mineral formation, but the remainder could be transported along bottom currents and via upwelling to sites of precipitation (Holland, 1984). With higher mantle heat flows on early Earth, combined with µM concentrations of sulfate in the Archean (Crowe et al., 2014b), the flux of iron to the ocean from hydrothermal alteration of the seafloor was likely also elevated above modern fluxes (Isley, 1995; Kump and Seyfried Jr, 2005). It has also been suggested that some of the most aerially extensive IF are co-eval with evidence for enhanced mantle-driven volcanism (Barley et al., 1997; Isley and Abbott, 1999; Rasmussen et al., 2012), further evidence for the importance of the hydrothermal iron source. It is generally agreed that hydrothermalism is the predominant iron source to IF, which in many cases is supported by rare earth element (REE) patterns, where a positive europium (Eu) anomaly indicates a high-temperature hydrothermal source (Bau and Moeller, 1993). A continental source of iron is also discussed for some IF (Alexander et al., 2008; Li et al., 2015; Raiswell, 2006), but the significance of a continental source likely depended on the amount of emergent land (Flament et al., 2008), and the oxygenation of terrestrial near surface environments and resulting iron mobility (Babechuk et al., 2019).

The sedimentology of Superior-type IF and associated sediments deposited during the Archean and Paleoproterozoic provide ample evidence for a gradient in dissolved iron concentrations, with higher iron concentrations in the deep ocean and lower concentrations in shallower waters. This is typified by deepwater IF, where sedimentary iron concentrations exceed 15 wt % and fine-grained clastics such as shales and mudstones deposited along the slope have total iron to aluminum ratios (Fe_T/Al) exceeding one (Raiswell et al., 2011), implying authigenic precipitation of iron-bearing minerals contributed additional iron above that present in detrital grains derived from continental crust (Taylor and McLennan, 1985). Precambrian carbonates, deposited at shallower depths than IF, sometimes contain wt % enrichments of iron (Eroglu et al., 2018; Sumner, 1997). These can be significant compared to Phanerozoic carbonates (i.e. Veizer et al., 1989), but generally imply less iron in shallow waters as compared to those in deeper waters. These general trends in sedimentary iron concentrations from shallow to deep are typically explained by a deep, anoxic basin supplying dissolved iron sourced from hydrothermal alteration of ocean crust (Beukes and Klein, 1992). Most models call for oxidation and/or precipitation of iron as upwelling water masses moved toward the surface ocean, although the proposed oxidation mechanisms vary (Posth et al., 2013b). Importantly, the interpretation of a gradient of iron concentrations with depth is observed in the stratigraphy of many other late Archean and Proterozoic IF-depositing basins varying in time and place, including the Transvaal basin preserved in South Africa (Beukes and Klein, 1992; Czaja et al., 2012), the Hammersley Basin in western Australia (Kaufman et al., 1990), and the Paleoproterozoic Animike Basin of North America (Simonson, 1985).

Additional constraints on paleoredox conditions of the shallow ocean in connection with IF-depositing basins have been estimated by the iron content and isotopic composition of carbonates. For instance, textures such as herringbone carbonate and the lack of micrite in the 2.521 Ga Gamohaan Formation were inferred to reflect the presence of an inhibitor to calcite formation in seawater, in this case Fe^{2+} (Sumner and Grotzinger, 1996). Inhibitors such as Fe^{2+} or Mn^{2+} act by slowing precipitation kinetics, or nucleation dynamics. The textural evidence for seafloor calcite in the Gamohaan Formation and correlative Frisco Formation, and deeper water siderite formation, has further been used to suggest that shallow waters may have had 20 µM or more Fe^{2+}, while deeper waters in equilibrium with siderite had up to 80 µM (Sumner, 1997). Invoking siderite as a seawater precipitate is, however, often incompatible with its light $\delta^{13}C$ values, which can signal diagenetic formation (sec. 3). Further geochemical work on the ~2.58 to 2.50 Ga Campbellrand-Malmani carbonate platform, including the Gamohaan Formation, focused on iron concentrations and isotopic compositions within carbonates deposited across a range of water depths. Iron concentrations and isotope compositions showed depth-dependent trends, which were modelled with a Rayleigh distillation equation to yield estimates of 61-928 µM Fe^{2+} in water overlying the slope, to 30-310 µM on the shelf itself (Eroglu et al., 2018), ranges that overlap with the calcite-siderite saturation and textural estimates (**Table 1**; Sumner, 1997).

From the summary in **Table 1**, it is clear that estimates of ferrous iron concentrations vary widely, both in space and time, and also depend upon the approach and assumptions. An underlying implication here is the non-conservative behavior of iron in aqueous systems – it plays the role of a nutrient and scavenged (i.e. mineral forming) element simultaneously – and

has temporally variable inputs. Although the residence time of iron in seawater was likely higher (a few hundred thousand to a few million years) under predominantly anoxic and low sulfate oceans than it is today (Johnson et al., 2003; Thibon et al., 2019), it would still be reacting to local and global changes in oxygen and pH, as well as the concentrations of other ions (i.e. carbonate, silicate) necessary to precipitate iron-bearing minerals. Dissolved Iron concentrations vary widely in the modern ocean, both vertically through the water column, as well as between different regions. These variations stem from local or regional sources, as well as water column cycling and sedimentary sinks. The range of estimates of iron concentrations for ferruginous oceans may indicate that sources, sinks, and processes for iron in the oceans varied in time and space, and there is no *a priori* reason to assume that iron concentrations would have been static. Each estimate should only be applied to the specific depositional system from which it was constrained.

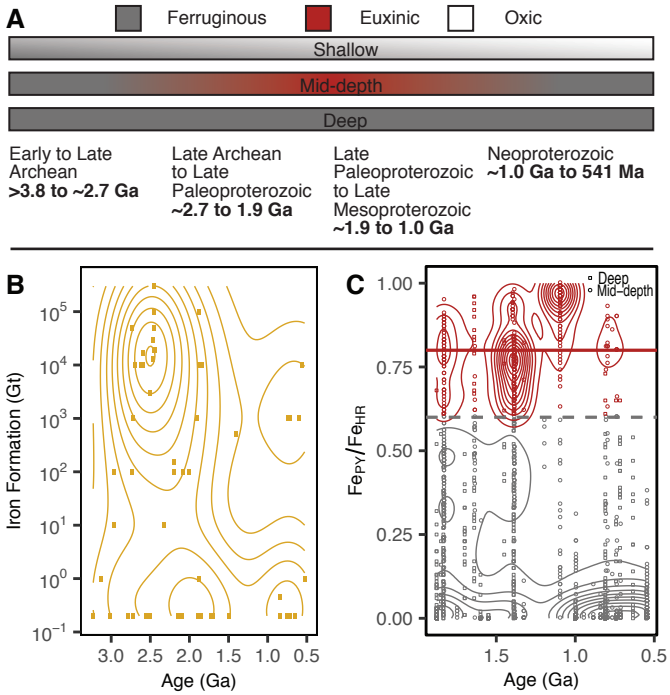

Figure 1. A. Summary of redox conditions within the Precambrian oceans. **B**. Individual Precambrian iron formations, as gigatons (Gt), plotted from data compiled by Bekker et al. (2010) and updated with Mid-Proterozoic data (Canfield et al., 2018; Sun et al., 2018). **C**. Proterozoic iron speciation data, plotted from data compiled by Guilbaud et al. (2015) with additional data from more recent studies (supplementary information). Horizontal lines denote thresholds of Fe_{PY}/Fe_{HR} for ferruginous (<0.6) and euxinic (>0.8). Contours in **B** and **C** are kernel density estimations, essentially smoothed, 2D histograms.

Paleoredox proxies in the Proterozoic and beyond

Iron Formations and associated sediments imply ferruginous conditions by virtue of being iron-rich chemical precipitates. Many carbonates and clastic marine sediments also contain iron enrichments above that which is added from detrital minerals. Several iron speciation techniques that quantify iron in minerals or phases with different reactivity toward

sulfide can be used to indicate the paleoredox conditions of anoxic, euxinic, or ferruginous. These techniques include Fe_T/Al (Lyons et al., 2003), highly reactive iron to total iron (Fe_{HR}/Fe_T), pyritized iron to total iron (Fe_{PY}/Fe_T) (Poulton et al., 2004b), and degree of pyritization or sulfidization (DOP or DOS), which are the ratios of sulfidized iron (Fe_{PY} and/or acid-volatile sulfide-associated iron, Fe_{AVS}) to the sum of pyritized/sulfidized iron and hydrochloric acid-extractable iron (Berner, 1970; Boesen and Postma, 1988). Highly reactive iron combines sufide-reactive iron extracted from carbonates, oxides, magnetite and pyrite, while a boiling hydrochloric acid extraction also extracts some iron that does not react with sulfide. Total iron includes all reactive iron phases and silicate-bound iron. Best practices for these techniques and analysis of results have recently been summarized by Raiswell et al. (2018).

When Fe_T/Al exceeds 0.66, anoxic conditions are indicated (Clarkson et al., 2014; Raiswell et al., 2018), although others advocate for a higher threshold (Cole et al., 2017). Anoxic conditions are indicated by elevated Fe_{HR}/Fe_T. Highly reactive iron minerals may precipitate from the water column after transport under ferruginous conditions, leading to enrichments over the detrital iron input in deposited sediments (Poulton et al. 2004a; Poulton and Canfield 2011; Raiswell and Canfield 2012). Anoxic conditions tend to have Fe_{HR}/Fe_T ratios >0.38, whereas Fe_{HR}/Fe_T <0.22 commonly indicates oxic conditions, and Fe_{HR}/Fe_T between 0.22 and 0.38 are considered equivocal. When accompanied by enrichments in Fe_{HR}/Fe_T (i.e. >0.38), elevated Fe_{py}/Fe_{HR} ratios of 0.6 to 0.8 (horizontal lines in **Figure 1c**) or above commonly suggest euxinic conditions, although particular care is required for samples in the range of 0.6-0.8 (Raiswell et al., 2018). Ferruginous conditions commonly have Fe_{py}/Fe_{HR} ratios <0.6 (Benkovitz et al., 2020; Poulton and Canfield, 2011). More recently, it has been demonstrated that the iron

386 extraction scheme can also be applied to carbonate-rich sediments when iron exceeds 0.5 wt %,
387 providing there is no evidence for additional iron supply through deep burial dolomitization
388 (Clarkson et al., 2014).
389 Trace element systematics should be used in concert with iron speciation to provide more
390 robust insight into local redox conditions instead of relying on iron speciation alone (cf. Raiswell
391 et al., 2018). The principle of sedimentary trace element enrichments as paleoredox indicator is
392 that trace metals often show a redox-dependent behavior, which causes their fractionation
393 and/or accumulation in sediments under oxic vs. anoxic and ferruginous vs. euxinic conditions
394 (see reviews by Tribovillard et al. 2006; Piper and Calvert 2009; Huang et al. 2015; Robbins et al.
395 2016). Molybdenum (Mo) enrichments can occur under oxic conditions due to reaction with
396 iron and manganese (oxyhydr)oxides, but scavenging by sulfide produces much greater
397 enrichments (Scott et al., 2008). Molybdenum enrichments are therefore a proxy for euxinic
398 conditions (Doyle et al., 2018; Scott and Lyons, 2012), although sustained and widespread
399 euxinic conditions can draw down the oceanic reservoir of Mo, resulting in muted enrichments
400 (Algeo, 2004). Uranium enrichments indicate anoxic conditions, but do not distinguish between
401 ferruginous and euxinic conditions (Algeo and Tribovillard, 2009; Partin et al., 2013). Chromium
402 (Cr) is scavenged to anoxic but not sulfidic sediments, but the reservoir of Cr can also been
403 drawn down with extended and/or widespread anoxia, muting enrichments (Reinhard et al.,
404 2013). Rhenium (Re) is preferentially buried under anoxic condition relative to oxic, has less of
405 an interfering detrital component than Cr or U, and may not be sensitive to sulfide (Kendall et
406 al., 2010; Sheen et al., 2018). Zinc (Zn) is preferentially buried under sulfidic conditions (Robbins
407 et al., 2013; Scott et al., 2012), while enhanced cobalt (Co) burial is associated with a larger Co

reservoir under ferruginous conditions (Swanner et al., 2014). Importantly, thresholding enrichments across units with varying mineral or sedimentary phases can lead to spurious results (Algeo and Liu, 2020).

Trace element isotope ratios are also employed paleoredox proxies, as fractionations can occur upon phase changes, and chemical and biological transformations of oxidation state and speciation, and have been reviewed independently (Anbar and Rouxel, 2007; Wasylenki, 2012). Positive $\delta^{97/95}$Mo occur when Mo has been scavenged to sediments under euxinic conditions, while negative values are more indicative of oxic conditions (Arnold et al., 2004). Mass balance models can help to constrain the extent of euxinia (Gordon et al., 2009; Kendall et al., 2011). Positive iron isotope (i.e $\delta^{56/54}$Fe) sedimentary values have been interpreted to indicate euxinic conditions and a pyrite sink, while negative values can indicate either localized microbial iron reduction or partial oxidation processes within ferruginous waters (Eroglu et al., 2018; Johnson et al., 2008b; Rouxel et al., 2005). Positive values in Selenium (Se) isotope ratios (i.e. $\delta^{82/78}$Se), can indicate anoxic and ferruginous conditions (Kipp et al., 2017; Wen et al., 2014). Elevated U isotope ratios ($\delta^{238/235}$U) can distinguish oxic conditions from anoxic and euxinic conditions, which are less positive (Andersen et al., 2014; Lau et al., 2019).

The deposition of IF indicates widespread ferruginous conditions in the Archean and Paleoproterozoic (**Figure 1**). This inference is also supported by the record of enhanced Co in IF, shales, and sulfides from this time (Swanner et al., 2014). The redox landscape begins to change by about 2.0 Ga when coupled Mo, U, and Fe isotopes indicate the appearance of euxinic conditions during the Shunga event (Asael et al., 2013). In the ~1.8 Ga Animike Basin of North America, a transition from oceans that deposited IF to ferruginous deep waters overlain by

euxinic mid-depth and oxic shallow waters in shales is indicated by iron speciation (Poulton et al., 2010, 2004a). This transition was also observed in a shift from IF to black shales deposited under euxinic conditions, which have positive Mo isotope values consistent with euxinia (Kendall et al., 2011).

Iron speciation measurements of clastic sediments deposited in the middle Proterozoic (~1.8-1.0 Ga) have led to a picture of widespread (in space and time) ferruginous conditions in the deep ocean (**Figure 1**; Guilbaud et al., 2015; Planavsky et al., 2011; Poulton et al., 2010; Poulton and Canfield, 2011; Sperling et al., 2015). A narrow range of Zn enrichments in shales during the entire Precambrian, and Re abundances during the mid-Proterozoic also support the inference of widespread ferruginous conditions with limited euxinia (Scott et al., 2012; Sheen et al., 2018). Combinations of Mo and Cr shale records and mass balance models indicate widespread anoxic conditions in the mid-Proterozoic, and although euxinia expanded after about 1.8 Ga, the areal extent was under 10% of the seafloor (Reinhard et al., 2013; Scott and Lyons, 2012). This view of limited euxinia is supported for the mid-Proterozoic by the U isotope record (Gilleaudeau et al., 2019). Despite this broad inference of widespread ferruginous conditions, studies of individual formations throughout the middle Proterozoic reflect a wide range in the redox structure of the oceans (**Figure 1**). This could reflect spatial and temporal variation, basinal vs. global conditions, the range of processes invoked in the interpretation of data, or perhaps the fidelity of the redox proxies to post-depositional processes.

There are numerous studies that point to more nuance in Proterozoic paleoredox. Molybdenum isotopes are used to infer episodic deep-water oxic conditions and manganese oxide formation in ~1.8 Ga sediments from the Animikie Basin depositing on the margin of

North America (Planavsky et al., 2018). This seems to be an exceptional case, as most other middle Proterozoic sites lack evidence for full water column oxidation and instead lie somewhere on a spectrum of ferruginous to euxinic with varying evidence for oxygen in overlying waters. Degree of pyritization and S isotopes of 1.7 and 1.6 Ga sediments from the MacArthur Basin of Western Australia indicate euxinic conditions, with sulfate concentrations estimated at 0.5 to 2.4 mM (Shen et al., 2002). There is evidence from iron speciation and rare earth element (REE) abundance patterns for intervals of enhanced shallow water oxygenation overlying ferruginous deep water at ~1.56 Ga (Zhang et al., 2018). Iron speciation of clastic sediments deposited at 1.4 Ga in the Roper Basin of Western Australia indicate a euxinic water column with overlying oxic water, despite sulfur isotopic evidence for low, perhaps sub-mM sulfate concentrations (Shen et al., 2003), an interpretation largely supported by DOP, Fe_T/Al, and Re, U, Mo, and vanadium (V) abundances (Kendall et al., 2009). At 1.4 Ga, shales deposited below wave-base in the Arlan Basin in Volgo-Ural region of Russia lack iron enrichments indicative of ferruginous conditions, and contained biomarker evidence potentially consistent with an oxic water column (Sperling et al., 2014). The low total organic carbon content (<0.2 %) of these sediments was interpreted to indicate oligotrophic conditions that allowed for deep oxygen penetration. From broadly age-correlative samples elsewhere in the Volgo-Ural region, iron speciation indicated deeper-water anoxic and ferruginous conditions, with overlying oxic conditions limited to only very shallow water (Doyle et al., 2018). The sediments studied by Doyle et al. (2018) likely were deposited in greater water depths with greater connection to the open ocean than those studied by Sperling et al. (2015). Similar-aged sediments from China were suggested to record a Mesoproterozoic OMZ, with overlying and underlying oxic waters

(Zhang et al., 2016). However, other workers interpret the V and biomarker data used to infer an OMZ in that study as rather consistent with anoxia (Planavsky et al., 2016).

A compilation of iron speciation measurements in late Middle Proterozoic to early Neoproterozoic (~1000 Ma to 742 Ma) fine-grained clastic sediments suggest widespread ferruginous conditions in shallow mid-depths of the oceans (**Figure 1**; Guilbaud et al., 2015). The authors interpreted this data to reflect a shift away from euxinic conditions detected in similar settings in the Middle Proterozoic (1.8 to 1.0 Ga). A 1.1 Ga, the intercratonic Taoudeni Basin, Morocco, records evidence for a shallow chemocline between oxic and euxinic conditions, but with episodic mid-depth and deeper water ferruginous conditions, based on iron speciation, C and S isotopes, and trace element (Fe, Al, Mo, V, Mn) enrichments within clastic sediments (Beghin et al., 2017; Gilleaudeau and Kah, 2015). Such epeiric seas were becoming increasingly common in the Middle Proterozoic but are distinct environments from those included in global compilations (e.g. **Figure 1**). The 742-800 Ma Neoproterozoic Chuar Group in Arizona records iron enrichments that signify ferruginous conditions (Johnston et al., 2010). The later Neoproterozoic (<742 Ma) was also characterized by anoxic and ferruginous conditions along continental shelves and in deeper basins, based on the abundance of highly-reactive iron minerals (Canfield et al., 2008). In both of these latter studies, ferruginous conditions were implicated below the mixed layer, with limited detection of euxinic conditions. Another Neoproterozoic example of predominantly ferruginous conditions is from 835-630 Ma sediments from Svalbard, evidence by both iron speciation, Fe_T/Al, and trace elements (Mo, U, V; Kunzmann et al., 2015). A 650 Ma carbonate reef in South Australia records iron and manganese enrichments, interpreted as evidence for ferruginous conditions in shallow and

deep reefal water (Hood and Wallace, 2014). The Edicaran-age Duoshontuo Formation (635-551 Ma) in South China records persistent ferruginous deepwater conditions below euxinic shelf waters through both iron speciation and sulfur isotope datasets (Li et al., 2010). Late Neoproterozoic (550-541 Ma) carbonates from Namibia document the presence of low oxygen, Mn^{2+}-bearing (manganiferous) waters below oxygenated surface waters, and above deeper ferruginous waters, based on REE patterns and trace element abundances (Tostevin et al., 2016; Wood et al., 2015).

Anoxic conditions seem to persist, at least locally, into the Phanerozoic Eon as indicated by redox-sensitive trace element abundance patterns, as well as iron speciation (Partin et al., 2013; Reinhard et al., 2013; Tostevin and Mills, 2020), and a continuation of ferruginous conditions has been advocated (Canfield et al., 2008; Poulton and Canfield, 2011; Sperling et al., 2015). Iron speciation measurements indicate ferruginous conditions in the early Cambrian and at the Permian-Triassic boundary (Clarkson et al., 2016; Goldberg et al., 2007). Phanerozoic MRB, with elevated concentrations of bulk iron, are thought to form from episodic incursions of a deep ferruginous water mass into oxic waters (Song et al., 2017). Importantly, these indicate lower dissolved iron concentrations than are inferred for the Precambrian (**Table 1**). The recently described early Cambrian-aged IF also records evidence for ferruginous conditions in deep waters (Z.-Q. Li et al., 2018), but notably $\delta^{82/78}Se$, Se abundances and iron speciation also indicate ferruginous conditions in several shale and carbonate sections during the Ediacaran to Cambrian transition (Wen et al., 2014). In several studies, the occurrence of ferruginous conditions has been linked to ocean anoxic events (OAE; Clarkson et al., 2016; März et al., 2008; Poulton et al., 2015; Song et al., 2017). As OAEs recur throughout the Phanerozoic, and are

often linked to major mass extinctions (Wignall and Twitchett, 1996), additional multi-proxy documentation of oceanic redox conditions will shed light on the timing of the ultimate demise of ferruginous conditions from the oceans. For the Phanerozoic, such studies will have important implications for the capacity of ferruginous conditions to exist as marine sulfate levels rose (Canfield and Farquhar, 2009).

3. The biogeochemistry of ferruginous oceans

Primary minerals and their formation and deposition pathways

Much work has focused on determining the original iron minerals precipitated out of ferruginous oceans and deposited to IF, but particular emphasis will be given here to Superior type IF deposited from the Neoarchean (about 3.8 Ga) to the Paleoproterozoic (about 1.8 Ga), as they are the most extensive, diverse, and best studied examples of sediments deposited in ferruginous oceans (**Figure 1**; Bekker et al., 2014). Many early studies of IF noted that ferrous, ferric, and mixed-valence iron minerals are present, with an oft-cited average oxidation state compiled from some Superior-type IF of $Fe^{2.4+}$ (Klein, 2005; Klein and Beukes, 1992). More recent microanalysis documents the dominance of Fe^{2+} in well-preserved IF, but also show intriguing observations of Fe^{3+} within typically ferrous minerals (Johnson et al., 2018). Revisiting some of the well-studied IF with newer analytical tools will yield precise mineralogy, elemental stoichiometry and oxidation state, as well as resolve primary from secondary minerals from different IF as well as different water depths within IF. Such careful studies, combined with experimental and computational approaches to constrain mineral formation

539 conditions, are already leading to a clearer picture of the diversity of conditions and primary
540 minerals that gave rise to Precambrian IF.

541 Models of IF genesis often invoke the need for an oxidation mechanism due to the
542 presence of mixed valent or ferric iron minerals in IF. Most of these mechanisms center around
543 biological pathways, although not exclusively. These include: 1) oxidation of Fe^{2+} by molecular
544 oxygen (O_2) produced by organisms such as the earliest evolved oxygenic phototrophic bacteria
545 (the Cyanobacteria; Cloud Jr., 1968), 2) direct oxidation of Fe^{2+} by anoxygenic photosynthetic
546 bacteria in the absence of oxygen (Kappler et al., 2005; Konhauser et al., 2002; Widdel et al.,
547 1993), or 3) direct chemical oxidation of Fe^{2+} by UV light (Cairns-Smith, 1978). The specifics of
548 each mechanism, and arguments for or against, and evidence of, have been extensively
549 reviewed (Koehler et al., 2010; Konhauser et al., 2017; Posth et al., 2013b).

550 Iron formations comprise several mineralogical facies, or lithofacies, where a primary
551 control on IF lithofacies was likely water depth along shelf-to-basin transitions on passive
552 margins (Beukes and Gutzmer, 2008; Beukes and Klein, 1992). These facies include oxide,
553 silicate, and carbonate (James, 1954). A previously defined sulfide facies is now excluded as a
554 true IF, as these are likely either carbonaceous shales or volcanogenic massive sulfide (VMS)-
555 related deposits (Bekker et al., 2010). The exact mineralogy of the facies is dependent on
556 metamorphic grade, but the lowest metamorphic grade IF generally encompass magnetite and
557 hematite from oxide-facies IF, chert, greenalite, and stilpnomelane from silicate-facies IF, and
558 siderite, ankerite, and ferroan dolomite from carbonate-facies IF (Klein, 2005).

559 Fine-grained hematite has been observed in some IF and interpreted as primary, for
560 instance in the 2.5 Ga Dales Gorge member of the Brockman Iron Formation (Ayres, 1972;

561 Morris, 1993), and the Mara Mamba Iron Formation (Ahn and Buseck, 1990). Iron formations
562 depositing in the Animikie Basin at around 1.8 Ga in North America have been argued to have
563 minor occurrences of primary hematite (James, 1954). A primary water column precipitate of
564 Fe^{3+}, such as a colloidal Fe^{3+} (oxyhdr)oxide (Ahn and Buseck, 1990) has been widely discussed.
565 Such poorly crystalline phases are generally what is detected in cultures of anoxygenic
566 photosynthetic bacteria (Kappler and Newman, 2004; Swanner et al., 2015c) and Cyanobacteria
567 producing oxygen in the presence of Fe^{2+} (Swanner et al., 2017). Hematite is not detected in
568 such studies, and water chemistry controls aging of primary precipitates to more crystalline
569 phases, such as goethite or lepidocrocite (Wu et al., 2014). Such poorly-crystalline precipitates
570 would have likely dehydrated and crystallized to hematite under diagenetic conditions (Posth et
571 al., 2013a). A secondary origin of Fe^{3+}, particularly the mineral hematite, has been argued for
572 some hematite within the 2.5 Ga Dales Gorge member of the Brockman Iron Formation based
573 on mineral replacement textures (Rasmussen et al., 2014). However, if post-depositional
574 oxidation is invoked, which it often is for hematite and magnetite ore (Taylor et al., 2001), it
575 requires a plausible oxidative mechanism consistent with regional geological events (Robbins et
576 al., 2019).

577 In contrast to some evidence supporting primary hematite, magnetite is generally
578 considered to have formed during diagenesis (Klein, 2005; Posth et al., 2013a). Magnetite
579 formation is generally ascribed to microbial reduction of Fe^{3+} (oxyhydr)oxides coupled to
580 organic carbon oxidation (Johnson et al., 2008a, 2005; Konhauser et al., 2005), which reconciles
581 the low organic carbon content (usually a few hundred ppm) of many IF. Magnetite also forms
582 experimentally during abiotic reaction of Fe^{3+} (oxyhydr)oxides and organic carbon at

583 temperatures of 170°C and pressures of 1.2 kbar (Halama et al., 2016; Posth et al., 2013a),
584 approximating low-grade metamorphic conditions. A green rust precursor has also been
585 proposed as part of an early formation pathway for magnetite in some IF (Halevy et al., 2017; Li
586 et al., 2017). Rasmussen and Muhling (2018) also argue that much IF magnetite is the product
587 of thermal decomposition of siderite.

588 A primary iron silicate precipitate has been suggested by many authors. Textural
589 evidence supports the primary nature of iron silicates in several IF of the Hammersley and
590 Transvaal Basins, formed either within the water column or sediments (Rasmussen et al., 2017,
591 2015, 2013). Diffraction-based analysis and mapping of iron within nanoscale greenalite and
592 stilpnomelane inclusions within chert layers of 2.5 Ga BIF from Western Australia and South
593 Africa also provide evidence for the primary nature of iron silicates (Johnson et al., 2018).
594 Experimental work documents that greenalite is a likely product of Fe^{2+}-silicate gels, with
595 formation favored under alkaline (i.e. pH 7.7-8.3) and likely deep-water conditions (Tosca et al.,
596 2016). Iron-bearing phyllosilicates can also be produced upon aging of green rust precipitated in
597 the presence of silica (Halevy et al., 2017).

598 Siderite ($FeCO_3$), ankerite [$Ca(Fe,Mg,Mn)(CO_3)_2$] and ferroan dolomite are the
599 predominate mineral phases in carbonate-facies IF, but are also common in oxide facies (James,
600 1954). Iron-bearing Ca-Mg carbonates are present in IF of lowest to highest metamorphic
601 grades (Klein, 2005). There has been much discussion of whether these phases precipitated
602 directly from seawater or formed later during sedimentary diagenesis or even metamorphism.
603 If siderite is a primary seawater precipitate, it would be a proxy for the chemical composition of
604 the ocean (Rosing et al., 2010), as carbonate exchanges with atmospheric CO_2 equilibrating in

605 the surface ocean and alkalinity generated during weathering. However, numerous lines of
606 evidence, discussed below, suggest siderite did not form in equilibrium with seawater (Dauphas
607 and Kasting, 2011; Gäb et al., 2017; Reinhard and Planavsky, 2011).

608 The $\delta^{13}C$ of siderite in IF is usually depleted from the assumed value of dissolved
609 inorganic carbon (DIC; including dissolved CO_2, H_2CO_3, HCO_3^- and CO_3^{2-}) in seawater ($\delta^{13}C \cong 0$
610 ‰; **Figure 2**; Supplementary Information). This led to the early suggestion that oceans were
611 stratified with respect to DIC and $\delta^{13}C$-DIC, with increasing DIC concentrations and
612 progressively lighter $\delta^{13}C$-DIC with depth. This hypothesis was based on the observation of
613 deep-water siderite with $\delta^{13}C$-DIC of about -5 ‰, and shallower limestones and dolomites with
614 $\delta^{13}C$-DIC closer to -1 ‰ (Beukes et al., 1990; Beukes and Klein, 1990; Carrigan and Cameron,
615 1991; Kaufman et al., 1990; Winter and Knauth, 1992). Other authors have interpreted a $\delta^{13}C$-
616 carbonate isotopic gradient within IF to invoke a stronger biological pump than the modern
617 ocean, which seems unlikely if primary productivity was lower in the Archean ocean compared
618 to modern (Fischer et al., 2009). The depleted $\delta^{13}C$-DIC (i.e. <-5 ‰) common in siderite data
619 compiled here (**Figure 2**; Supplementary Information) is generally ascribed to diagenetic
620 formation in sediments, via organic carbon oxidation coupled to microbial Fe^{3+} (oxyhydr)oxide
621 reduction (Heimann et al., 2010; Johnson et al., 2013; Perry et al., 1973), but higher
622 temperature abiotic reactions with organic carbon are also feasible (Köhler et al., 2013). During
623 diagenetic formation, the depleted $\delta^{18}O$ composition of Fe^{3+} (oxyhydr)oxides can be transferred
624 to the carbonate (see discussion below). The iron isotopic composition can also inform the
625 formation pathway, with positive $\delta^{56}Fe$ values inherited from diagenetically reduced Fe^{3+}
626 (oxyhydr)oxides, while negative $\delta^{56}Fe$ values may reflect the isotopic composition of iron in

627 seawater, partial reduction of Fe^{3+} (oxyhydr)oxides (Heimann et al., 2010; Johnson et al.,
628 2008b), or a hydrothermal Fe source of $\delta^{56}Fe \cong 0$ ‰ (Jiang and Tosca, 2019). Strontium (Sr)
629 isotopes have been proposed as a way to parse the primary vs. diagenetic origins of
630 Precambrian carbonates, with uniform $^{87}Sr/^{86}Sr$ representing seawater in Ca-Mg carbonates of
631 late Archean age, while non-uniform and more radiogenic (i.e. higher) $^{87}Sr/^{86}Sr$ in IF siderite and
632 ankerite interpreted as incorporation of Sr from clays during diagenetic formation (Johnson et
633 al., 2013).

634 Original studies of light $\delta^{13}C$-DIC in siderite IF pointed to precipitation from mantle-
635 derived carbon in hydrothermally-influenced seawater, consistent with other geochemical
636 signatures in those carbonates, e.g. REE, patterns and low organic carbon (Beukes et al., 1990;
637 Beukes and Klein, 1990; Kaufman et al., 1990). Precipitation of siderite from such fluids is
638 possible based on work in experimental (Jiang and Tosca, 2019) and natural systems (Bahrig,
639 1988). The presumed average value of mantle $\delta^{13}C$-DIC measured from hydrothermal vents of -
640 6.5 ‰ (Shanks III, 2001) is nearly identical to both the extent of $\delta^{13}C$-DIC stratification
641 observed in the redox-stratified Black Sea (-5 to –7‰) (Deuser, 1970; Fry et al., 1991), and the
642 average $\delta^{13}C$ depletion of siderite samples in our database (-6.23 ‰; **Figure 2**; Supplementary
643 Information). Given that the scale of the Black Sea basin may be similar to that of major
644 Superior type IF basins (Ohmoto et al., 2006), extending the analogy of the observed Black Sea
645 $\delta^{13}C$-DIC stratification to the Superior IF basin scale is feasible. Hence, a wider range of primary
646 marine $\delta^{13}C$ signatures may be reflected in ancient ferruginous environments (Jiang and Tosca,
647 2019; Wittkop et al., 2020b).And while a diagenetic interpretation of siderite $\delta^{13}C$ depletion is
648 clearly feasible in many cases (see Konhauser et al. (2017) for the conventional diagenetic

649 interpretation of these signatures), recent work also demonstrates that a more nuanced view
650 of δ ^{13}C signatures in Archean siderites is consistent with a link between photoferrotrophy,
651 methane cycling, and the paucity of organic carbon observed in IFs (Thompson et al., 2019).
652

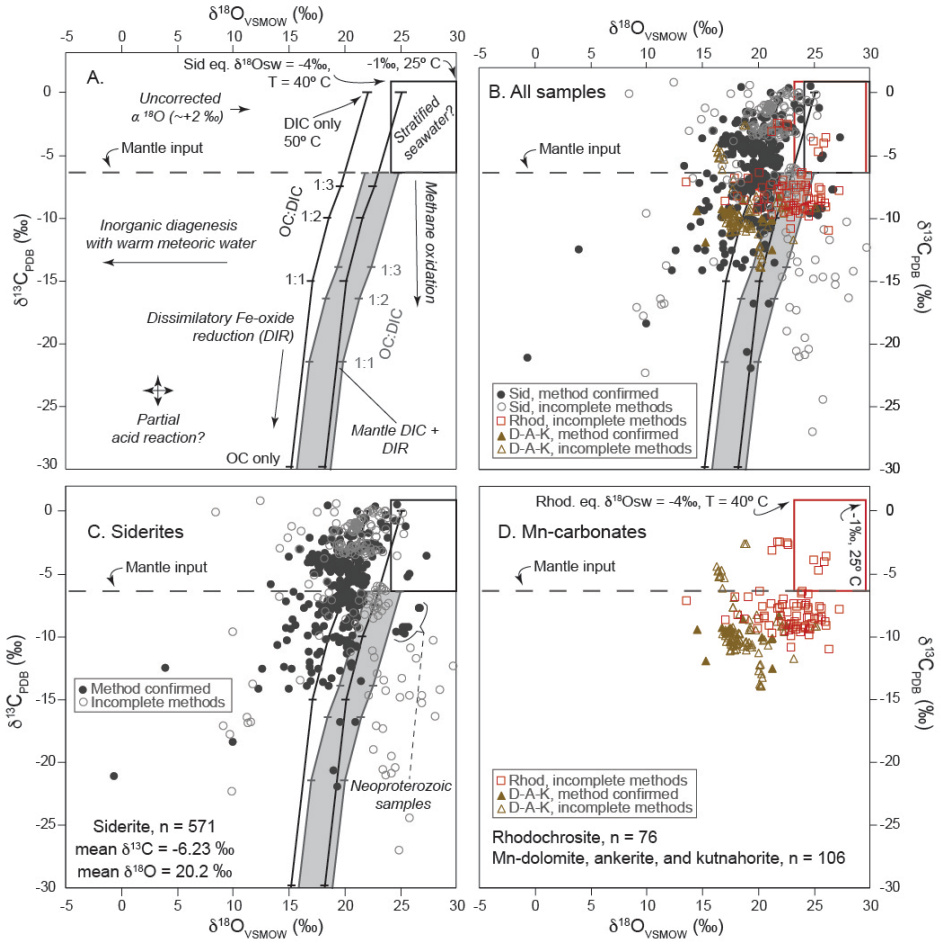

653
654
655 **Figure 2**. Cross plots from a database Precambrian Fe- and Mn-carbonate δ^{13}C and δ^{18}O
656 (Supplementary Information), including siderites (Sid), rhodochrosites (Rhod), and Mn-enriched
657 dolomites (D), ankerites (A), and kutnohorite (K). **A**. The range of processes potentially recorded
658 in Fe- and Mn-carbonate isotope records. The box shows a range of potentially stratified
659 seawater siderite values based on d^{18}O equilibrium siderite (Sid) and seawater at 25° to 40° C

660 and -1 ‰ to -4 ‰, representing a range from an ice-free ocean value (Muehlenbachs, 1998) to
661 an upper limit on estimates of a more depleted ancient marine $\delta^{18}O$ reservoir (e.g. Galili et al.,
662 2019) using the fractionation factor of Zhang et al. (2001), and the presumed $\delta^{13}C$ value of
663 mantle input (Shanks III, 2001; horizontal dashed line). A relatively small fractionation factor
664 between C in siderite and HCO_3^- at ~25° C (~+0.5 ‰) is not considered (Jimenez-Lopez and
665 Romanek, 2004). The paired diagonal lines show the $\delta^{13}C$ and $\delta^{18}O$ evolution of diagenetic
666 siderite generated from dissimilatory iron reduction (DIR) assuming a range of ratios (horizontal
667 ticks in diagonal lines) of marine DIC (0‰ by convention) and organic carbon (OC, -30‰),
668 replotted from Heimann et al. (2010) who adopted a higher-temperature siderite ^{18}O
669 fractionation factor from Carrothers et al. (1988). The gray diagonal box shows the DIR
670 relationships detailed from Heimann et al. (2010) shifted to adopt a mantle $\delta^{13}C$-DIC input of -
671 6.5‰. In contrast, methane oxidation potentially shifts $d^{13}C$-DIC lower without significantly
672 impacting $\delta^{18}O$. Metamorphism or interaction with warm diagenetic fluids influenced by
673 meteoric waters lowers $\delta^{18}O$ (Jaffrés et al., 2007). Siderite samples that were not corrected for
674 the acid-digestion fractionation factor ($\alpha_{CO2\text{-}siderite}$) will be shifted ~+2 ‰. The impact of
675 incomplete acid reaction on siderite samples is potentially complex (Fernandez et al., 2016). **B**.
676 All samples relative to the fields discussed in **A**. Closed symbols have a confirmed analytical
677 method; open symbols show samples where analytical method could not be fully verified. **C**. All
678 siderite samples in the database (n = 571). A handful of samples plot within a reasonable range
679 for hydrothermally influenced or stratified seawater. A greater proportion of samples show
680 diagenetic ^{18}O alteration but ^{13}C compositions within a range predicted for hydrothermally
681 influenced or stratified seawater. While the majority of the samples plotting within the

682 methane oxidation zone have unconfirmed analytical methods (predominantly from the
683 Mesoproterozoic Xiamaling iron formation; Canfield et al., 2018), a subset of samples from a
684 recently described Neoproterozoic siderite occurrence plot in this space as well (Hiatt et al.,
685 2020). **D**. All Mn-carbonate samples, including rhodochrosites, and Mn-enriched dolomites,
686 ankerites, and kutnohorite [see Heimann et al. (2010) for discussion of Fe-ankerites]. There is
687 less agreement regarding analytical methods for Mn-carbonates, but a range of $\delta^{18}O$ for
688 rhodochrosite based on fractionation factors of Kim et al. (2009) is shown using the same
689 constraints on seawater composition as **A**. Most samples appear to plot in a diagenetic field,
690 but a handful of samples (principally from the Cryogenian Datangpo Formation; Yu et al., 2016)
691 plot in a space consistent with an origin from stratified seawater or methane oxidation.
692
693 There are isolated examples of extremely light $\delta^{13}C$ in siderite, for instance as light as -
694 28 ‰ (Canfield et al., 2018), which could alternatively be produced if DIC is sourced either from
695 methane oxidation or direct remineralization of organic carbon, although a methane source
696 was not evaluated for that study. Isotopically light $\delta^{13}C$ of siderite can also implicate
697 metamorphism, which can be parsed when paired with oxygen isotopes (Carrigan and
698 Cameron, 1991; Kaufman et al., 1990; Li et al., 2013), as carbonates from metamorphosed IFs
699 typically plot with extremely low $\delta^{18}O$ (Yang et al., 2015). But such alteration generally
700 produces lighter $\delta^{18}O$ without altering $\delta^{13}C$, assuming a rock-buffered diagenetic environment
701 (Jaffrés et al., 2007; Knauth and Kennedy, 2009), though new approaches utilizing Ca- and Mg-
702 isotopes have shown significant promise in evaluating such assumptions in Ca-carbonates (e.g.
703 Ahm et al., 2019). The $\delta^{13}C$ and $\delta^{18}O$ signatures of hydrothermal fluids have divergent

pathways, producing for instance negative $\delta^{13}C$ and positive $\delta^{18}O$ (Shanks III et al., 1995), creating the potential for a unique signature of a hydrothermally influenced siderite. However, many ancient siderites instead display a co-varying isotopic depletion in both $\delta^{13}C$ and $\delta^{18}O$ (**Figure 2**), which may be linked to diagenetic reduction of Fe^{3+} (oxyhydr)oxides (Heimann et al., 2010). Despite this, a handful of siderite samples plot within a range potentially consistent with equilibrium with seawater that is either influenced by a hydrothermal input, or otherwise stratified with respect to DIC composition (**Figure 2**).

Included in the updated siderite isotope database (**Figure 2**) are manganese carbonate samples (Supplementary Information), as environments favorable to producing ferruginous sediments may also overlap with those that generate Mn-enriched sediments (Bekker et al., 2014; Maynard, 2010; Roy, 2006; Wittkop et al., 2020b). The $\delta^{13}C$ and $\delta^{18}O$ of these Mn-enriched carbonates display many similarities with siderites, including a majority of samples likely representing diagenetic environments (**Figure 2**). But as with siderite samples, some Mn -carbonates also plot within a range of $\delta^{13}C$ and $\delta^{18}O$ that reflect a potential origin from stratified seawater, and likewise warrant additional detailed study.

Although the record is intermittent, the $\delta^{13}C$ and $\delta^{18}O$ of siderites and Mn-enriched carbonates do display some interpretable temporal trends. The $\delta^{13}C$ of these samples generally plots below the values of co-eval Ca-carbonates (**Figure 3**), though a subset of samples—particularly those from the ~1.85 Ga Animikie Basin of North America—overlap with the values observed from Ca-carbonates (Carrigan and Cameron, 1991; Winter and Knauth, 1992). A large population of Transvaal Basin samples from South Africa also overlap with $\delta^{13}C$ values that are within a range between presumed surface seawater and mantle input. As with Ca-carbonates,

the $\delta^{18}O$ of Fe- and Mn-carbonates becomes generally lighter with increasing age, although the origin of this trend in Ca-carbonates is subject to much debate. A diagenetic influence on siderite $\delta^{18}O$ may explain this observation (Heimann et al., 2010; further discussion below), as most siderite samples—particularly those older than the Animikie Group—plot below the lower limit for permissible seawater $\delta^{18}O$ (**Figure 3**).

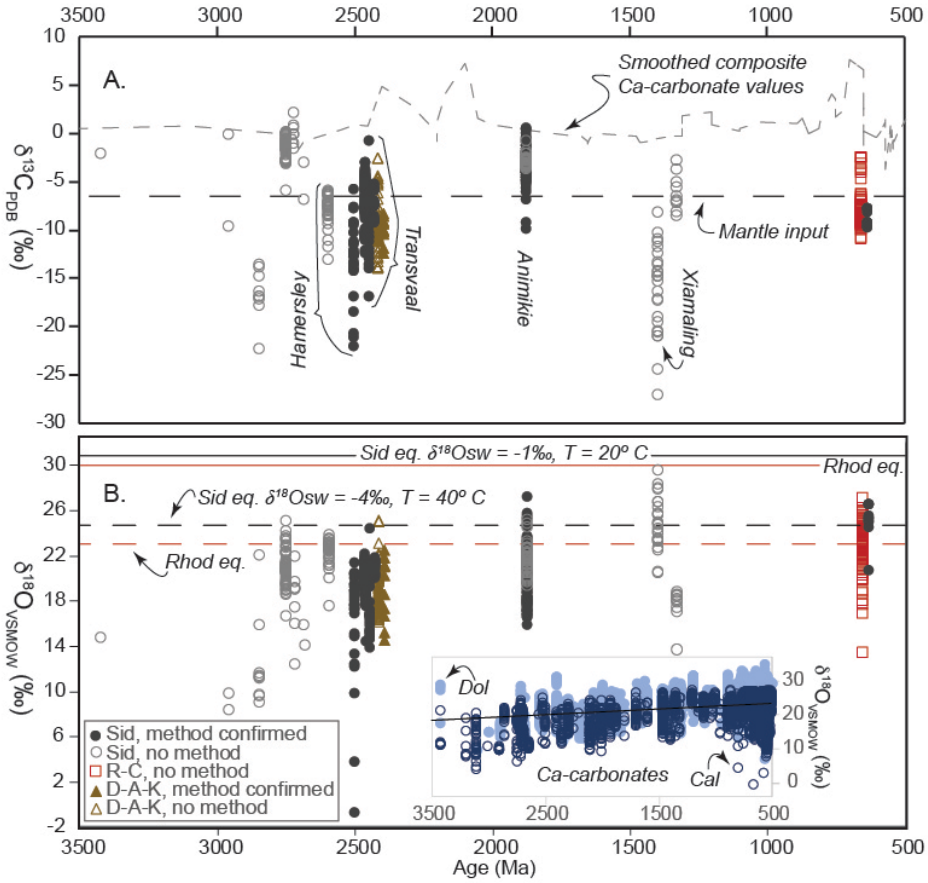

Figure 3. Database of Precambrian Fe- and Mn-carbonate $\delta^{13}C$ and $\delta^{18}O$ (Supplementary Information), including siderites (Sid), rhodochrosites (Rhod), and Mn-enriched dolomites (D), ankerites (A), and kunohorite (K). **A**. Plot of sample carbonate $d^{13}C_{VPDB}$ versus age (sample geochronology updated following Bekker et al. (2014), where possible. Closed symbols are

738 samples where an analysis method is confirmed; open symbols indicate samples where the
739 analysis method could not be fully validated. Light-gray dashed line of smoothed values from
740 Ca-carbonates (dolostones and limestones; Shields and Veizer, 2002) is shown for reference.
741 The darker, straight dashed line is the presumed $d^{13}C$ value of mantle input (Shanks III, 2001).
742 Sample groups from major IF basins are highlighted. Note that, regardless of analytical method,
743 a large population of samples fall within a range of $\delta^{13}C$ that lies between Ca-carbonate values
744 and mantle input. **B**. Plot of sample Fe- and Mn-carbonate $\delta^{18}O_{VSMOW}$ versus age as in **A**.
745 Horizontal lines show $d^{18}O$ equilibrium values between Fe/Mn-carbonates and a range of
746 seawater compositions. The top solid line shows $\delta^{18}O$ equilibrium between siderite (Sid) and
747 seawater at 20° C and -1 ‰ (an ice-free ocean value; Muehlenbachs, 1998) using the
748 fractionation factor of Zhang et al. (2001); the red solid line below shows the equilibrium value
749 of rhodochrosite (Rhod) under the same conditions using the fractionation factor of Kim et al.
750 (2009). Utilizing these same fractionation factors, the black dashed line marks $\delta^{18}O$ equilibrium
751 between siderite and seawater at 40° C and -4 ‰, representing an upper limit on estimates of a
752 more depleted ancient marine $\delta^{18}O$ reservoir (e.g. Galili et al., 2019); the red dashed line below
753 represents rhodochrosite $\delta^{18}O$ equilibrium under these same conditions. An inset shows the
754 trend of Ca-carbonate $\delta^{18}O$ over the same time interval, with calcite (Cal) in open circles and
755 dolomite (Dol) in closed circles (data from Shields and Veizer, 2002). Fewer samples plot within
756 a range of reasonable seawater values, though there is considerable disagreement regarding
757 interpretation of past seawater $\delta^{18}O$. While Fe- and Mn-carbonates follow the same general
758 trend of decreasing $\delta^{18}O$ with increasing age, the impact of analytical method potentially

759 manifests more prominently in $\delta^{18}O$ records, with an up to 2 ‰ increase in samples without
760 phosphoric acid fractionation correction (Rosenbaum and Sheppard, 1986).
761
762 Siderite is virtually unknown in Neoproterozoic iron formations (Cox et al., 2013), which
763 differ with earlier Precambrian (particularly Superior-type) IFs in other important aspects
764 including deposition in predominantly rift basin environments and a lack of silica-enriched
765 phases (Bekker et al., 2014). But Hiatt et al. (2020) recently documented siderite varves from
766 the Cryogenian (Neoproterozoic, ~635 Ma) Jacadigo Basin of Brazil. A small $\delta^{13}C$ dataset
767 presents relatively high $\delta^{18}O$ values for Precambrian siderites (**Figure 2**), which may reflect a
768 direct influence of seawater, or an initial genesis in cold water followed by later diagenetic
769 lowering of $\delta^{18}O$.
770 There remain considerable challenges in the interpretation of $\delta^{13}C$ and especially $\delta^{18}O$
771 of siderite. Perhaps chief among these is the persistent debate and uncertainty regarding the
772 $\delta^{18}O$ of seawater (Galili et al., 2019; e.g. Jaffrés et al., 2007; Johnson and Wing, 2020).
773 Furthermore, IF siderite frequently co-occurs with chert, and it has long been recognized that
774 quartz and carbonate $\delta^{18}O$ can equilibrate during diagenesis (Becker and Clayton, 1976), though
775 equilibrium between chert-siderite $\delta^{18}O$ in the Gunflint Formation has also been interpreted as
776 evidence of precipitation from a common water mass (Winter and Knauth, 1992). Siderite
777 stable isotope analysis also requires an extended reaction time (up to 48 h), correction for ^{18}O-
778 phosphoric acid fractionation (Rosenbaum and Sheppard, 1986), and careful assessment of
779 potential impact of organic carbon contamination in sample processing (Lebeau et al., 2014;
780 Oehlerich et al., 2013). Unfortunately, many recent studies did not fully document if these

781 methods were followed in their studies. While the ^{18}O correction for siderite acid digestion is a
782 relatively straightforward ~2‰ depletion, the impact of partial reaction on both $\delta^{13}C$ and $\delta^{18}O$
783 is a potentially greater unknown. It is imperative that future work on siderite $\delta^{13}C$ and $\delta^{18}O$
784 hews more closely to established methods to reduce these uncertainties, consistent with
785 broader community efforts to improve quality control in proxy studies (Planavsky et al., 2020).
786 Recent validation of a new open-vessel method for siderite digestion will significantly aid in
787 these efforts (Fernandez et al., 2016).

788 *In situ* isotopic analysis offers a potential to re-evaluate the relationship discussed
789 above, which is entirely based on analysis of bulk samples using IRMS techniques. In particular,
790 the associations between carbonate textures and isotopic signatures described in earlier
791 literature (Carrigan and Cameron, 1991; Winter and Knauth, 1992) suggest that some well-
792 preserved samples may have the potential to archive the composition of the earliest diagenetic
793 fluids impacting the sediments, if not seawater itself. The potential for isotopic fractionation
794 between siderite and precursor phases such as chukanovite (Jiang and Tosca, 2019) or green
795 rust (Halevy et al., 2017; Vuillemin et al., 2019b) also has yet to be addressed by experiments.

796 Other arguments against direct precipitation of siderite from the water column come
797 from experiments. Jiang and Tosca (2019) argue that as supersaturation is required to form iron
798 carbonates, the pCO_2 values may be possible only where DIC-rich hydrothermal fluids are
799 emitted (i.e. Bahrig, 1988). Such a suggestion has been made for BIF-associated siderites in the
800 Mesoproterozoic Jingtieshan BIF (Yang et al., 2018). Jiang and Tosca (2019) also argue that
801 direct siderite precipitation from seawater is in competition with iron silicate precipitation.
802 Direct precipitation from a water column is also difficult to reconcile with the slower kinetics of

803 siderite precipitation and higher saturation states required as compared to calcite (Jiang and
804 Tosca, 2020; Jimenez-Lopez and Romanek, 2004). However, most of these scenarios assume a
805 homogenous precipitation of siderite at supersaturation, which may be unrealistic in a natural
806 setting. Siderite nucleation on a pre-existing surface, perhaps on the seafloor (e.g.
807 heterogeneous precipitation; Jiang and Tosca, 2019) might lower the thermodynamic barriers
808 to direct precipitation, but such scenarios have yet to be fully explored in experiments, though
809 a recent study including calcite-siderite transformation demonstrates the promise of this
810 approach (Lin et al., 2020). It is also important to note that while experimental data clearly
811 demonstrate slow growth rates for inorganic siderite, they also show that in contrast to
812 dolomite (e.g. Land, 1998), low temperature siderite precipitation is feasible on scales that are
813 geologically reasonable, for example, an extended period (weeks to months) of crystal growth
814 in an undisturbed seafloor environment with chemically favorable conditions. Another
815 consideration is that iron carbonate precipitated experimentally under conditions that simulate
816 past oceans is generally ferrous hydroxy carbonate, not siderite (Gäb et al., 2017). Additional
817 laboratory experiments replicating such environments – including various nucleation centers
818 and communities of microbes – may help clarify these relationships.
819 Siderite can also be produced from thermal reduction of Fe^{3+} (oxyhydr)oxides with
820 organic carbon under low-grade metamorphic temperatures of 170°C and pressures of 1.2 kbar
821 (Köhler et al., 2013; Posth et al., 2013a). This process did not go to completion when microbial
822 biomass and biominerals were used (Halama et al., 2016), suggesting that the reactivity of
823 organic carbon and/or of Fe^{3+} (oxyhydr)oxides precursors is important to its preservation. It has
824 also been suggested based on similar experiments that siderite texture is related to the iron to

organic carbon ratio, with higher ratios favoring the development of spheroidal to rhombohedral siderite, and lower ratios favoring massive siderite (Köhler et al., 2013).

Iron isotopes recorded by the iron minerals under discussion have been suggested to track the redox state of the ocean through time, by recording trends in seawater $\delta^{56}Fe$ through time. One of the most abundant iron-bearing minerals forming in diverse sediments through time is pyrite (FeS_2). The $\delta^{56}Fe$ composition of pyrites shifted from predominantly negative prior to 2.3 Ga, to mostly <-0.5 ‰ and predominantly positive afterward (Busigny et al., 2014; Rouxel et al., 2005). Negative $\delta^{56}Fe$ has been interpreted to reflect partial oxidation of dissolved iron in an anoxic ocean, with heavy iron preferentially going into Fe^{3+} (oxyhydr)oxides (preserved as magnetite, hematite), while residual light aqueous Fe^{2+} was precipitated as pyrite (Eroglu et al., 2018; Rouxel et al., 2005). Subsequent diagenetic reduction of Fe^{3+} (oxyhydr)oxides has also been proposed as a source of negative $\delta^{56}Fe$, as microbes preferentially reduce light iron from Fe^{3+} (oxyhydr)oxides (Heimann et al., 2010; Johnson et al., 2008b). This mechanism requires partial reduction in order to record negative $\delta^{56}Fe$ in sedimentary minerals, and that 90 % of all sedimentary iron was recycled by Fe^{3+} reduction to produce negative $\delta^{56}Fe$ in the seawater reservoir.

Key biogeochemical processes in ferruginous oceans

The persistence of ferruginous conditions in the ocean throughout the Precambrian necessitates an understanding of how life, specifically microbial life, interacted with iron. Fundamental to this is determining the amount of oxygen in the environment, as it controls whether the microbial community was aerobic or anaerobic. Geochemical inferences from the

847 rock record presently suggest that oxygen in the atmosphere passed a threshold of 10^{-5} present
848 atmospheric level (PAL; currently about 20 %) at 2.33 Ga (Luo et al., 2016). Proterozoic
849 estimates range from 0.1 to 1 % PAL (Cole et al., 2016; Planavsky et al., 2014b), up to 10 % PAL
850 (Crockford et al., 2018; Zhang et al., 2016), while still others have estimated oxygen contents
851 much closer to modern (Blamey et al., 2016; Large et al., 2019; Steadman et al., 2020).
852 Numerous studies document at least low amounts of oxygen in the surface ocean beginning in
853 the Archean (Anbar et al., 2007; Czaja et al., 2012; Kendall et al., 2010; Planavsky et al., 2014a)
854 and throughout the Proterozoic (sec. 2). This topic has also been reviewed recently (Catling and
855 Zahnle, 2020; Lyons et al., 2014).

856 A major question in understanding the redox evolution of Earth's ocean and atmosphere
857 through time is in determining how oxygen built up in the atmospheric reservoir despite the
858 existence of oxygen sinks (Kasting, 2013). Considerations include 1) how productive the
859 biosphere was; and 2) the efficiency of carbon burial and preservation. Primary productivity,
860 when carried out by oxygenic photosynthetic organisms, offers a primary control on oxygen
861 production, and in turn an oxidant for Fe^{2+}, H_2, sulfur, and CH_4 that kept the oceans and
862 atmosphere reducing. However, burial of organic carbon isolates a photosynthetically produced
863 reductant from oxidation by oxygen, which over time allows for the reservoir of atmospheric
864 oxygen to build up. Both of these are necessary components to the oxidation of the oceans and
865 atmosphere through time, and ultimately, the disappearance of ferruginous oceans.

866 Global productivity is widely assumed to have been lower in the Proterozoic oceans
867 (Anbar and Knoll, 2002). A coupled atmospheric-ecosystem modeling study indicated 40x lower
868 marine primary productivity in the Archean as compared to modern oceans, when considering

869 a biosphere unable to perform oxygenic photosynthesis (Kharecha et al., 2005). However, direct
870 evidence in the form of either the gross amount primary productivity (GPP) by the early
871 biosphere is difficult to discern, as sediments record indicators of net productivity (NPP) after
872 water column and diagenetic processing. Triple oxygen isotope measurements of terrestrial
873 evaporitic sulfate deposits have been employed as a proxy for GPP, as they directly sample the
874 ratio of stratospheric to tropospheric oxygen produced by oxygenic photosynthesis (Crockford
875 et al., 2018). These results indicate that GPP was likely lower in the Proterozoic, between 6-41
876 % of modern pre-anthropogenic levels.
877 Innovations in evolution notwithstanding, how might have the chemical conditions
878 within ferruginous oceans have regulated primary productivity to these lower levels? Johnston
879 et al. (2009) suggested that the predominance of anoxygenic photosynthesis in the Proterozoic
880 ocean decoupled organic carbon production from oxygen production. Importantly, this model
881 relies on hydrogen sulfide as a readily available electron donor in the photic zone throughout
882 the Proterozoic oceans. Although many studies document euxinic conditions in the water
883 column (Sperling et al., 2014), these tend to be spatially limited, sometimes in restricted
884 settings, with the deeper ocean and open ocean settings still dominated by ferruginous
885 conditions (Doyle et al., 2018). Ferruginous conditions may have persisted in much of the
886 oceans, despite a buildup of sulfate that could have fueled development of water column
887 euxinia. Organic carbon burial may have also been insufficient to drive complete sulfate
888 reduction in many ocean regions (Johnston et al., 2010). Primary productivity in predominately
889 ferruginous oceans could have also relied on Fe^{2+}-dependent anoxygenic photosynthesis

890 ("photoferrotrophy"), which produces organic carbon in a molar ratio of 1:4 to iron oxidized,
891 according to the stoichiometry below:
892 $HCO_3^- + 4Fe^{2+} + 10H_2O + light\ (h\nu) = CH_2O + 4Fe(OH)_3 + 7H^+$ (eq. 1)
893 This limited amount of organic carbon production, tied to the availability of iron, could have
894 placed an upper limit on primary production (Konhauser et al., 2005). For instance Canfield
895 (2005) estimated rates of primary production by photoferrotrophs in such a scenario that were
896 7-22 x lower than modern marine primary production. Phosphate (P) limitation in the
897 Precambrian (discussed below) may have also favored photoferrotrophs, as a greater Fe:P ratio
898 is required by photoferrotrophs as compared to cyanobacteria, which do not require as much
899 iron (Jones et al., 2015).
900 Further controls on primary productivity in light of evidence for oxygenic photosynthesis
901 well before the GOE often center around the role of nutrient limitation, particularly nitrogen
902 (N) and phosphorus (P). One idea is that ammonium (NH_4^+) in the oceans would not have been
903 consumed by oxygen-dependent ammonium oxidation and/or subsequent denitrification prior
904 to the appearance of oxygen in the marine system (Fennel et al., 2005). Such a pathway
905 accounts for fixed nitrogen loss in deoxygenated regions of the modern oceans, which limit
906 subsequent primary productivity (Codispoti and Christensen, 1985). The anaerobic ammonium
907 oxidation (anammox) process, whereby ammonium is oxidized by bacteria using nitrite (NO_2^-)
908 as an electron donor, is also responsible for fixed nitrogen loss in OMZ regions of the ocean
909 today (Dalsgaard et al., 2012), but importantly still requires an oxidant (nitrite) formed through
910 oxygen-requiring nitrification. Oxygenic photosynthesis could have therefore produced a

911 negative feedback on nitrogen availability, as oxygen's appearance spurred the development of
912 an aerobic cycle that led to marine fixed nitrogen loss.
913 Negative $\delta^{15}N$ in organic carbon from anoxic Archean environments has been
914 interpreted as reflecting incomplete uptake of non-limiting ammonium (Yang et al., 2019),
915 suggestive that nitrogen may not have always been a limiting nutrient for primary productivity.
916 Phylogenetic inferences point to a mid-Proterozoic acquisition of genes encoding for the N_2-
917 fixing nitrogenase enzyme (Boyd et al., 2011), which would have allowed fixed nitrogen
918 production. Yet near zero $\delta^{15}N$ from 3.2 Ga rocks are difficult to explain by abiotic processes,
919 indicating that biological N_2 fixation could be a much older process (Stüeken et al., 2015).
920 Similar findings support active N_2 fixation in ~2.9 Ga Pongola Supergroup (Ossa Ossa et al.,
921 2019). Others have used similar isotopic arguments to advocate for the appearance of N_2
922 fixation during the GOE (Luo et al., 2018). This may be copacetic with rising availability of Mo in
923 Proterozoic oceans due to enhanced oxidative weathering (Scott et al., 2008). Molybdenum is
924 required for efficient nitrogenase activity in Cyanobacteria (Glass et al., 2009; Zerkle et al.,
925 2006). Negative $\delta^{15}N$ in 1.88 Ga sediments from the Animikie basin point to active N_2 fixation,
926 and non-limiting fixed nitrogen to fuel primary productivity associated with the development of
927 euxinic mid-depth waters, which can scavenge Mo to sediments, but apparently did not exhaust
928 the Mo supply for N_2 fixation in the Animikie basin (Godfrey et al., 2013).
929 Phosphate availability has been put forward as a regulator of early marine primary
930 productivity. Scavenging of phosphate through adsorption on variably charged Fe^{3+}
931 (oxyhdr)oxides was suggested as a mechanism for phosphate limitation given evidence for
932 deposition of mixed-valent iron minerals to IF (Bjerrum and Canfield, 2002). Subsequent work

933 cast doubt on this scenario given that dissolved silica higher before the Phanerozoic origin of
934 silicifying organisms. Silica co-precipitation with Fe^{3+} (oxyhydr)oxides limits the amount of
935 phosphate adsorption to Fe^{3+} (oxyhdr)oxides (Konhauser et al., 2007). Experimentally
936 determined adsorption constants measured in the presence of silica were used to determine
937 the Archean seawater phosphate recorded by IF, estimated at 5.25 ± 2.63 µM (Konhauser et al.,
938 2007). Subsequent experiments in a more realistic seawater matrix revised these estimates
939 downward, to between 0.04 to 0.13 µM (Jones et al., 2015). The significance of Fe^{3+}
940 (oxyhdr)oxides phosphate scavenging pathway likely depends on the extent to which Fe^{3+}
941 (oxyhdr)oxides in IF are primary (sec. 2).
942 A temporal record of marine phosphate concentrations has been assembled via
943 phosphorus abundances in IF (Planavsky et al., 2010) and in shales (Reinhard et al., 2016). Both
944 records indicate increasing phosphate burial beginning in the Neoproterozoic, echoing the
945 consensus of phosphate-limited primary productivity through the Archean and much of the
946 Proterozoic. Phosphate limitation in the mid-Proterozoic has been argued to have throttled the
947 rise of atmospheric oxygen at this time (Derry, 2015). The Proterozoic marine phosphate
948 reservoir is proposed to have been buffered by precipitation the mineral vivianite
949 ($Fe_3(PO_4)_2 \cdot 8H_2O$ or an Fe^{3+}-phosphate (Derry, 2015; Reinhard et al., 2016), but green rust has
950 also been suggested (Halevy et al., 2017). This model predicts that vivianite or other phosphate-
951 bearing phases should be deposited in sediments from that time, although the ultimate
952 preservation potential of such minerals is not clear. Vivianite is not often reported in
953 Precambrian marine sediments, but does form in recent marine sediments below the sulfate-
954 methane transition zone (Liu et al., 2018), and at sites of high organic carbon deposition

(Dijkstra et al., 2016). It has also been detected in some ferruginous and euxinic lake sediments (Cosmidis et al., 2014; Vuillemin et al., 2019a; Xiong et al., 2019).

More intense ultraviolet (UV) radiation in the upper 30 m of the ocean has been discussed as having inhibited primary productivity in the Archean, due to a lack of ozone (Cockell, 2000). Radiation exposure has been proposed to have been mitigated by mineral sunscreens, notably Fe^{3+} (oxyhdr)oxides and/or silica (Bishop et al., 2006). Gauger et al. (2015) noted that photoferrotrophs have the advantage of producing their own iron-based mineral sunscreen in the course of anoxygenic photosynthesis. However, Fe^{3+}(oxyhdr)oxides-silica co-precipitates did not seem to confer much protection on cyanobacteria, suggesting they might have been more susceptible to the higher UV exposure on early Earth (Mloszewska et al., 2018). Yet another source of toxicity to cyanobacteria could be Fe^{2+} itself. Reactive oxygen species (ROS) likely mediate toxicity if Fe^{2+} is fluxing into a zone of oxygen production, such as when ferruginous deep water upwelled to deposit IF (Swanner et al., 2015a).

The $\delta^{13}C$ of marine carbonates provides some constraint on changes in the global carbon cycle through time. The $\delta^{13}C_{carb}$ records marine $\delta^{13}C_{DIC}$ with <1‰ offset (Zeebe and Wolf-Gladrow, 2001). The fractionation factor (Δ_c) is the difference between $\delta^{13}C_{carb}$ and $\delta^{13}C_{org}$ during carbon fixation. Changes in the fraction of organic carbon (f_{org}) removed from Earth's surface environment may reflect changes in the total amount of primary productivity, oxygen produced, and overall productivity of the biosphere via the following mass balance (Havig et al., 2017):

$$\delta^{13}C_{carb} = \delta^{13}C_{mantle} + f_{org}(\Delta_c) \quad \text{(eq. 2)}$$

A decrease in Δ_c between in the $\delta^{13}C_{carb}$ and $\delta^{13}C_{org}$ in marine sedimentary records throughout the Proterozoic has been taken as an indication of increasing carbon burial through time, with this interpreted as a cause of the rise of oxygen through time (Des Marais et al., 1992). Examination of such a mass balance and the $\delta^{13}C_{carb}$ and $\delta^{13}C_{org}$ records have also been used to argue for shifts from dominantly chemical to biochemical carbonate precipitation in the Proterozoic (Bartley and Kah, 2004). Elaboration of this mass balance into models that incorporate feedbacks from weathering, volcanism and atmospheric processes inform where these additional feedbacks exert influence (Kump and Arthur, 1999). More nuanced approaches also consider that variations in these isotopic records can be caused by dominance of different microbial metabolisms (e.g. Havig et al., 2017). For instance, elevated $\delta^{13}C_{carb}$ have also been interpreted as evidence for active methanogenesis (Hayes and Waldbauer, 2006).

Methane likely contributed to carbon cycling in ancient ferruginous environments, but the proportion of the carbon cycle conducted via methane is subject to debate. Complicating the matter is the fact that there is no direct proxy for the presence of methane on early Earth because dissolved or gaseous methane escapes the location where it forms. However, methane is unique among carbon compounds in having extremely light $\delta^{13}C$. When biologically formed, methane is often 40 ‰ or more lighter than the starting carbon substrate (Whiticar, 1999). Therefore, many studies invoke methane cycling in depositional environments where 1) $\delta^{13}C$ of organic carbon is extremely isotopically depleted (e.g. biomass from organisms who consumed methane); or 2) where extremely light $\delta^{13}C_{DIC}$ was generated by oxidation of methane, which was then incorporated into carbonate minerals.

997 Genomic data and isotopic records are consistent with methanogens representing an
998 early appearing microbial lineage (Schopf et al., 2018; Ueno et al., 2006; Wolfe and Fournier,
999 2018). The role of methane as an important greenhouse gas in the Precambrian atmosphere is
1000 widely discussed (Catling and Claire, 2005; Claire et al., 2006; Feulner, 2012). Methanogenesis
1001 has been interpreted to be a major pathway for degradation of organic carbon produced by
1002 primary productivity within anoxic oceans (Canfield et al., 2006; Goldblatt et al., 2006; Kharecha
1003 et al., 2005; Ozaki et al., 2018; Pavlov et al., 2003), although others have suggested a more
1004 muted role (Laakso and Schrag, 2019).
1005 Hayes (1994) highlighted a global negative excursion of kerogen $\delta^{13}C$ to its lowest values
1006 in the geologic record (-60 ‰) and attributed it to methanotrophy, microbial oxidation of
1007 methane. Aerobic methanotrophy at an oxycline has also been invoked to explain depleted $\delta^{13}C$
1008 in organic carbon near the GOE (Bekker and Kaufman, 2007). Hinrichs (2002) noted that such a
1009 signal could be consistent with either aerobic or anaerobic methanotrophy. Following from this
1010 was the suggestion that the early methane cycle may have been regulated primarily by
1011 anaerobic oxidation of methane (AOM) coupled to sulfate (Stüeken et al., 2017), potentially
1012 representing a major CH_4 sink over geologic time (Olson et al., 2013). Others have also invoked
1013 AOM utilizing alternative electron acceptors, such as Fe^{3+} (oxyhydr)oxides (Lepot et al., 2019).
1014 Methanotrophy seems to have been common in the Neoarchean, particularly within closed-
1015 basin environments (Flannery et al., 2016). Others have argued against a vigorous methane
1016 cycle to explain depleted $\delta^{13}C$ in kerogen. Slotznick and Fischer (2016) suggested on the basis of
1017 carbonate $\delta^{13}C$ and a geochemical model, that acetogenesis using the acetyl-CoA metabolisms
1018 could have been responsible for the Archean kerogen excursion. This model permits the genesis

1019 of $\delta^{13}C$-depleted kerogens without necessitating precursor photosynthetic biomass (e.g. Lepot
1020 et al., 2019) or methanotrophy.

1021 Finally, a highly localized influence of methanogenesis and methanotrophy on marine
1022 DIC and carbonate $\delta^{13}C$, such as within a redox-stratified basin, has been postulated as late as
1023 the Ediacaran (Ader et al., 2009). It has also been argued that carbonate carbon signatures of
1024 methanotrophy would have been muted by higher DIC concentrations, particularly in the
1025 Archean (Slotznick and Fischer, 2016). Although these examples demonstrate that there is
1026 much interest in exploring the methane cycle of early Earth, few studies can explicitly link the
1027 putative influence of methane to redox proxies. Thus, an opportunity exists to explore signals of
1028 methanogenesis in ancient environments.

1029 Direct fossil evidence of bacteria, particularly those involved in iron cycling in
1030 ferruginous settings is rare from early Precambrian rocks. Evidence for Fe^{2+}-oxidizing bacteria
1031 has been put forward based on microfossils reminiscent of modern, aerobic Fe^{2+}-oxidizing
1032 bacteria such as *Gallionella* sp. who make organic twisted stalks that become coated with iron
1033 minerals (Chan et al., 2004), or *Leptothrix* sp. who make long, mineralized organic sheaths
1034 (Kunoh et al., 2017). Similar "Gunflint" microfossils have been found worldwide in ca. 1.8 Ga
1035 iron formations and carbonates (Barghoorn and Tyler, 1965; Cloud, 1965; Papineau et al., 2017;
1036 Planavsky et al., 2009; Wilson et al., 2010). The temporal restriction of these microfossils has
1037 been suggested to arise from a limited period of time for an interface between deep
1038 ferruginous and shallow oxic oceans (Knoll, 2003). With our increased understanding that a
1039 ferruginous to oxic interface existed in the oceans through much of the Precambrian (sec. 2),
1040 temporally-limited chemical conditions are unlikely to explain the limited occurrence of

1041 Gunflint-type microfossils. The bias is unlikely to be preservational, as experimental work
1042 suggests some organic and iron-mineralized structures from Fe^{2+}-oxidizing bacteria can be
1043 preserved up to 250°C and 140 MPa (Picard et al., 2015). Furthermore, documentation of
1044 intracellular iron minerals by some thick-walled taxa has led to the suggestion that at least
1045 some of these Gunflint-style microorganisms may rather be cyanobacteria, as intracellular
1046 mineralization is unlikely for aerobic Fe^{2+}-oxidizing bacteria (Lepot et al., 2017).
1047 Nitrifying organisms and denitrifying organisms likely originated after the introduction
1048 of oxygen into the environment, which was needed to fuel an aerobic nitrogen cycle, as
1049 discussed above. Evidence for oxidative nitrogen cycling by the time of the GOE comes from the
1050 heavier $\delta^{15}N$ in organic carbon by this time, produced when the lighter $\delta^{15}N$ in ammonium are
1051 preferentially nitrified and lost from the ocean as N_2, enriching the nitrogen source for biomass
1052 (Beaumont and Robert, 1999; Kipp et al., 2018; Luo et al., 2018; Zerkle et al., 2017). An increase
1053 in the $\delta^{15}N$ composition of kerogen in late Archean shales deposited from ferruginous water
1054 has therefore been interpreted for the onset of oxidative nitrogen cycling due in overlying
1055 waters (Godfrey and Falkowski, 2009). Busigny et al. (2013) suggested that elevated $\delta^{15}N$ in
1056 shales and BIF from the Hamersley Basin, encompassing anoxic oceans to redox-stratified
1057 oceans with oxygen in surface waters, could also involve uptake of ammonium and a
1058 completely anaerobic nitrogen cycle. In the mid-Proterozoic, aerobic nitrogen cycling in
1059 shallower water above a deeper ferruginous ocean may have led to nitrogen loss that favored
1060 N_2-fixing Cyanobacteria over other eukaryotes (Stüeken, 2013). Another consequence of the
1061 onset of aerobic nitrogen cycling, especially in stratified ferruginous oceans, is that abiotic
1062 reaction of nitrite, an intermediate in denitrification, with Fe^{2+} could have produced the

greenhouse gas nitrous oxide (N_2O), which could have been part of the solution of the Proterozoic Faint Young Sun paradox (Stanton et al., 2018).

4. Past ferruginous lakes

Although much recent literature addressed biogeochemical processes occurring in ancient ferruginous oceans (sec. 3), or on modern processes occurring in lakes that are presently ferruginous and meromictic (sec. 6), opportunity also exists to investigate the sediment records of past ferruginous lakes. These "paleoferruginous" lakes can either be no longer ferruginous, or no longer extant lake systems. Sediment records of paleoferruginous lakes as old as the Mesoproterozoic have been identified (Cumming et al., 2013; Slotznick et al., 2018). However, variability in the pH of lacustrine systems (Stüeken et al., 2019) as well as high rates of clastic sedimentation (Lyons and Severmann, 2006) may be complicating factors in interpreting the redox records of ancient lakes.

Younger lacustrine sediments offer the opportunity to clarify the relationships between redox proxies and environmental conditions. Recent work on long sediment records from Lake Towuti, Indonesia, has provided insights into the relationships between porewater chemistry, microbial activity, and diagenetic iron mineral genesis (Vuillemin et al., 2019b, 2019a, 2018). Although water monitoring data are limited, modern Lake Towuti appears to maintain redox stratification but with relatively low and seasonally-variable concentrations of dissolved Fe (max. ~2.5 µM; Costa et al., 2015). The ferruginous nature of the Lake Towuti sediment record appears to reflect allochthonous iron inputs from lateritic soils and ultramafic rocks of its watershed (Costa et al., 2015; Hasberg et al., 2019). Such a system provides a further

1085 opportunity to assess the relationships between ultramafic rock weathering and lacustrine
1086 depositional processes and make Lake Towuti particularly valuable to studies of lacustrine
1087 deposition on Mars (e.g. Goudge et al., 2017).

1088 Other examples of paleoferruginous lake records are known primarily through
1089 paleoclimate investigations, but they are generally less well-known from a geobiological and
1090 geochemical context. Paleoferruginous lakes are particularly valuable in that they archive
1091 geochemical records of transitions from ferruginous to euxinic or oxic conditions (e.g. Felder
1092 and Gaupp, 2006)—mirroring changes experienced in Earth's ancient oceans (sec. 2)—but with
1093 minimal imprint of deep burial diagenesis or metamorphism. In the paragraphs that follow we
1094 will highlight the potential for additional work in paleoferruginous lakes using two examples.
1095 These include a small temperate lake which was ferruginous as recently as several hundred
1096 years ago, and a large tropical lake, which appears to have cycled in and out of ferruginous
1097 conditions repeatedly over the past ~140 Kyr. Otter Lake is a Pleistocene kettle lake located in
1098 southeast Michigan, USA, from which a Holocene sediment core containing sequences of Fe-
1099 and Mn-carbonate varves has been previously described (Wittkop et al., 2014). However, Otter
1100 Lake's surface sediments are not particularly iron-rich, and the lake does not appear to be
1101 ferruginous (or meromictic) today. Lake Malawi is a large tropical (12°S, 34.5°E) meromictic
1102 freshwater lake in the tectonically active Great Rift Valley of Africa (Katsev et al., 2017). A
1103 drilling campaign in 2005 recovered over 500 meters of core from two sites in Lake Malawi
1104 (Scholz et al., 2011a). In modern Lake Malawi water column sulfate levels are low (~15 µM),
1105 dissolved hydrogen sulfide is present at mid-water depths at low µM concentrations, and
1106 dissolved iron is a significant component of surface sediment porewaters (J. Li et al., 2018).

Geochemical and mineralogical records of Fe-deposition in paleoferruginous lakes

The application of iron speciation measurements (sec. 2) to lakes has not always yielded results that are consistent with the redox characteristics of the overlying water column (Rico and Sheldon, 2019; Slotznick et al., 2018; Stüeken et al., 2019). Using data from Lake Malawi and Otter Lake, we will argue that the presence of siderite in sediments enriched in bulk iron can be used as a reliable indicator of the presence of paleoferruginous conditions. Furthermore, bulk iron enrichment and the presence of siderite can be evaluated without the application of specialized techniques. As siderite is present in both Otter Lake and Lake Malawi sediments (Scholz et al., 2011b; Wittkop et al., 2014), the following discussion will explore these occurrences of siderite in the context of what is presently known about the sediment records of iron deposition in these lakes.

Otter Lake sediments are generally iron-rich and contain up to 20 wt% Fe-carbonates in discrete intervals within the late Holocene (<6 ka) sediments (Wittkop et al., 2014). Carbonates in Otter Lake sediments occur in mm-scale laminae, which radiocarbon dates and lamination counts confirm to be varves, seasonally deposited each year. The sediments are also enriched in organic carbon (up to 70 %). The carbonates are manganoan siderites as confirmed by quantitative X-ray diffraction (XRD) with sediment abundance of up to 19 % by weight, and appear to have precipitated in oxygen isotopic equilibrium with modern lake water with modified DIC (Wittkop et al., 2014). Clumped O-isotope analysis confirmed that the siderite precipitated in a cold environment on the lake floor or within sediments (van Dijk et al., 2019).

X-ray fluorescence (XRF) data (**Figure 4**) demonstrates that the sediments of Otter Lake are enriched in bulk iron (up to 60 % Fe_2O_3 on a carbon-free basis, or about 20 % Fe_2O_3 of bulk, where Fe_2O_3 is the total Fe measured by XRF), with siderite deposition occurring largely during intervals of high Fe_2O_3:SO_3. Manganese enrichments in Otter Lake sediments are also strongly—but not exclusively—linked to carbonate deposition. Perhaps most intriguingly, Otter Lake continued to deposit iron-enriched sediments for nearly 1,000 years after major siderite deposition ceased. Although the iron mineralogy of this section of the record could not be determined by XRD, a more sensitive analysis of Fe-mineralogy in the Otter Lake record may provide additional insights into the processes which drove a transition from ferruginous to the fully oxic conditions observed today, and whether or not the sediments record an intermediate phase of euxinic conditions. Although these questions will need to be addressed in future work, the existing evidence highlights the potential for future paleoredox work on the Otter Lake

record.

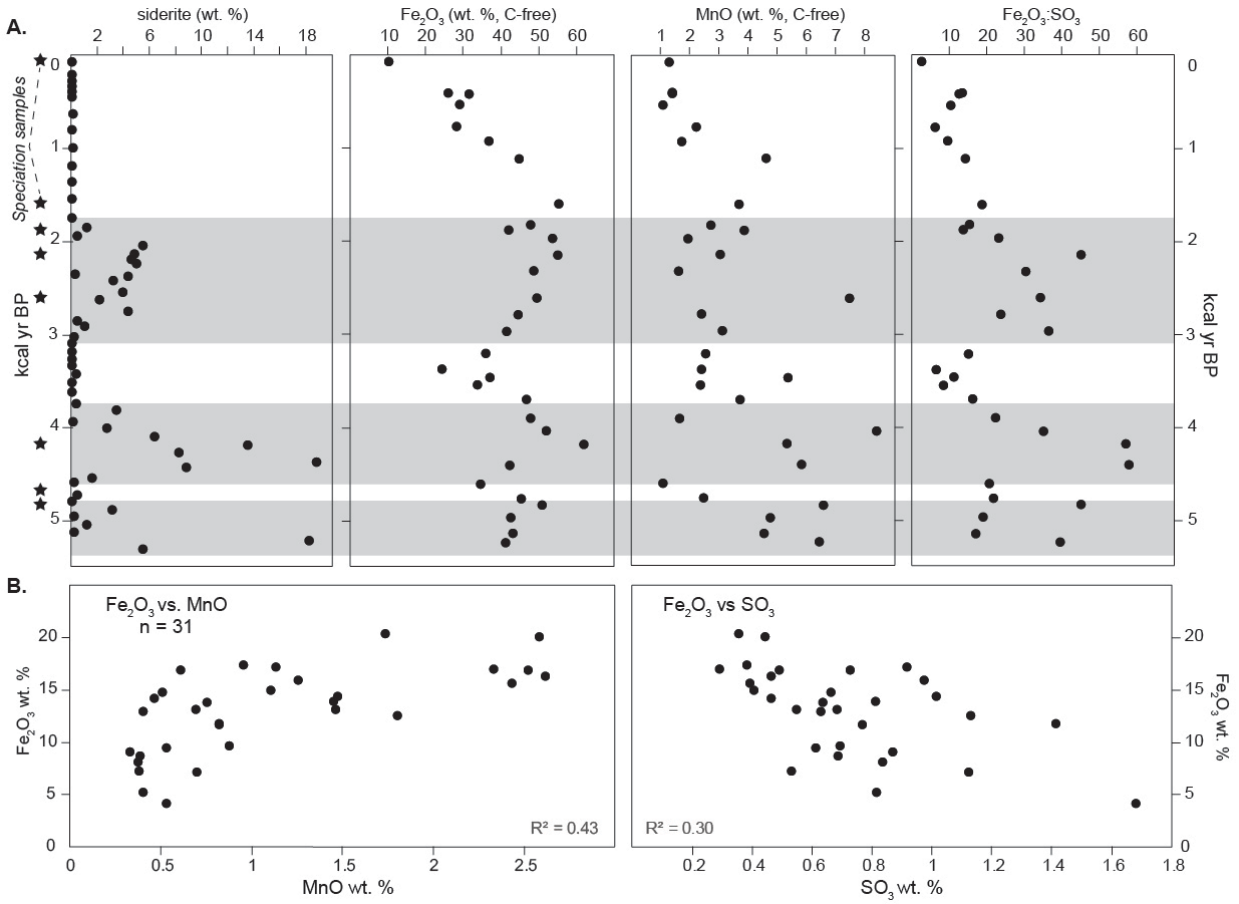

Figure 4. Geochemistry and mineralogy of the Otter Lake sediment core. **A**. Plots of siderite abundance (replotted from Wittkop et al., 2014), bulk sediment Fe_2O_3 (carbon-free basis, total Fe expressed as Fe_2O_3), MnO (carbon-free basis), and the ratio of Fe_2O_3 to SO_3 .Ferruginous conditions (grey bars) are indicated by enhanced siderite accumulation and high values of bulk sediment Fe_2O_3. Variables plotted versus sediment age in thousands of calendar years before present (kcal yr BP) using the age model from Wittkop et al., (2014). The speciation samples refer to samples in **Figure 9**. **B**. Cross plots of Otter Lake sample XRF showing relationships between Fe_2O_3 and MnO, and Fe_2O_3 and SO_3.

Lake Malawi also contains iron-enriched sediments and carbonates hosted in a starkly contrasting geological and hydroclimate environment. The long sediment cores from Lake Malawi were initially obtained to generate a high-resolution record of late Pleistocene tropical climate extending to 140,000 years before present (Brown, 2011; Johnson et al., 2011; Lane et al., 2013; Scholz et al., 2011a). Lake Malawi sediments range in lithology from finely laminated, organic rich (up to 8 % total organic carbon; TOC) muds to massive carbonate-rich muds and sands (Scholz et al., 2011a). Generally, laminated muds are thought to reflect lake highstands while massive carbonate rich intervals are thought to reflect lowstands associated with intense drought conditions. Scholz et al. (2011b) noted that siderite occurs in both nodular and laminated contexts in the Lake Malawi 1C core and is most notable in sediments aged 117-124 ka; they interpret the lack of calcite and presence of siderite to suggest a stratified water column capable of dissolving calcite.

Previously collected XRF core scans (method described by Brown, 2011) coupled with new XRD-XRF analysis of selected Lake Malawi samples provides a window into the paleoferruginous conditions recorded in the Lake Malawi cores (**Figure 5**). Intervals of enhanced iron deposition in Lake Malawi are inferred by semi-quantitative XRF scans of Fe/Ti (**Figure 5**), which demonstrate episodic spikes above a modal value of 52.3 for the combined long Lake Malawi record in the 1B and 1C cores (Scholz et al., 2011a). **Figure 5** also shows XRD spectra from two samples in Fe/Ti enriched zones in Lake Malawi core 1C, which confirm the presence of siderite, as well as quantitative XRF data demonstrating that these sediments are iron-enriched (Fe_2O_3 up to 41.8 wt. % on a carbon-free basis). Vivianite has also been detected (Scholz et al., 2011a). Cross plots of individual sample quantitative XRF demonstrate that iron

and Mn deposition are closely linked in Lake Malawi, and that the most iron-enriched Lake Malawi samples correspond to high sediment Fe_2O_3:SO_3.

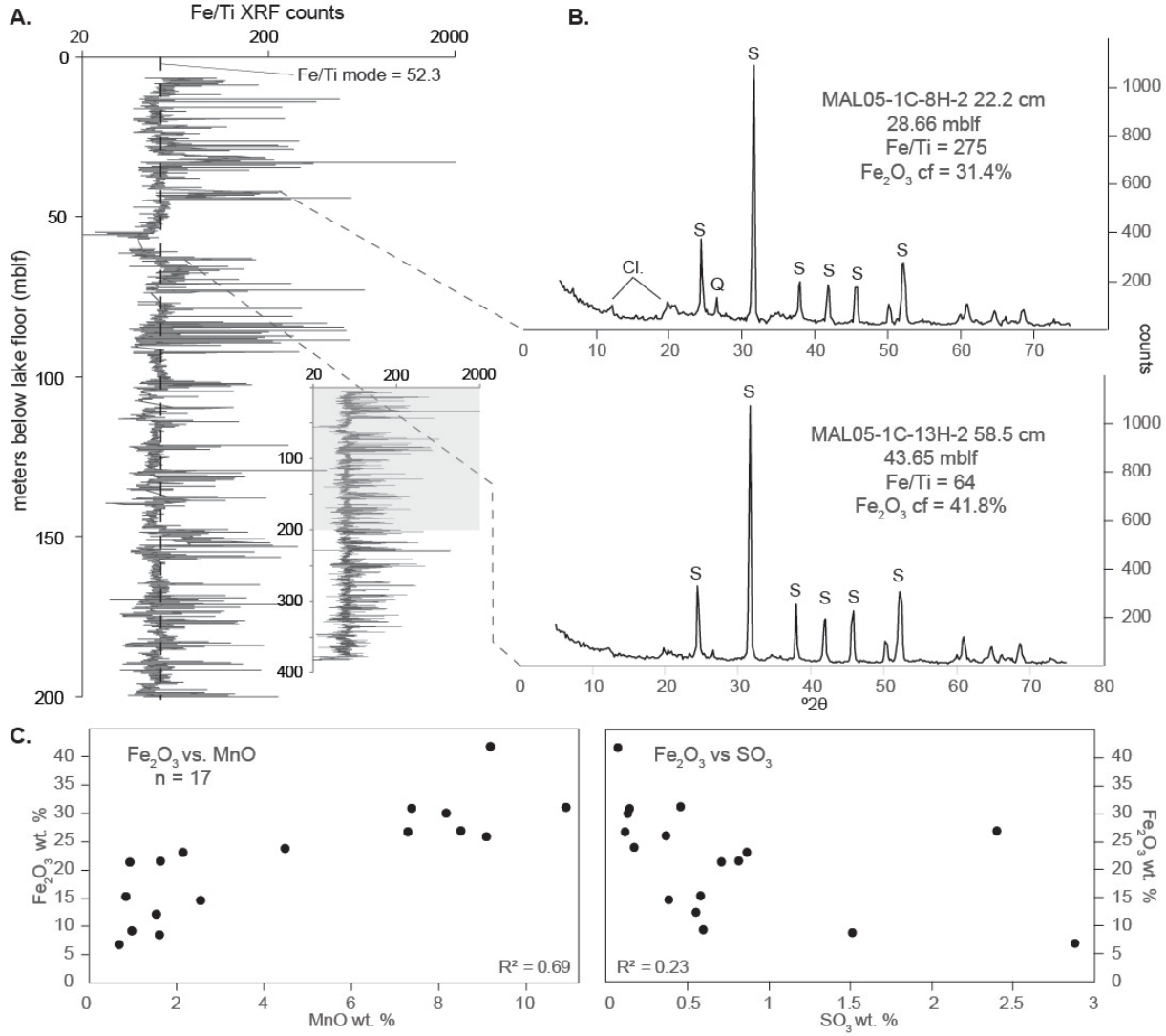

Figure 5. Geochemistry and mineralogy from the Lake Malawi drill cores collected in 2005 (Scholz et al., 2011a). **A**. Plot of core 1B and 1C XRF core scan Fe/Ti ratio, showing multiple cycles of excess Fe/Ti likely representing ferruginous conditions. **B**. Sediment XRD scans from samples in two separate intervals of excess Fe/Ti showing a dominance of siderite (S) relative to siliciclastics such as quartz (Q) or clay minerals (Cl.). Quantitative XRF from the same samples demonstrates Fe_2O_3-enriched sediments up to 42 % on a carbon-free basis (with sediment Fe

1182 expressed as Fe_2O_{3T}). **C**. Cross plots of individual sample XRF data showing strongly linked cycles
1183 of Fe_2O_3 and MnO deposition, and an antithetical relationship between sediment Fe_2O_3 and SO_3
1184 deposition.
1185
1186 Lake Malawi sediments appear to represent a particularly rich archive of dynamic redox
1187 cycling directly influenced by environmental changes. Mega-droughts are evident in the Malawi
1188 record, which influenced chemical cycling in the lake through changes in lake level, altering the
1189 carbonate compensation depth and the availability and transport of weathered materials from
1190 the watershed (Brown, 2011). Therefore, iron minerals in the Lake Malawi cores may represent
1191 a range of sources including detrital siderite from older continental sequences, diagenetic
1192 minerals precipitated during phases of organic-rich deposition, and water-column or lake floor
1193 precipitates formed through carbonate cycling in stratified waters.
1194
1195 *Lacustrine siderite petrography, microanalysis, and speciation*
1196 The presence of siderite in both Otter Lake and Lake Malawi offers an opportunity to
1197 compare differences and similarities in the examples that may provide insight into the
1198 occurrence of siderite in the rock record. Electron probe microanalysis (EPMA) maps of varved
1199 carbonate sediments from Otter Lake display a consistent manganoan component, together
1200 with trace amounts of calcium (Ca). These maps demonstrate that Ca, when present, is found in
1201 the crystal core, and is overgrown by a Mn-enriched zone, and that both are embedded in an
1202 Fe-enriched rim (**Figure 6**). Iron is most strongly concentrated in carbonate crystals, with lower
1203 concentrations within the amorphous sediment matrix; in contrast, Mn is concentrated more

strictly within carbonate crystals. Diffraction patterns from EPMA-analyzed intervals are most consistent with a phase in rhodochrosite-siderite solid solution, rather than kutnohorite (Wittkop et al., 2014).

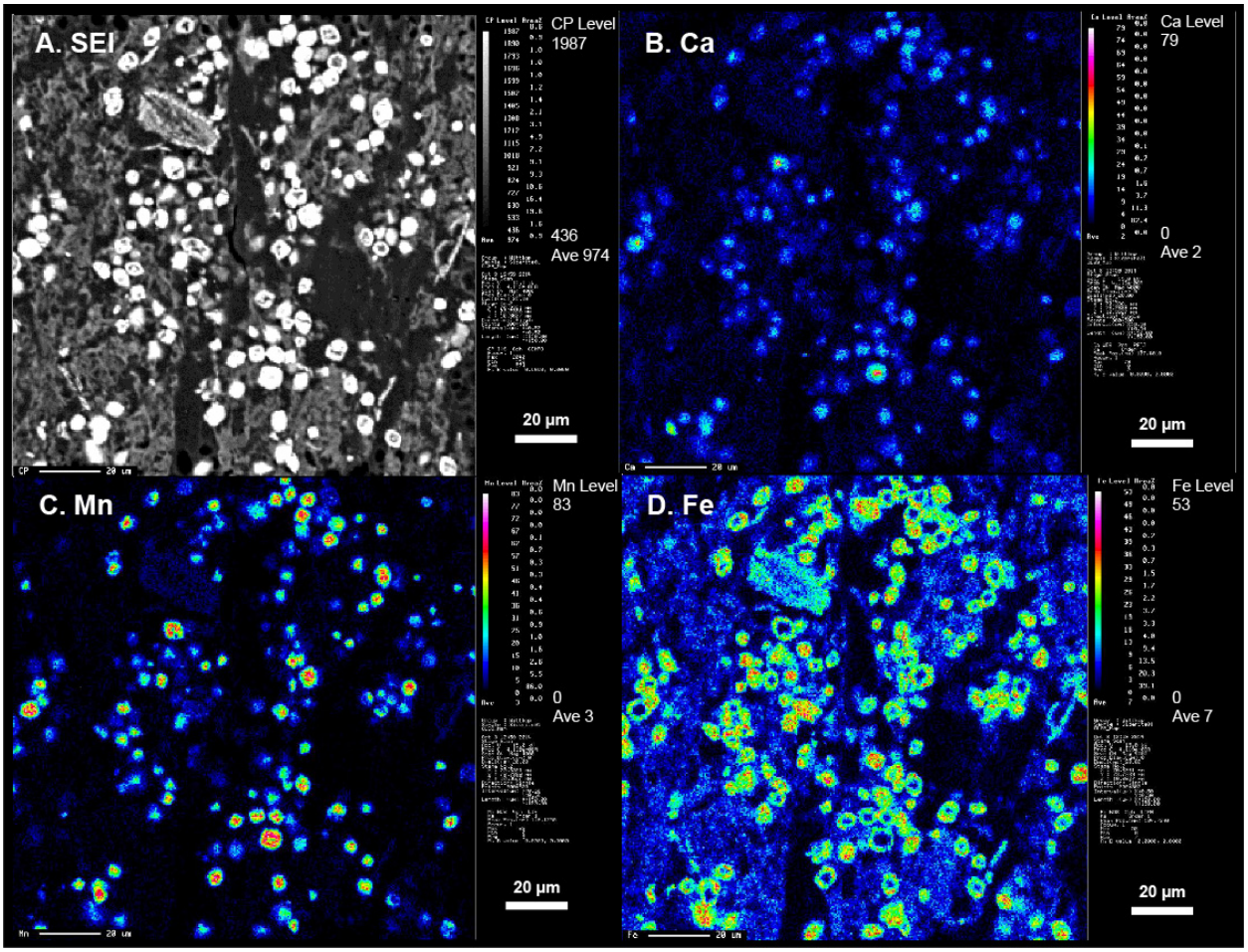

Figure 6. Electron probe microanalysis (EPMA) maps of Otter Lake carbonate crystals. **A**. Secondary electron image. **B**. Relative Ca concentration. **C**. Relative Mn concentration. **D**. Relative Fe concentration. Note the enrichment of Ca and Mn in carbonate crystal cores, versus Fe-enrichment in carbonate crystal rims as well as diffuse concentrations in the sediment matrix.

1215

1216 The Fe-Mn carbonates in Lake Malawi cores occur in structureless sediments and display
1217 textures such as radiating sprays of larger, twinned crystals, which cross-cut original
1218 horizontality (**Figure 7**; **Figure 8**). In contrast, the Otter Lake carbonates are smaller, more
1219 spherical, and show evidence of polarization crosses (**Figure 8**). Spherical structures and
1220 polarization crosses have also been linked to late diagenetic Fe-carbonates (Köhler et al., 2013),
1221 but their presence in Otter Lake sediments suggests they may be polygenetic. Although their
1222 morphologies differ, both the Otter Lake and Lake Malawi examples exhibit Mn concentration
1223 in their crystal cores, although Fe also appears to be strongly concentrated in the Lake Malawi
1224 carbonate crystal cores, and Ca appears to be more evenly distributed in Lake Malawi
1225 examples.

1226

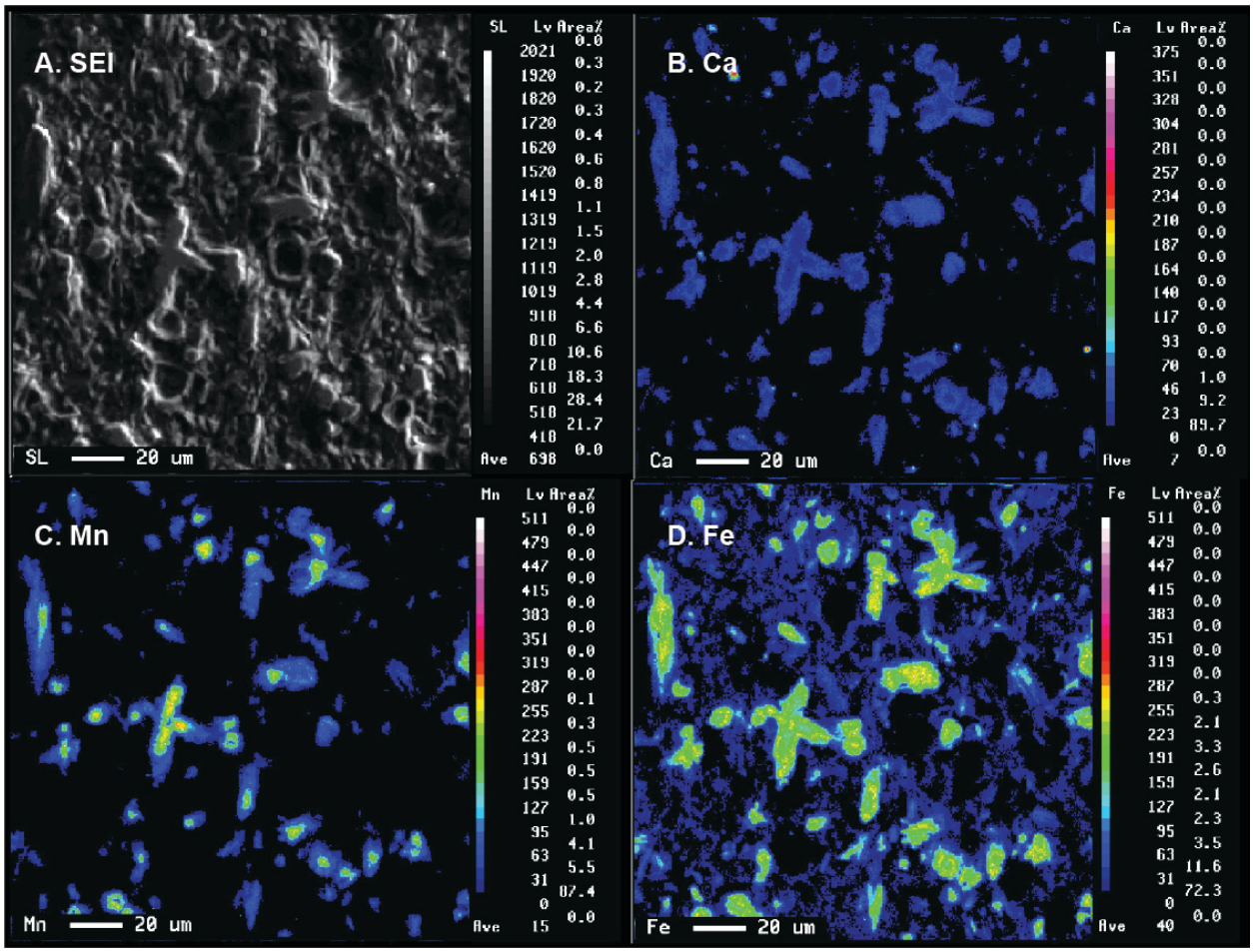

Figure 7. Electron probe microanalysis (EPMA) maps of Lake Malawi carbonate crystals. **A**. Secondary electron image. **B**. Relative Ca concentration. **C**. Relative Mn concentration. **D**. Relative Fe concentration. Note the strong concentration of Mn in carbonate crystal cores similar to the OL example. However, in contrast to the Otter Lake example, Ca is more evenly distributed in the crystals. Additionally, iron is also enriched in Lake Malawi crystal cores in comparison to Otter Lake but is present in low abundance in the sediment matrix in both lakes.

Microprobe spot analyses from Lake Malawi and Otter Lake carbonates normalized to Ca-Mn-Fe show that Lake Malawi samples analyzed from two different locations in the core separated by approximately 15 m of sediments range from 40-80 % Mn-carbonate (**Figure 9**).

The relative consistency of the Lake Malawi carbonate compositions may indicate a more stable diagenetic environment. In contrast, Otter Lake crystals analyzed from two intervals of core separated by about 2 meters of sediment range from 10-95 % Mn. The wider range of composition in the Otter Lake samples is consistent with fluctuating conditions in a lake water column, where ratios of elements may change seasonally or through long-term basin evolution (sec. 5), though the wide range of Fe concentrations could also derive from the EPMA beam measuring more Fe-enriched rims versus Fe-poor crystal cores in some cases (**Figures 6 & 7**).

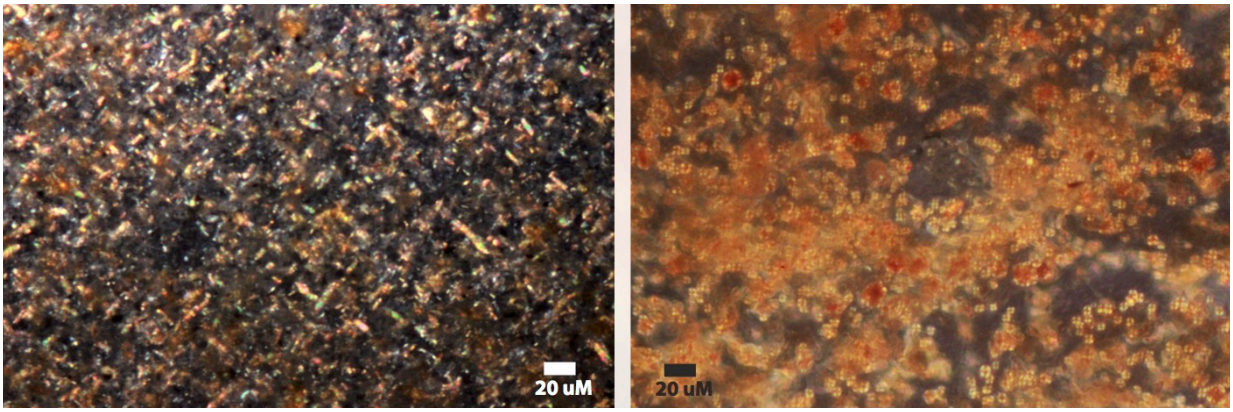

Figure 8. Polished petrographic thin section images of lacustrine iron carbonates. Left, Lake Malawi sample displaying cross cutting fabric relative to plane of deposition (parallel to long axis of image) and larger elongate crystals. Right, photomicrograph of Otter Lake carbonates showing smaller, more spherical crystal forms, and the presence of polarization crosses.

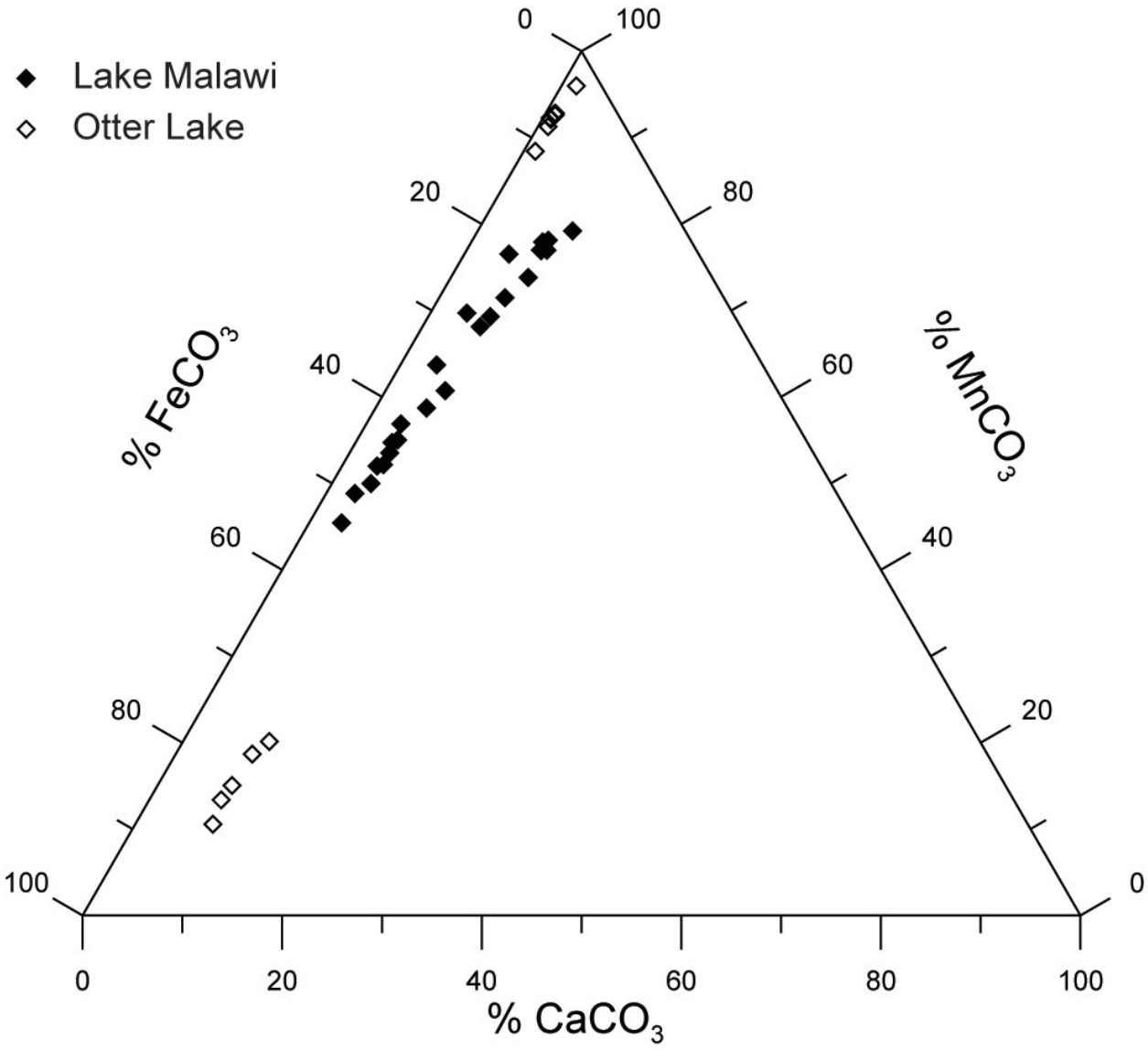

Figure 9. Normalized composition of Lake Malawi (closed diamonds) and Otter Lake (open diamonds) carbonates compiled from microprobe analysis. One Otter Lake sample plots in the Lake Malawi field. Note the greater variability in Otter Lake carbonates relative to Lake Malawi.

Further differences in the Lake Malawi and Otter Lake siderite occurrences can be observed in bulk iron speciation. Samples were extracted from a modified protocol based on the method of Poulton and Canfield (2005). Concentrations of both Fe and Mn were analyzed in the extracted

solutions owing to the significant abundance of Mn in both systems. Sulfur species were not extracted. The concentration of Fe and Mn in speciation data (**Figure 10**) suggest carbonates comprise up to ~12 % of sediments by weight. This is similar to quantitative XRD abundance reported from Otter Lake, although quantifying siderite is not straightforward (Ordoñez et al., 2019; Wittkop et al., 2014). Both lakes' sediments show that reservoirs of highly reactive iron persist in sediments, but only Lake Malawi samples showed a significant component of magnetite. Lake Malawi magnetite was in a molar ratio of approximately 1.5:1 relative to iron-carbonates, consistent with diagenetic co-precipitation of carbonate and magnetite (Heimann et al., 2010). This suggests that much of the of the iron reservoir in Otter Lake remained in a highly reactive but reduced form that was not available for diagenetic reduction, possibly as a green rust phase. As iron speciation analysis was performed in oxic conditions, identification of such a metastable phase was not possible.

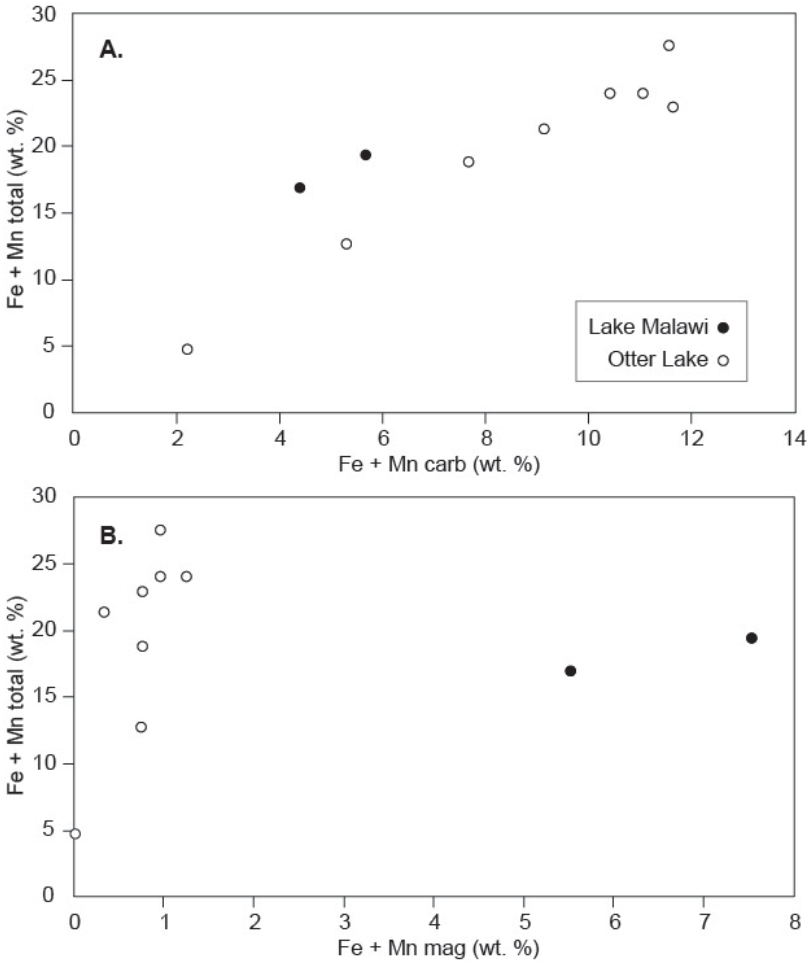

Figure 10. Iron and manganese speciation from selected Lake Malawi and Otter Lake samples. **A**. Total extracted Fe and Mn as weight percentage of dry sediment, versus Fe and Mn extracted from the carbonate fraction, also expressed as weight percentage of dry sediment. Note the similar trend of increasing total Fe and Mn with increasing carbonate in both systems. **B**. Total extracted Fe and Mn versus magnetite associated Fe and Mn, expressed as in **A**. Note that Lake Malawi samples exhibit significantly higher proportion of sediments as magnetite relative to Otter Lake. This is potentially representative of diagenetic co-precipitation of Fe-carbonate and magnetite (e.g. Heimann et al., 2010), or an enhanced aeolian flux of detrital magnetite to Lake Malawi.

Although Otter Lake and Lake Malawi are vastly different freshwater systems in terms of size and regional geology, the siderite occurrences have noteworthy similarities and key differences. Water-column dissolution of calcite below the calcite compensation depth appears to be a factor in both cases, as Otter Lake retains calcite in littoral sediments, and Lake Malawi contains calcite-rich intervals associated with mega-droughts. Significant lake level changes are also common to both systems, as each display geochemical changes associated with variable clastic influx tied to lake level variability (Brown, 2011; Wittkop et al., 2014). Finally, the similarity between Lake Malawi and Lake Towuti siderites appears to clarify aspects of a diagenetic pathway for siderite precipitation (cf. Vuillemin et al., 2019b). Initial precipitation forms Mn-enriched siderite, while later growth leads to increasingly rhombohedral forms with increased Ca substitution (Vuillemin et al., 2019b). The presence of Ca in siderite crystals and not the sediment matrix (and apparent slight enrichment in crystal rims) in Lake Malawi supports the hypothesis that Ca is incorporated passively from porewater during late crystal growth. The co-occurrence with magnetite in Lake Malawi and Lake Towuti could be ascribed to diagenetic co-precipitation (Heimann et al., 2010), a precursor authigenic phase (Vuillemin et al., 2019b), or perhaps detrital influx. While other pathways for Fe-carbonate genesis in the Malawi example may be entertained (for instance, Fe-carbonate replacement of a pre-existing spindle-shaped gypsum crystals), the similarities between Towuiti and Malawi carbonate morphologies are more likely driven by processes universal to iron diagenesis in organic-rich sediments.

The fine-grained siderites in the Otter Lake are more difficult to ascribe to the diagenetic mechanisms proposed from tropical lakes. Instead, finely laminated examples more closely resemble well-preserved micro-banded siderites from ancient iron formations (Carrigan and Cameron, 1991; Morris, 1993). These textural differences, combined with a lower proportion of co-eval magnetite, and apparent nucleation on Ca-carbonates rather than passive incorporation from porewater, are consistent with potential initial precipitation from the sediment water interface, potentially nucleating on Ca-carbonates (e.g. Wittkop et al., 2020b), followed by subsequent growth in porewaters that may have remained in oxygen isotopic equilibrium with waters above the sediments, but reflecting enhanced iron and DIC concentrations.

Although the concentration of Fe in Otter Lake carbonate crystal rims could also be taken as evidence pointing to a strictly diagenetic pathway for siderite precipitation, this would not preclude the presence of a ferruginous water mass. Rather, the presence of Fe-enriched carbonate rims may simply reflect the slower precipitation kinetics of siderite (see discussion in sec. 3), which would require more time for crystal growth relative to other carbonates, and which would be expected to continue in ferruginous environments where porewater redox conditions would be similar to an overlying ferruginous water mass. Recent detection of Fe-carbonate phases in the water column of ferruginous Lake Matano (Bauer et al., 2020) indicates the possibility that primary water column processes play a role in the genesis of some Fe-carbonates. Our initial analysis of the Otter Lake and Lake Malawi sediments, combined with recent insights regarding diagenetic mineral growth from Lake Towuti (Vuillemin et al., 2019b, 2019a), suggest that exploring the geochemical and mineralogical records of paleoferruginous lakes is promising avenue for future research.

We are aware of several additional examples of paleoferruginous lakes in the literature. Ferruginous laminated sediments are found in Elk Lake, Minnesota and it is thought the deep basin of this lake was likely meromictic in the past (Megard et al., 1993). Siderite varves from Meerfelder Maar in Germany also point to a past ferruginous meromictic interval (Brauer et al., 2008). Vivianite-rich laminated sediments indicate ferruginous conditions during the Pleistocene in Devils Lake, Wisconsin, these indicators disappear 11,000 years after the onset of lake sedimentation (Williams et al., 2015). An Eocene-aged lake on the Seward peninsula records siderite varves that disappear as the lake filled in (Dickinson, 1988), interpreted to reflect a past ferruginous meromictic lake.

5. Ferruginous meromictic lakes

Meromictic lakes are permanently stratified into a mixolimnion (i.e. upper mixed layer) and a monimolimnion, which has higher density waters that are resistant to mixing with the mixolimnion. In the temperate zone, seasonal stratification of lakes is common due to solar heating of the mixolimnion and cooler denser water below the photic zone. This thermal stratification is disrupted in the fall when the mixolimnion cools (or warms in spring) - wind-driven upwelling then disrupts the density gradient and allows mixing. In meromictic lakes, the monimolimnion remains permanently denser because of dissolved substances or persistent temperature gradients, which stabilize the water column from mixing. The specific factors stabilizing tropical meromictic lakes are discussed extensively elsewhere (Katsev et al., 2017; Lewis Jr., 1996). Importantly for the current discussion, dissolved iron can also increase water

density and stabilize a lake against mixing, or the maintenance of dissolved iron can simply be promoted by other physical or chemical factors that cause the water column to stratify.

The size and shape of the lake are critical in determining whether it becomes meromictic. Lakes that are relatively deep in comparison to their surface area mix less efficiently (Gorham and Boyce, 1989). A lake's relative depth (Z_r) is calculated from its maximum depth (Z_m) and its surface area (A_0):

$$Z_r = \frac{50 * Z_m * \sqrt{\pi}}{\sqrt{A_0}}, \qquad \text{or in percent: } Z_r = \frac{Z_m * 88.6}{\sqrt{A_0}} \qquad \text{(eq. 3)}$$

Lakes with Z_r > 4 % are physically resistant to mixing, and more likely to be seasonally or permanently stratified (Walker and Likens, 1975; Wetzel, 2001).

Another critical factor is fetch, or the distance across which wind can move (Gorham and Boyce, 1989; Lewis Jr., 1996), and the depth of mixing generally increases with fetch (Mazumder and Taylor, 1994). Several studies propose additional empirical relationships between morphometric attributes of a lake in combination with additional factors such as wind stress and internal waves (Gorham and Boyce, 1989; Kirillin and Shatwell, 2016).

Numerous authors have sought to define different types of meromixis based on probable causal agents (Boehrer and Schultze, 2008; Hall and Northcote, 2012; Schultze et al., 2017; Stewart et al., 2009; Walker and Likens, 1975). Four categories are acknowledged in recent literature: Type I) Ectogenic refers to dense, saline waters increasing density stratification, usually from active or relict seawater input; Type II) Crenogenic meromixis develops when saline water infiltrates the lake through springs or seeps within the basin; Type III) Biogenic meromixis is induced by biological pumping of ions into bottom waters through dissolving (bio)minerals or decomposition of settling organic carbon; and Type IV) Cryogenic

affects mainly Arctic lakes and develops when salts are frozen out, and dense salty water descends to the bottom of the lake. Another recently recognized type of ectogenic meromixis is termed “cultural” (Koretsky et al., 2012; Sibert et al., 2015), and affects lakes in urban areas in temperate regions when road deicing salts applied in the watershed increase bottom water density (Novotny et al., 2008). Biogenic meromixis can also result from anthropogenic eutrophication or changes in land use that affect the productivity of a lake (Culver, 1977; Hongve, 1980). Finally, thermogenic meromixis is maintained by temperature gradients, with weak salinity gradients developing as a consequence (Katsev et al., 2017)

The occurrence of “iron-meromixis” has been identified by some authors when a high concentration of dissolved iron in bottom waters stabilizes a meromictic water column against mixing (Boehrer et al., 2017, 2009; Campbell and Torgersen, 1980; Hongve, 2002; Kjensmo, 1967). Ferruginous meromictic lakes are sometimes stabilized by other solutes such as bicarbonate (Rodrigo et al., 2001), or even sodium and chloride ions from de-icing salts (Lambrecht et al., 2018; Sibert et al., 2015). Therefore, we will use the term ferruginous meromictic to describe lakes that are both ferruginous and meromictic, without implying that iron has a relationship to the stability of the water column. Yoshimura (1936) suggested a 5 mg L^{-1} (~90 µM) threshold for his “siderotrophic” lakes. However, “ferruginous”, implies the presence of dissolved ferrous iron, reflecting the dominance of Fe^{3+} as a terminal electron accepting process vs. others (i.e. oxygen, nitrate, sulfate; Canfield and Thamdrup, 2009), or an external supply of iron that outpaces its removal, regardless of concentration (sec. 1).

Meromictic lakes are thought to be rare, with just several hundred documented worldwide (Anderson et al., 1985; Stewart et al., 1965, 2009; Walker and Likens, 1975;

1393 Yoshimura, 1937). **Table 2** is a compilation of natural basins (i.e. no mining pits) that comprise
1394 circumneutral (i.e. pH 6-8) ferruginous meromictic lakes and which have previously been
1395 reported in the literature. Ferruginous lakes comprise just a fraction of meromictic lakes
1396 worldwide. However, dissolved iron is not often measured or reported for meromictic lakes,
1397 and so ferruginous meromixis could be more widespread even among the known meromictic
1398 lakes. Several lakes have been excluded from this list. For instance, ferruginous Nordbytjernet
1399 in Norway was originally described as meromictic (Hongve, 1974), but has since experienced
1400 mixing due to hydrological changes (Hongve, 1999). Lake Glubok in Russia may be becoming
1401 meromictic due to eutrophication, and contains up to 180 μM iron in bottom water
1402 (Shaporenko and Shil'krot, 2006).
1403

Table 2. Known Ferruginous Meromictic lakes worldwide.

Lake	Location	Max. diss. Fe	A_o (m^2)	Z_m (m)	Z_r (%)	Reference
*Skratjern	Norway	877 µM	8,600	12.5	11.9	Hongve 1980
*Canyon Lake	MI, USA	1,594 µM	10,000	22.5	19.9	Smith 1940; Lambrecht et al., 2018
*Paul Lake	MI, USA	120 µM	12,000	12.2	9.9	Taillefert et al., 2002
Lake La Cruz	Spain	1,000 µM	14,500	24	17.7	Rodrigo et al., 2001
*Ljøgodttjern	Norway	1,480 µM	23,400	16.3	9.4	Hongve 1980
*Vilbergtjern	Norway	98 µM	24,000	17	9.7	Hongve 1980
*Bakketjern	Norway	296 µM	24,100	14.8	8.4	Hongve 1980
Hall Lake	WA, USA	750 µM	31,100	16.2	8.1	Balisteri et al., 1994
*Skjennungen	Norway	625 µM	34,000	17.8	8.6	Kjensmo 1967
*Brownie Lake	MN, USA	1,605 µM	50,000	14	5.5	Swain 1984; Lambrecht et al., 2018
*Valkiajärvi	Finland	6,758 µM	78,500	25	7.9	Meriläinen 1970
*Lake 120	Canada	4,200 µM	93,000	19	5.5	Campbell & Torgersen 1980
Kuznechikha	Russia	3,850 µM	93,000	20	5.8	Gorlenko et al., 1980
*Woods Lake	MI, USA	360 µM	107,000	13	3.5	Sibert et al., 2015
*Lake of the Clouds	MN, USA	11,070 µM	120,000	31	7.9	Anthony 1977
*Store Aaklungen	Norway	6,071 µM	132,000	32.5	7.9	Kjensmo 1967
*Lake Svetloe	Russia	240 µM	146,000	39	9.0	Savvichev et al., 2017; Kokryatskaya et al., 2017
Oha Lampi	Russia	1,780 µM	154,000	16	3.6	Dubinina & Derygina 1969
Lake Pavin	France	1,184 µM	440,000	92	12.3	Michard et al., 1994
Lake Nyos	Cameroon	4,410 µM	1,580,000	210	14.8	Teutsch et al., 2009
Sikaribetuko	Japan	1,550 µM	3,450,000	99.5	4.7	Yoshimura 1936
Kabuno Bay of Lake Kivu	Dem. Rep. of Congo	1,200 µM	4,800,000	120	4.9	Lliros et al., 2015
Lake Monoun	Cameroon	5,180 µM	609,000	96	10.9	Sigurdsson et al., 1987
Lake Matano	Indonesia	140 µM	164,000,000	590	4.1	Crowe et al., 2008

*indicates lakes of glacial origin

1404

Aside from a few studies, the source of iron to ferruginous meromictic lakes has not been extensively addressed in the literature. Some studies of ferruginous lakes suggested dissolved iron is sourced from the lake sediments themselves (Nürnberg and Dillon, 1993). This idea of an internal cycle of iron is attractive and not invalid – under anoxic and non-sulfidic conditions Fe^{3+} (oxyhydr)oxides will be reductively dissolved by the activity of Fe^{3+}-reducing microorganisms in the presence of a supply of sedimentary organic carbon. However, iron is a non-conservative element that is permanently removed to sediments through precipitation and deposition of iron-bearing minerals, such as iron phosphates (e.g. vivianite; Cosmidis et al., 2014; Vuillemin et al., 2019a), iron carbonates (e.g. siderite; Vuillemin et al., 2019b; Wittkop et al., 2014), Fe^{3+} or mixed-valent (oxyhydr)oxides (Bauer et al., 2020; Crowe et al., 2008b), or mixed valent green rusts (Zegeye et al., 2012). This implies that iron must be resupplied from an external source other than the sediments to maintain a reservoir of iron in the lake (cf. Davison, 1993).

Iron budgets for several ferruginous meromictic lakes have been created. In Lake Pavin, France, the supply of iron via sublacustrine springs into the mixolimnion derived from volcanism is required to achieve mass balance with iron removal to sediments, although there has been no direct determination of iron fluxes from this source (Aeschbach-Hertig et al., 2002; Assayag et al., 2008; Michard et al., 1994). Weathering and erosion of tropical soils with abundant Fe^{3+} (oxyhydr)oxides provides iron to Lake Matano (Crowe et al., 2008b), as a hydrothermal source of iron could not be identified (Crowe et al., 2011). An iron budget from Lake 120 in Canada does not specify the source of iron but notes that external iron inputs are required. Surface

1426 water was thought to recharge at the chemocline depth after transiting through an adjacent
1427 bog (Campbell and Torgersen, 1980).
1428 Additional ferruginous meromictic lakes have some constraint on the likely iron source.
1429 Ferruginous Kabuno Bay of meromictic Lake Kivu likely sources its iron through sub-lacustrine
1430 springs derived from volcanism (Ross et al., 2015), similar to Lake Pavin. Iron-bearing surface
1431 waters likely supply Lake Nordbytjernet, but sublacustrine iron concretions also indicate
1432 discharge of iron-bearing groundwaters (Hongve, 1974). Others also invoke reducing
1433 groundwater in supplying iron, despite the lack of direct data (Kjensmo, 1967; Yoshimura,
1434 1931). In iron budgets of temperate but non-meromictic lakes, atmospheric deposition, stream
1435 input from organic carbon-rich soils, and recycling from sediments were noted, with recycling
1436 thought to be the largest source (Nürnberg and Dillon, 1993). However, groundwater sources
1437 were not quantified, and if this unaccounted-for source is significant, mass balance approaches
1438 could overestimate the inputs from sedimentary recycling.
1439
1440 *Identification of ferruginous meromictic lakes*
1441 Considering the utility of ferruginous meromictic lakes for understanding past
1442 ferruginous oceans (sec. 4 and sec. 6), it would be useful to find more. To do this, it would be
1443 helpful to establish criteria to screen for likely meromixis from commonly available data. We
1444 propose a strategy to identify possibly meromictic temperate lakes based on morphometry and
1445 susceptibility to mixing. Morphometric data, such as maximum or average depth and surface
1446 area, are commonly available from local, regional, or national agencies. Identifying whether
1447 these lakes are ferruginous requires more detailed regional chemical or geological information,

1448 but we present a case study on what types of regional characteristics might be useful. We
1449 specifically focus on temperate lakes of likely glacial origin (as opposed to karstic, volcanic,
1450 etc.), as this describes more than half of the ferruginous meromictic lakes in **Table 2**.

1451 **Figure 11** shows a compilation of the area A_0 and the relative depth Z_r for some
1452 temperate meromictic and non-meromictic lakes. Only temperate lakes mentioned in **Table 2**
1453 are included, tropical or volcanic ferruginous meromictic lakes (Lakes Sikaribetuko, Matano,
1454 Monoun and Nyos, and Kabuno Bay of Lake Kivu), are excluded. The compilation includes
1455 meromictic lakes (including some ferruginous) from Massachusetts, Maine, Minnesota,
1456 Michigan, New York, Wisconsin, Ontario and Quebec, and Finland (Anderson et al., 1985;
1457 Stewart et al., 2009), and meromictic and non-meromictic lakes from Norway (Hongve, 2002,
1458 1977). Non-meromictic lakes from temperate areas of North America of likely glacial origin
1459 were compiled from several sources (Dupuis et al., 2019; Molot et al., 1992; Myrbo, 2008;
1460 Myrbo and Shapley, 2006; Orihel et al., 2015; Schiff et al., 2017; Striegl and Michmerhuizen,
1461 1998). Data are provided in Supplementary Information.

1462 Surface area is related to fetch, and prior studies have indicated that lakes with small
1463 surface areas are less likely to mix (Mazumder and Taylor, 1994). Another study documented a
1464 maximum length of 250 m for meromictic lakes (Salonen et al., 1983). In a Norwegian study
1465 (Hongve, 2002), meromixis was only observed in lakes with a $A_0 < 0.3$ km^2. For temperate lakes,
1466 a A_0 of less than 0.5 km^2 seems to be a natural cutoff as all temperate meromictic lakes shown
1467 in **Figure 11** have a $A_0 < 0.5$ km^2.

1468

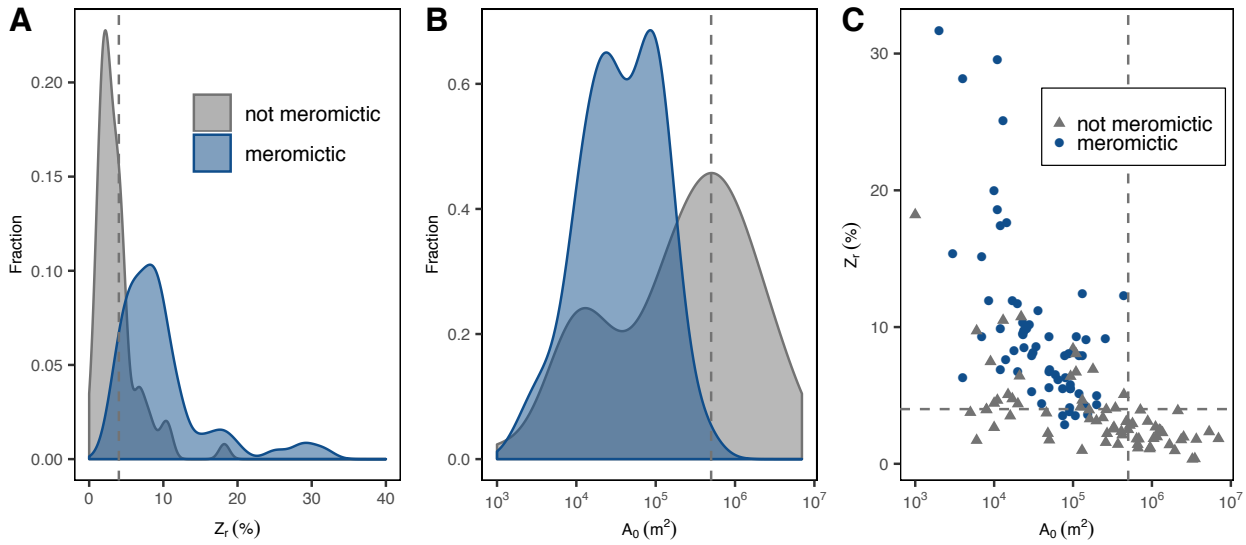

1469

1470 **Figure 11.** Histograms of temperate meromictic and not meromictic lakes based on the

1471 morphometric parameters **A**. relative depth (Z_r) and **B**. surface area (A_0). **C**. A scatter plot of the

1472 data, where dashed lines denote A_0 of 0.5 km^2 and Z_r of 4 %.

1473

1474 There is a considerable range in the Z_r of meromictic lakes (**Figure 11**), and a number of

1475 non-meromictic lakes have a Z_r > 4 %, a threshold noted to limit mixing (Wetzel, 2001). While a

1476 Z_r > 4 % may physically limit mixing, a salinity gradient is also necessary to stabilize meromixis

1477 (Hongve, 2002; Salonen et al., 1983). For lakes that have a sufficiently small surface areas and a

1478 Z_r just below 4 %, enhanced salinity may be a large enough factor for meromixis. For instance,

1479 Woods Lake in Michigan, USA (Z_r of 3.5 %) has become meromictic as a result of road salt use

1480 (Sibert et al., 2015). Lakes with a $Z_r \leq 4$ % can also have weak salinity gradients that might be

1481 vulnerable to occasional mixing. This scenario was observed in ferruginous Lake Nordbytjernet,

1482 originally reported as meromictic, and which has a Z_r of 3.8 % and A_0 just under 0.3 km^2

1483 (Hongve, 2002, 1999). Other authors have suggested that a criteria of Z_r > 8 % could define

meromixis (Salonen et al., 1983). A higher Z_r may be necessary for meromixis in regions where waters are likely to be more dilute, whereas lakes that are heavily influenced by anthropogenic contaminants, such as road salt, may become meromictic at $Z_r \leq 4$ %.

Several natural processes could produce a basin with $Z_r \geq 4$ %, which - as described above - might poise a lake to develop meromixis. Lake basins carved in karstic terrain can be quite deep relative to their surface area, and many meromictic lakes are known from karstic regions (Alcocer, 2017; Ciglenečki et al., 2017), including ferruginous La Cruz in Spain (Camacho et al., 2017a). Morphometry resulting in high Z_r and meromixis is sometimes attributed to faulting in exposed bedrock that has been weathered or further carved by glacial ice or outwash. This is likely the case with Store Aaklungen (Kjensmo, 1967) and Canyon Lake (Lambrecht et al., 2018).

There is a strong bias in the literature toward identification of meromictic lakes in Europe and North America, which has been attributed to a higher concentration of limnological studies in those areas (Zadereev et al., 2017). Another major factor in the sheer number of lakes in northern temperate regions is the commonality of glacial origins. Numerous meromictic lakes in Norway, for instance, are sheltered kettle lakes in thick glacial deposits (Hongve, 1980). Thousands of kettle lakes were also formed in North America at the edges of retreating glaciers by ice blocks buried in sediments that were covered by glacial outwash. Kettle lakes tend to be small and less than 50 m deep, and can have a rounded shape (Wetzel, 2001), dimensions conducive to the elevated Z_r values that characterize many temperate in meromictic lakes (**Figure 11**).

If this broad relationship between glacial origins and meromixis scales, the morphometric attributes of the millions of temperate kettle lakes worldwide may poise some fraction of these lakes toward meromixis. If true, this hypothesis might also be useful to predict areas where more meromictic lakes can be found. For instance, a deglaciated and lake-rich region of Northeast Poland contains numerous lakes with laminated sediments, often with $A_0 <$ 0.3 km^2 and high Z_r (Tylmann et al., 2013).

While there are more elaborate methods to determine whether lakes may be prone to meromixis, the approach proposed here has the advantage of utilizing two metrics (A_0 and Z_m) that are commonly reported in the literature or in government databases. We used Minnesota as a case study for identifying additional lakes that may be meromictic using the Z_r and A_0 criteria set out above. Minnesota has 11,842 lakes greater than 10 acres (0.04 km^2). The Z_r values of 1,986 Minnesota lakes are available from the Minnesota Department of Natural Resources (DNR; Supplementary Information). Of these, 33 have $A_0 < 0.5$ km^2 and $Z_r > 4$ % and are natural lakes (as opposed to mining pits or other artificial basins; **Table 3**). Bathymetric data is only available for a relatively small portion of the many lakes in Minnesota. However, if our dataset is representative, Minnesota lakes have physical features conducive to meromixis at a rate of 1.7 %, which equates to 197 lakes in the entire state. In comparison, a similar analysis done in Finland just 0.36 % of lakes smaller than 0.3 km^2 were suspected to be meromictic using a much higher threshold for meromixis of $Z_r \geq 10$ % (Hakala, 2004). Yet the one example of a ferruginous meromictic lake in Finland, Valkiajärvi, has a Z_r of 7.9 % (Meriläinen, 1970), suggesting such a stringent Z_r threshold may be unwarranted.

Table 3. Minnesota lakes (of 1,986) with morphometric attributes conducive to meromixis.

Lake	County	A_o (m^2)	Z_m (m)	Z_r (%)
Adams	Itasca	48441	14.3	5.8
Ahsub	Lake	244151	23.8	4.3
Alice	Itasca	164363	18.3	4.0
Bear	Lake	73936	21.0	6.8
Benfield	Carlton	104559	24.7	6.8
Benjamin	Benjamin	134113	38.9	9.4
Brownie	Hennepin	44086	14.7	6.2
Church	Carver	64790	16.5	5.7
Crappie	Hubbard	93729	22.2	6.4
Crooked	Itasca	420387	33.5	4.6
Cub	St. Louis	30129	11.9	6.1
Deep	Clearwater	176625	23.1	4.9
Fadden	Wright	81467	14.6	4.5
George	Stearns	34597	9.6	4.6
Hazel	Cass	59643	11.5	4.2
Hidden	Hennepin	30906	8.5	4.3
Little Bass	Itasca	104381	25.7	7.1
Little Cedar	Wright	146318	17.9	4.2
Little Elbow	St. Louis	21610	9.9	6.0
Little Thunder (East Bay)	Cass	1044384	17.3	4.4
Minnie	Stearns	107395	16.8	4.5
Morgan	Wadena	93053	17.5	5.1
North	Dakota	38558	9.8	4.4
North Little Long	Hennepin	211501	23.2	4.5
Peavey	Hennepin	36940	16.5	7.6
Pleasant	Pleasant	89063	20.8	6.2
South Berthiaume	Wright	79565	22.2	7.0
South Little Long	Hennepin	69586	13.1	4.4
St. Joe	Carver	79116	15.8	5.0
Unnamed (Cassidy)	Wright	61132	11.2	4.0
Unnamed (Hidden)	Wright	31966	9.4	4.7
Unnamed (Nickel)	Itasca	57490	12.1	4.5

Wabasso	Ramsey	173286	22.2	4.7

Table 4 shows lakes previously literature reports of meromictic lakes in Minnesota (Anderson et al., 1985; Stewart et al., 2009). Of these, Brownie Lake is the only lake also identified as meromictic in **Table 3**. What is notable from comparison of **Table 3** and **Table 4** is that a number of potentially meromictic lakes occur in Hubbard and Clearwater Counties. Parts of these counties are encompassed in Itasca State Park. The lakes within the park are generally in morainic depressions with forested ridges rising 30 m above (Baker and Brook, 1971), conducive to physiography and wind sheltering favoring meromixis.

Table 4. Minnesota lakes reported to be meromictic.

Lake	**County**	**A_o (m^2)**	**Z_m (m)**	**Z_r (%)**	**Reference**
Tin Cup	Clearwater	65000	6.7	2.33	Stewart et al., 2009
Ozawindib (Squaw)	Clearwater	610000	24	2.72	Baker and Brezonik, 1971
Josephine	Hubbard	30000	10.3	5.27	Baker & Brook, 1971
Lower LaSalle	Hubbard	980000	60	5.37	Baker & Brook, 1971
Swain's Pond	Lake	4000	4.5	6.31	Anthony 1977
Deming	Hubbard	50000	17	6.74	Baker & Brook, 1971
Budd	Clearwater	20000	10.8	6.77	Baker & Brook, 1971
Spring	Ramsay	12000	8.5	6.88	Stewart et al., 2009
Arco	Hubbard	14000	10.2	7.64	Baker & Brook, 1971
Elk	Clearwater	100000	30	8.41	Anderson et al., 1985
Rivalry	Lake	17000	17.5	11.89	Anthony 1977

Looking only at the morphometric data of the Minnesota lakes, it is impossible to know whether these potentially meromictic lakes are also ferruginous. The presence of iron in meromictic lakes requires a sustained external source, as detailed above. In ferruginous meromictic lakes where the iron source has been identified, it is often some type of

groundwater or sublacustrine spring, with a clear exception being the tropical soil erosion that supplies iron oxides to Lake Matano. A role for groundwater may not be surprising, given that anoxic conditions are generally required for iron to be extensively mobile in circumneutral water (sec. 2). Aquifers and aquitards can have very limited exchange with the atmospheric oxygen. Where sufficient organic carbon is present, perhaps particularly in unconsolidated sediments such as glacial till, groundwater can accumulate Fe^{2+} due to the reduction of ferric iron minerals (Barnes et al., 2011).

Numerous ferruginous meromictic lakes reported in the literature were noted for their occurrence in or adjacent to moraines or other glacial drift (Campbell and Torgersen, 1980; Hongve, 1980; Kjensmo, 1967; Lambrecht et al., 2018). Similarly, other ferruginous meromictic lakes formed in areas of known Late Quaternary glaciations (Demidov et al., 2004; Ojala and Saarnisto, 1999). Lake of the Clouds in northeastern Minnesota (**Table 3**), conversely, is formed in iron-rich bedrock carved by glacial erosion (Anthony, 1977), a setting thought to give rise to millions of ferruginous lakes in boreal regions (Schiff et al., 2017).

Minnesota, the area of our case study, exhibits a surficial geology of predominantly glacial drift and glacial landforms, a legacy from multiple glacial advances during the late Quaternary. The area also has regions with iron-rich bedrock (Johnson et al., 2016). The geochemistry of glacial sediments is known to influence the ionic composition of lakes in the upper Midwest (Gorham et al., 1983). The glacial aquifers and aquitards in the upper Midwest are known to have low redox conditions, particularly those deposited during the latest Wisconsin-aged advance (Erickson et al., 2018; Erickson and Barnes, 2005; Simpkins and Parkin, 1993).

To assess whether iron-rich groundwater is widespread in Minnesota, we retrieved total iron on groundwater from private and municipal wells from the Minnesota Pollution Control Agency's (PCA; Supplementary Information). The total iron concentrations within 618 wells drilled into quaternary aquifers were interpolated using the natural neighbor method in ArcGIS to create a map of groundwater iron concentrations (**Figure 12**). The map shows iron-rich groundwater widely distributed throughout the state. The highest iron regions visibly overlap the extent of the Wisconsin-aged glaciation, i.e. are from wells drilled into sediments of the Des Moines Lobe, the most aerially extensive glacial lobe in Minnesota surficial geology.

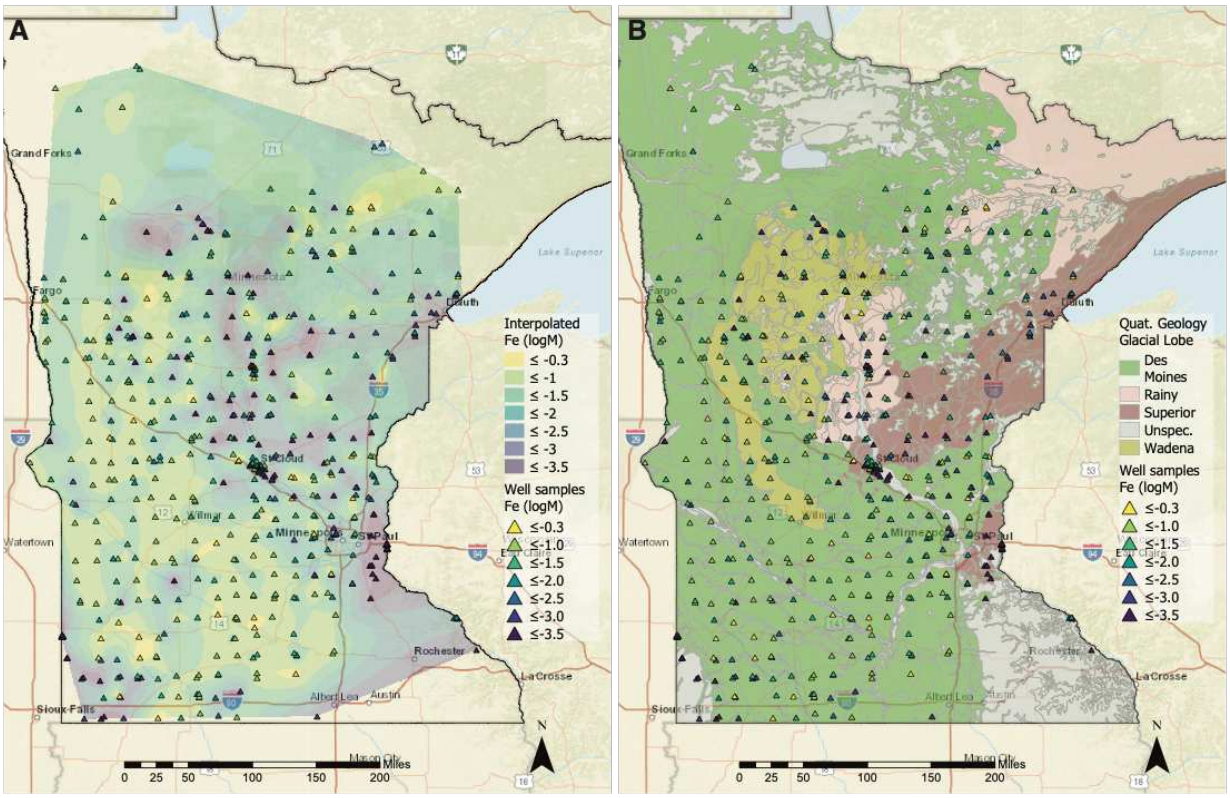

Figure 12. A. Individual wells (triangles) colored by their total iron concentration (as log molar), with shading representing interpolation. The proposed study areas are outlined. **B**. Wells

overplotted on the lobes of the Laurentide ice sheet in Minnesota (source: Minnesota Geological Survey).

We hypothesize that the source of sediments to glacial drift, and thus aquifer material, would have produce distinct differences in the total iron content of the resulting groundwater. We therefore determined the total iron values for wells within the glacial lobes represented in Minnesota (Des Moines, Rainy, Superior, Wadena, or Unspecified – areas glaciated by a different lobe or not glaciated at all). The results indicate that the highest total iron concentrations occur within the Des Moines lobe (**Table 5**). Wells in unspecified areas had the lowest total iron concentrations. To test the hypothesis that the lobe's identity had a significant influence on the total iron values, we performed a pairwise ANOVA with a Tukey HSD post-hoc test at 95 % intervals between all possible pairs of the average log molar (M) total iron concentrations in the five lobes: Des Moines. Rainy, Superior, Wadena and Unspecified. Des Moines to Superior, Des Moines to Unspecified, Rainy to Unspecified, Superior to Wadena and Wadena to Unspecified were all significantly different based on a $p<0.001$ (1 %; **Table 5**). The Rainy to Superior comparison was borderline significant ($p=0.0199$). All other pairs are not significantly different.

Table 5. Statistics for total Fe concentrations of 618 MN wells.

Glacial Lobe	Number of wells	Mean Fe (log M)	Std. dev. Fe (log M)	Tukey HSD p values:				
				Des Moines	Rainy	Superior	Wadena	Unspecified
Des Moines	389	-1.96	0.89	--	0.4988	**<0.00001**	0.9695	**<0.00001**
Rainy	53	-2.19	1.19	--	--	*0.0199*	0.9202	**<0.00001**
Superior	52	-2.75	0.97	--	--	--	**0.0005**	0.5155
Wadena	70	-2.04	1.02	--	--	--	--	**<0.00001**
Unspecified	54	-3.04	1.05	--	--	--	--	--

For Tukey HSD, bold indicates a significant difference, italics indicate borderline significant difference.

These results support the hypothesis that the total iron concentration of groundwater in Minnesota are related to the origin of the glacial aquifers. The reasons that one lobe's till would produce aquifers with higher iron have yet to be elucidated, but may be related to the iron content of the till, which is in turn related to its provenance (Wittkop et al., 2020a). Surface-groundwater interactions have dramatic implications for both water and elemental fluxes to lakes in Minnesota where these processes have been studied (Dean et al., 2006; Jones et al., 2013). But if such surface groundwater interactions are widespread, they may be a ubiquitous mechanism for sustaining ferruginous lakes.

Another potential source of iron to lakes in Minnesota could be from peatlands. Peatlands are aerially extensive in the postglacial northern temperate zone (Jungkunst et al., 2012), and mobilize significant quantities of iron, solubilized by humic substances (Gorham, 1957; Jirsa et al., 2013). Peatlands are commonly mentioned in the literature as a source of iron to lakes through streams or shallow seepage (Campbell and Torgersen, 1980; Kjensmo, 1962; Nürnberg and Dillon, 1993). North-central and northeastern Minnesota is dominated by peatlands, including bogs and fens, which can be significant sources of humic-bound iron in

runoff (Jirsa et al., 2013; Krachler et al., 2016). The concentrations of iron in rainwater-fed (bogs) or groundwater-fed (fens) peatlands in Minnesota can be several tens of µM (Robbins et al., 1997; Urban et al., 1987), indicating this as an additional possible iron source to Minnesota lakes, and possibly other postglacial lakes worldwide.

Meromixis has been recognized as a stage in lake evolution. For those lakes that have a natural basin with a high Z_r, they may start meromictic, but over time, sedimentation eventually fills in the basin, shallowing it and promoting mixing. This is often seen as a transition from meromictic to holomictic (Hakala, 2004; Wittkop et al., 2014). The history of mixing can be inferred from a lake's sedimentary record. The presence of laminated sediments indicates holomixis, with annually laminated sediments (varves) indicating meromixis (Anderson et al., 1985). Numerous lakes in Minnesota contain ferruginous laminated sediments, although not all are meromictic. In some modern, glacially-formed ferruginous meromictic lakes, both in North America in Scandinavia, authors have noted a dynamic equilibrium between ferruginous and non-ferruginous and/or meromictic and holomictic conditions (Campbell and Torgersen, 1980; Hongve, 1999, 1980). Fluctuations between meromixis and holomixis can result due to a weak salinity gradient that can be easily disrupted by changes in a lake's hydrology.

Although meromixis can be a natural stage of a lake, human influence such as manipulation of water levels or addition of solutes can induce meromixis. Changes in water level due to canal building (Swain, 1984) and water use in the lake or adjacent, hydrologically connected lakes (Hakala, 2004) have led to the onset of meromixis in some ferruginous meromictic lakes. In Brownie Lake, this onset of meromixis is associated with an increase in burial of iron to sediments (Tracey et al., 1996). Meromixis may also become more common

due to increasing global average temperatures associated with climate change that enhance stratification (Nisbet et al. 2014). Land-use changes due to agriculture can affect the drainage system and increase dissolved solutes that help to stabilize the lake against mixing (Tilman et al. 2001; Hakala 2004). For example, use of road salt in the temperate regions may increase salinity-driven stratification, poising urban lakes towards meromixis (Koretsky et al., 2012; Lambrecht et al., 2018; Novotny et al., 2008; Sibert et al., 2015). Therefore, it is likely that the occurrence rate of meromictic lakes will increase, both due to discovery and due to anthropogenic factors.

6. The biogeochemistry of ferruginous meromictic lakes

Photosynthesis & Primary Productivity

One of the early motivators for the use of ferruginous meromictic lakes as analogues for ferruginous oceans was to test the hypotheses that photoferrotrophs were 1) major primary producers, and 2) had a major role in Fe^{2+} oxidation and deposition of iron-bearing minerals to the seafloor (Crowe et al., 2008a). Therefore, a premium has always been placed on finding ferruginous meromictic lakes where the chemocline between oxygen and ferrous iron is illuminated, so that Fe^{2+} and light are in sufficient supply to fuel photoferrotrophy. In this regard, the large tropical lakes, Matano and the ferruginous Kabuno Bay of Lake Kivu have been particularly valuable, because oligotrophic conditions give rise to clear water columns with deep light penetration (Crowe et al., 2014a; Llirós et al., 2015). Additionally, a weak thermal stratification allows for substantial vertical migration of the chemocline seasonally (Katsev et al., 2017). Other sunlit chemoclines exist in karstic Lake La Cruz in Spain (Walter et al., 2014),

and glacially-formed Brownie Lake in Minnesota (Lambrecht et al., 2018). A limitation of smaller meromictic lakes in the temperate zone in this regard is that they often have deep oxyclines (Lambrecht et al., 2018), eutrophic conditions, or humus-derived color (Hakala, 2004; Hongve, 1980), which can impede light penetration to the chemocline.

The keen interest in establishing whether photoferrotrophy contributes significantly to carbon fixation and other biogeochemical cycles of ferruginous meromictic lakes has precedent from the study of anoxygenic photosynthesis in sulfidic meromictic lakes and sulfidic seas. Sulfidic stratified systems frequently contain populations of anoxygenic photosynthetic bacteria in the anoxic photic zone. Visually apparent bacterial plates are commonly observed near the chemocline of meromictic sulfidic lakes (but also sulfidic seas, such as the Black Sea), as well as absorption maxima, enhanced bacterial DNA, or enrichments in bacterial sulfur-cycling genes (Dickman and Ouellet, 1987; Gorlenko et al., 1978; Hand and Burton, 1981; Kuznetsov, 1968; Ludlam, 1996; Lunina et al., 2013; Manske et al., 2005; Morana et al., 2016; Mori et al., 2013; Parkin and Brock, 1980; Rogozin et al., 2010; Savvichev et al., 2005; Storelli et al., 2013; Takahashi and Ichimura, 1968; Tonolla et al., 2017). Anoxygenic photosynthetic bacteria have been shown to contribute significantly to total carbon fixation in some of these systems (Gorlenko et al., 1978; Kuznetsov, 1968), and to a lesser extent in others (Savvichev et al., 2017). Dense bacterial plates can also contribute significantly to light attenuation (Ludlam, 1996), which could inhibit photosynthetic organisms from growing deeper in the water column.

Populations of anoxygenic photosynthetic bacteria have been found in the anoxic zone of several ferruginous lakes, where sufficient sunlight is present to support carbon fixation (Camacho et al., 2017b; Crowe et al., 2008a; Llirós et al., 2015; Walter et al., 2014). However,

1673 the presence of anoxygenic photosynthetic 16S rRNA sequences, even those closely related to
1674 known photoferrotrophs, is not sufficient to demonstrate that photoferrotrophy is occurring.
1675 Photoferrotrophs belong to several phylogenetically distinct taxa including the classes
1676 Alphaproteobacteria ("purple non-sulfur bacteria", PNSB) and Gammaproteobacteria ("purple
1677 sulfur bacteria", PSB), as well as the family *Chlorobiaceae* (themselves comprising the entirety
1678 of the "green sulfur bacteria", GSB). The most well-studied isolates are the PNSB *R. ferrooxidans*
1679 strain SW2 (Ehrenreich and Widdel 1994) and *R. palustrius* strain TIE-1 (Jiao et al. 2005), and
1680 the GSB *C. ferrooxidans* strain KoFox (Heising et al. 1999). Additionally, these organisms contain
1681 bacteriochlorophyll (Bchl) pigments that distinguish them from eukaryotic phytoplankton and
1682 cyanobacteria. For instance, Bchl *e* is a pigment associated with low-light adapted GSB
1683 (Overmann et al., 1992), such as *C. ferrooxidans* (Heising et al., 1999). The presence of
1684 anoxygenic photosynthetic organisms can be identified by pigment analysis in addition to 16S
1685 rRNA gene sequencing. However, many anoxygenic photosynthetic bacteria are also capable of
1686 using electron donors in addition to or instead of Fe^{2+}, including hydrogen sulfide, but also
1687 molecular hydrogen (H_2), other forms of reduced sulfur, and small organic acids (Ehrenreich and
1688 Widdel, 1994; Hegler et al., 2008; Heising et al., 1999; Jiao et al., 2005; Laufer et al., 2017;
1689 Straub et al., 1999; Widdel et al., 1993). Also, examples exist of bacteria oxidizing Fe^{2+} as a side
1690 reaction, rather than as an electron source for photosynthesis and carbon fixation, and thus are
1691 not true photoferrotrophic primary producers (Heising and Schink, 1998; Kopf and Newman,
1692 2012; Poulain and Newman, 2009). Therefore, to implicate anoxygenic photosynthetic
1693 organisms in iron cycling and primary productivity in a ferruginous lake, it is necessary to

1694 demonstrate Fe^{2+} and light-dependent carbon fixation *in situ,* in addition to 16S rRNA or
1695 pigments analysis.
1696 In Lake Matano, the presence of a Bchl *e* peak was documented just below the Fe^{2+}-
1697 oxygen chemocline at more than 100 m depth (Crowe et al., 2008a). Twenty-five percent of the
1698 microbial community at the depth where Bchl *e* was detected belonged to the *Chlorobiaceae*
1699 based on 16S rRNA sequences within the water column (Crowe et al., 2014a). These organisms
1700 possessed genes for sulfur oxidation, indicating that sulfide, present at low µM concentrations,
1701 was likely to be the electron donor for photosynthesis than Fe^{2+}. Carbon fixation at the
1702 chemocline attributable to anoxygenic photosynthesis was negligible to total primary
1703 productivity in the lake, likely due to the extreme light limitation in the chemocline (Crowe et
1704 al., 2014a). Savvichev et al. (2017) found GSB closely related to *C. ferrooxidans* in the Fe^{2+}-
1705 bearing chemocline of ferruginous meromictic Lake Svetloe in Russia during the winter months.
1706 The rate of anoxygenic photosynthetic carbon fixation was 2.5x that of oxygenic photosynthesis
1707 at the chemocline, although it was not unambiguously demonstrated that anoxygenic
1708 photosynthesis was using Fe^{2+} as an electron donor, as H_2S was available from microbial sulfate
1709 reduction at these depths. These studies highlighted the need to not just detect anoxygenic
1710 phototrophs, but to perform additional measurements to infer whether or not they are actively
1711 coupling photosynthetic Fe^{2+} oxidation to carbon fixation. Put concisely, finding the organisms
1712 at the scene of the crime does not necessarily implicate them as the criminals. Additional
1713 physical evidence is necessary.
1714 Both purple bacteria and GSB populate the illuminated chemocline of ferruginous Lake
1715 La Cruz, Spain (Walter et al., 2014). In this system, Fe^{2+} stimulated light-driven carbon fixation in

the presence of an inhibitor of photosystem II in oxygenic photosynthesis [3-(3,4-dichlorophenyl)-1,1-dimethylurea; DCMU], indicating the role of photoferrotrophy to carbon fixation in Lake La Cruz. A unique aspect of this study was quantification of a light-dependent Fe^{2+} oxidation rate, 2.6 µmol L^{-1} h^{-1} (Walter et al., 2014). The authors note this is on the low end of rates measured with pure cultures (Hegler et al., 2008; Kappler et al., 2005; Wu et al., 2014). However, the number of photoferrotrophic cells was not directly measured in Lake La Cruz. A lower cell density in Lake La Cruz vs. in culture could account for this difference. An enrichment culture from the lake, which was composed of 80 % GSB closely related to *Chlorobium ferrooxidans*, was also able to perform light dependent Fe^{2+} oxidation.

One ferruginous water body where photoferrotrophs have been documented to be a significant part of the microbial community, and contribute significantly to primary productivity, is Kabuno Bay, a sub-basin of Lake Kivu in the Democratic Republic of Congo (Llirós et al., 2015). Several hundred µM Fe^{2+} is present in the illuminated Fe^{2+}-oxygen redoxcline, and about 30 % of the 16S rRNA sequences retrieved from this depth were closely related to a GSB isolate known to oxidize Fe^{2+} rather than sulfide (*Chlorobium ferrooxidans* strain KoFox). Furthermore, up to 28 % of primary productivity in the photic zone was attributed to photoferrotrophy (Llirós et al., 2015). *In situ* and *ex situ* incubations of the *Chlorobiaceae* community demonstrated that these organisms were oxidizing Fe^{2+} via anoxygenic photosynthesis, with negligible use of sulfide, and a closely-related isolate from the site was also able to perform photoferrotrophy (Llirós et al., 2015). Iron oxidation rates were 4.1 µmol L^{-1} h^{-1}. *Chlorobium phaoferrooxidans*, a photoferrotroph with 99 % 16S rRNA similarity to *C. ferrooxidans* has also been isolated from Kabuno Bay (Crowe et al., 2017).

Photoferrotrophy may have a wider impact than in just the illuminated Fe^{2+}-oxygen redoxclines of ferruginous, meromictic lakes. Berg et al., (2016) found evidence for light-driven iron cycling in sulfidic, meromictic Lake Cadagno in Spain. Iron cycling was rapid in the zone of the Fe^{2+}-oxygen redoxcline, where ferrous iron appeared in micromolar quantities, but above the depth of sulfide appearance. Enrichments of anoxygenic phototrophs from the chemocline performed light-driven CO_2 fixation, although the oxidation of Fe^{2+} was difficult to discern, likely due to rapid scavenging by Fe^{3+}-reducers in the enrichment culture. Another unique aspect of this system was the dominance of purple bacteria, *Chromatium* sp. in the zone of putative photosynthetic Fe^{2+} oxidation. *Chromatium* sp. made up more than 60 % of the microbial community, while the GSB *Chlorobium* sp. made up 4.9 to 6.4 % of the microbial species. The light intensity at the zone of Fe^{2+} oxidation in this lake was 0.5-3.2 µmol quanta m^{-2} s^{-1}, higher than other ferruginous lakes where photoferrotrophy was implicated. GSB likely have lower light requirements, and are observed to populate deeper portions of water columns that are also inhabited by purple bacteria (Camacho et al., 2017b).

Other putative biomarkers indicative of microbes that could have inhabited anoxic portions of sunlit water columns (i.e. anoxygenic phototrophs) have been proposed. For example, the presence of the carotenoids chlorobactane and isorenieratane in the rock record have been linked to green-colored and brown-colored GSB (Mallorquí et al., 2005; Summons and Powell, 1987, e.g. 1986). Similarly, the carotenoid okenane strictly infers the presence of PSB (Brocks et al., 2005; Brocks and Schaeffer, 2008). In addition, sedimentary derivatives of Bchl *a* and *b* provide evidence for PSB and PNSB, and Bchl *c*, *d*, and *e* for GSB (see Table 5 in

1759 Castañeda and Schouten, 2011 for a review of sedimentary pigments and their target
1760 organisms).

1761 There is a limited ability of specific pigments in past marine sediments to infer water
1762 column redox conditions. For instance, the presence of the aforementioned carotenoids in the
1763 rock record has typically inferred euxinic conditions, since many GSB and purple bacteria can
1764 oxidize hydrogen sulfide (see references above). However, the oceans were commonly
1765 ferruginous, not euxinic, for much of early Earth's history (sec. 2). Photoferrotrophs have been
1766 documented to oxidize sulfur species in addition to Fe^{2+} (Laufer et al., 2017; Straub et al., 1999),
1767 and they can perform cryptic iron cycling in euxinic meromictic lakes (Berg et al., 2016).
1768 Chlorobactene, a carotenoid distinguishing GSB that have been found in the rock record has
1769 been extracted from the photoferrotroph *C. ferrooxidans* (Hegler et al., 2008).

1770 Walter et al. (2014) documented a possible inorganic biosignature of photoferrotrophy
1771 in the water column of ferruginous Lake La Cruz in Spain. A secondary Fe^{3+} peak was present
1772 below the Fe^{2+}-oxygen redoxcline and was attributed to oxygen-dependent Fe^{2+} oxidation. This
1773 interpretation was supported with Fe^{2+}-dependent carbon uptake experiments at that depth.
1774 However, the influence of cyanobacteria on Fe^{2+}-oxidation resulting in the secondary Fe^{3+} peak
1775 remains ambiguous, and photoferrotrophs are likely also supported by sulfide, which exceeded
1776 100 µM in anoxic waters (Walter et al., 2014). Although the anoxic Fe^{3+} peak is a promising
1777 geochemical signature, it needs to be confirmed in other low-sulfide systems.

1778 Photoferrotrophs may also leave a distinct biosignature in the carbon speciation and
1779 isotopic composition of ferruginous lakes. Equation 1 predicts that active photoferrotrophs will
1780 draw down DIC concentrations, produce Fe^{3+}, and generate acidity. Hence, high-resolution

profiling of lake water DIC and pH, in addition to particulate Fe^{3+}, would be useful to indicate photoferrotrophic activity. Another anticipated influence of photoferrotrophy on carbon cycling is more positive $\delta^{13}C_{DIC}$ shifts due to preferential fixation of ^{12}C- DIC during carbon fixation. This enrichment should co-locate to an anoxic Fe^{3+} peak and be below any heavy $\delta^{13}C_{DIC}$ attributable to oxygenic photosynthesis in the oxic zone. Savvichev et al. (2017) also noted a shift to heavier $\delta^{13}C_{DIC}$ at the depth of maximum anoxygenic photosynthetic carbon fixation in Lake Svetloe, although cyanobacteria were likely also contributing to a peak in oxygenic photosynthetic carbon fixation and the isotope shift at this depth. A heavy $\delta^{13}C_{DIC}$ peak was also observed at the chemocline of Brownie Lake, Minnesota (**Figure 13**; Wittkop et al., 2020b), but overlap with a subsurface Chlorophyll *a* (Chl *a*) peak, indicating that detailed work is needed to decouple anoxygenic vs. oxygenic photosynthetic contributions to carbon fixation.

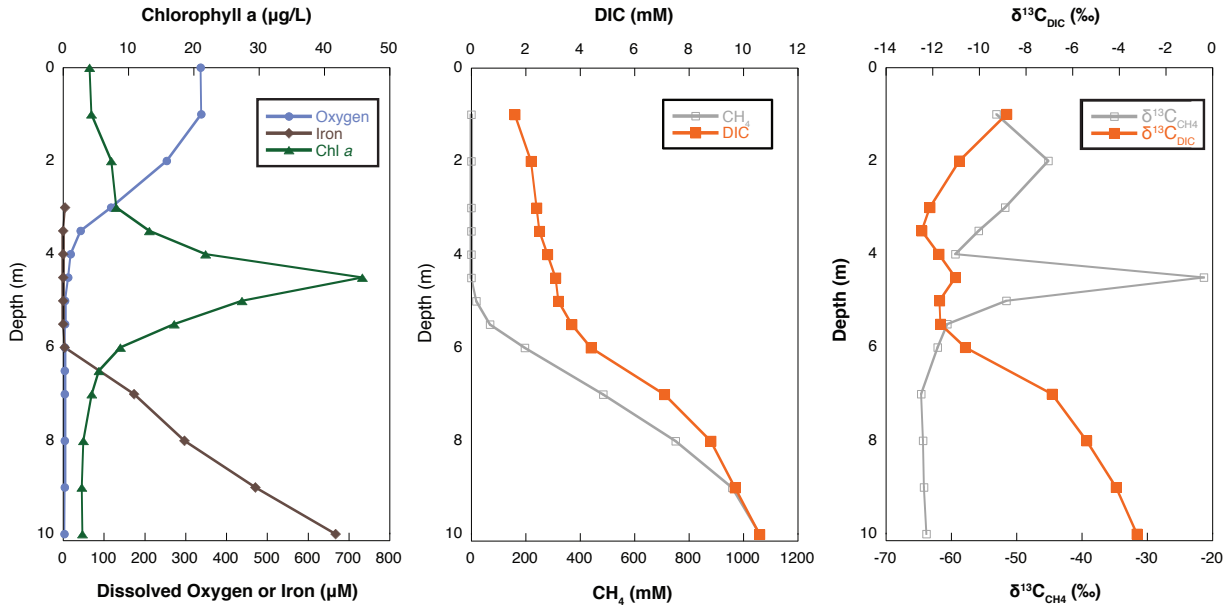

Figure 13. Depth-resolved trends at ferruginous Brownie Lake, Minnesota, USA (May 2017). The dissolved iron-oxygen redoxcline coincides with a subsurface chlorophyll maximum, and distinct

1795 shifts in $\delta^{13}C_{DIC}$ and $\delta^{13}C_{CH4}$. Photosynthetic carbon fixation (oxygenic and/or anoxygenic) and
1796 methane oxidation both have the capacity to modulate the $\delta^{13}C_{DIC}$, yet these processes are
1797 likely occurring at similar depths in Brownie Lake.

1798 Photoferrotrophy has been argued to be a common pathway in millions of holomictic or
1799 dimictic lakes in temperate and boreal zones, which may also be commonly ferruginous (Schiff
1800 et al., 2017). These authors tenuously link their detection of 16S rRNA sequences that are
1801 closely related to photoferrotrophs living in other ferruginous lakes to active photoferrotrophy
1802 in boreal lakes. Importantly, they did not conduct incubations that directly demonstrated
1803 photoferrotrophic activity, such as tracking carbon fixation with light/dark and Fe^{2+} or H_2S
1804 supplied incubations (e.g. Llirós et al., 2015), or tracking light and Fe^{2+}-dependent carbon
1805 fixation in lighted incubations in comparison to incubations amended with the photosystem II
1806 inhibitor DCMU (Walter et al., 2014). They utilized $\delta^{56}Fe$ variations in dissolved and particulate
1807 iron in the water column and a $\Delta^{56}Fe_{part\text{-}diss}$ of +1-2 ‰ (i.e. the difference between $\delta^{56}Fe$ of
1808 particulate and dissolved iron) below the Fe^{2+}-oxygen redoxcline as an indicator of
1809 photoferrotrophic Fe^{2+} oxidation. However, the $\delta^{56}Fe$ data did not have sufficient spatial
1810 resolution through the water column in combination with other lines of evidence (16S rRNA,
1811 Bchl pigments, carbon fixation measurements) to support this inference. Furthermore,
1812 insufficient evidence was given to falsify a competing hypothesis, specifically that these isotopic
1813 trends could be explained by abiotic or other biotic pathways for Fe^{2+} oxidation. The $\Delta^{56}Fe_{part\text{-}diss}$
1814 between dissolved Fe^{2+} and rapidly precipitated Fe^{3+} (oxyhydr)oxides is similar for
1815 photoferrotrophy, nitrate-dependent Fe^{2+} oxidation, and indirect, O_2-mediated Fe^{2+} oxidation
1816 by cyanobacteria (Croal et al., 2004; Kappler et al., 2010; Swanner et al., 2017). These scruples

aside, if ferruginous (and/or meromictic) lakes are more common than previously recognized (sec. 5; Schiff et al., 2017), there may be a significant contribution of photoferrotrophy to carbon fixation in freshwaters globally (Morana et al., 2016). Ferruginous lakes with seasonal stratification are likely to be far more common than ferruginous meromictic lakes, and so the importance of this alternative style of primary productivity could be worth evaluating on the landscape or global scale.

In addition to primary productivity attributed to photoferrotrophy, the presence of Fe^{2+} in the photic zone may influence oxygenic photosynthetic organisms. Understanding how the presence of Fe^{2+} regulates their primary productivity of oxygenic phototrophs has potentially even more far-ranging implications for the carbon cycle of millions of potentially ferruginous lakes suggested by Schiff et al. (2017). Although anoxygenic photosynthesis by Cyanobacteria using sulfide as an electron donor is well-documented (Cohen et al., 1975; Hamilton et al., 2018), an analogous process has not been documented with Fe^{2+} (Swanner et al., 2015b). Ferruginous lakes with sunlit Fe^{2+}-oxygen redoxclines seem to be a promising place to look. Further feedbacks between Fe^{2+} and primary productivity are also possible. For instance, the efficiency of carbon fixation by cyanobacteria under ferruginous conditions could be limited due to Fe^{2+} toxicity (Swanner et al., 2015a). In this capacity, the interaction of oxygen, Fe^{2+} and light may increase the concentration of reactive oxygen species (ROS), due either to Fenton-type reactions occurring outside of the cell, or in relation to iron homeostasis, Mehler reactions, and repair of oxidative damage. Such toxicity is likely more acute in high-light and well-oxygenated environments, where Fe^{2+} is supplied advectively (Swanner et al., 2015a). Iron can also be a limiting or co-limiting nutrient within the nutriclines of stratified regions of the

1839 modern ocean (Hogle et al., 2018), and a similar scenario could have played out within Fe^{2+}-
1840 oxygen redoxclines within ferruginous oceans.

1841 In ferruginous meromictic lakes, light is often a limiting factor at the Fe^{2+}-oxygen
1842 redoxcline. It is under these conditions that a perhaps even more important regulation of
1843 photosynthesis by Fe^{2+} occurs. Consider the ubiquitous subsurface chlorophyll maxima (SCM)
1844 observed in stratified marine systems, which often form areally extensive layers (i.e. SCML;
1845 Cullen, 1982; Hopkinson and Barbeau, 2008). In stratified water columns, marine SCML are
1846 characterized by a high chlorophyll to carbon ratio, and can (but may not) correspond to an
1847 increase in photosynthetic biomass (Cullen, 1982). While density gradients in salinity stratified
1848 waters are important in determining the depth of the SCML, biological factors, such as
1849 responses to light, nutrient availability and grazing are generally more important (Kononen et
1850 al., 1998). Light levels in SCML are generally 1-5 % of surface irradiance, yet these layers can
1851 contribute significantly to total primary productivity (Cullen and Eppley, 1981). SCML may also
1852 be more important than near-surface phytoplankton in new production in marine systems,
1853 (Silsbe and Malkin, 2016), as they intercept remineralized nutrients at the nitricline, which
1854 often occurs at the same depth as the SCML (Cullen, 2015). Many different types of
1855 phytoplankton are detected in marine SCML, including cyanobacteria and diatoms (Hopkinson
1856 and Barbeau, 2012).

1857 Subsurface chlorophyll maxima are thought to be common in seasonally or permanently
1858 stratified lakes in addition to marine systems (Ludlam, 1996). There has been little direct study
1859 of the dynamics of oxygenic phytoplankton in ferruginous lakes, yet SCM have been observed in
1860 some ferruginous meromictic lakes (Boehrer et al., 2017). Cyanobacteria (*Synechococcus* sp.)

made up 24 % of 16S rRNA sequences in the chemocline of ferruginous meromictic Lake Svetloe, and they likely contributed significantly to carbon fixation at depth (Savvichev et al., 2017). In addition to Chl *a*, the accessory pigment phycocyanin was absent, but phycoerythrin was detected at this depth and attributed to cyanobacteria. Phycoerythrin is synthesized as an adaptation to low-light in *Prochlorococcus* sp., and specifically to harvesting blue light, which penetrates deeper in the water column (Overmann and Garcia-Pichel, 2013). A SCM was also detected at the Fe^{2+}-oxygen redoxcline of Brownie Lake (**Figure 13**). In lakes with a sunlit Fe^{2+}-oxygen redoxcline, iron may not limit growth of oxygenic phototrophs, and growth could instead be limited by light and/or other nutrients. Exploring these controls within a chemically stratified ferruginous system will refine our understanding of how nutrient availability controlled primary productivity and the balance of new production and export from ferruginous oceans.

Subsurface turbidity peaks were abundant in a subset of Wisconsin (USA) lakes, and referred to as "microstratification" (Stewart et al., 1965). In these lakes, enhanced turbidity was linked to higher bacterial abundance (Whitney, 1938). Subsurface turbidity peaks were also found in four other putatively meromictic lakes (Deming, Josephine, Budd, Arco) in Itasca State Park in Minnesota (Anderson et al., 1985; Stewart et al., 2009). Some of the chemocline turbidity peaks contained filamentous cyanobacteria, while even deeper peaks contained cryptomonads and green algae (Baker and Brook, 1971). Four of the lakes studied are thought to be meromictic, with ferruginous bottom waters **(Table 4**; Baker and Brook, 1971). The SCM in Brownie Lake (**Figure 13**), which corresponds to variations in $\delta^{13}C_{DIC}$ and $\delta^{13}C_{CH4}$, which could result from oxygenic or anoxygenic photosynthesis, or methanotrophy, all of which occur near

1883 the chemocline (Lambrecht et al., 2020, 2018). Importantly, in permanently stratified lakes,
1884 density gradients can be important in explaining the accumulation of Chl *a* or biomass, but are
1885 often impossible to disentangle from gradients of nutrients, light, and temperatures (Burnett et
1886 al., 2006).

1887 A final consideration on primary productivity is the importance of chemoautotrophic
1888 carbon fixation in anoxic lakes. Savvichev et al. (2017) noted that during the winter in Lake
1889 Svetloe, most carbon fixation was attributed to dark processes, presumably
1890 chemolithoautotrophy, such as oxidation of hydrogen sulfide with nitrate. In Lake Kuznechikha,
1891 oxygenic and anoxygenic photosynthesis were most significant to summer carbon fixation, but
1892 dark fixation was not negligible (Gorlenko et al., 1980). Populations of putative
1893 chemolithoautotrophic iron and sulfur-oxidizing microbes have been observed in Lake Pavin
1894 (Berg et al., 2019; Lehours et al., 2007). The importance of chemolithoautotrophic carbon
1895 fixation therefore should not be ignored, particularly in winter when light is limiting or in lakes
1896 where light does not illuminate the chemocline.

1897 Another type of photosynthesis that could be potentially important in stratified lakes is
1898 aerobic anoxygenic photosynthesis. The aerobic anoxygenic phototrophs (AAP) are
1899 taxonomically and morphologically diverse and are ubiquitous in the environment. For
1900 example, a recent study showed AAP were detected in every freshwater interrogated (Ferrera
1901 et al., 2017). These organisms can be distinguished from oxygenic phototrophs based on the
1902 presence of Bchl *a*, although this pigment is also synthesized by other anoxygenic phototrophs
1903 (Yurkov and Hughes, 2013). They grow under oxic conditions and are obligate heterotrophs
1904 because they lack the enzyme RuBisCO, which is necessary for the Calvin cycle of

1905 photosynthesis (see Yurkov and Hughes, 2013 and references therein). AAP can augment their
1906 energy production through light-driven anaplerotic reactions, which feed intermediates into the
1907 TCA cycle (Yurkov and Hughes, 2013), and this ability provides a competitive advantage against
1908 other heterotrophs. In contrast to other photosynthetic organisms discussed to this point, AAP
1909 consume organic carbon rather than synthesize it. Nevertheless, the potential of AAP to cycle
1910 carbon, distinct from non-photosynthetic heterotrophs, may be large globally (Kolber et al.,
1911 2001, 2000), but has only been emphasized for marine systems.

1912 When parsing which types of photosynthetic reactions will be supported at different
1913 depths in ferruginous lakes, light should be a first order constraint, both in terms of quantity,
1914 the amount of irradiance, and its quality for photosynthetic organisms, namely its wavelength.
1915 Photosynthetically active radiation (PAR) are photons with wavelengths between 400-700 nm,
1916 which comprise the majority of wavelengths utilized by photosynthetic organisms, but each
1917 class of phototroph synthesizes pigments specialized in absorption of light of specific
1918 wavelengths (which are also potential organic biomarkers, discussed above). In Cyanobacteria,
1919 for instance, Chl *a* and accessory pigments such as phycocyanin give rise to strong absorption of
1920 light around 430 nm and 660 nm, and 605 nm, respectively. In purple bacteria, Bchl *a* or *b* is the
1921 dominant light-harvesting complex with light absorption patterns around 375 nm and 770 nm,
1922 and 400 nm and 790 nm (Oren, 2011). In addition to absorption and attenuation of light by
1923 photosynthetic microbes, certain wavelengths can also be attenuated by other substances in
1924 the environment, with water absorbing red and infrared light, and “yellow substances” or
1925 dissolved organic carbon (DOC) in lakes preferentially absorbing UV and blue light (Overmann
1926 and Garcia-Pichel, 2013).

Oxygenic phototrophs need the highest light quantities to sustain growth, with an oft-cited requirement 1 % of surface PAR, although a true lower limit is thought to be 0.01 µmol quanta m^{-2} s^{-1} (Raven et al., 2000). In Brownie Lake in May 2017 (**Figure 13**), the SCM occurred at 4.5 m with 0.6 µmol quanta m^{-2} s^{-1}. The lowest detectable PAR was 0.02 µmol quanta m^{-2} s^{-1} at 5.5 m. If a stratified community of photosynthetic organisms exist, purple bacteria should be just below, as they require anoxic conditions, but also longer wavelengths that are attenuated more readily in the water column. Purple bacteria have been observed in Lake La Cruz at 0.1 % of surface PAR, although absolute PAR values were not given (Camacho et al., 2017b). Green sulfur bacteria should be the deepest-dwelling phototrophs in the water column, both because of their utilization of the shorter/blue wavelengths that persist in deep waters and their tolerance of low light (Overmann and Garcia-Pichel, 2013). The lower light limit needed to support GSB communities has been suggested to be less than 0.00075 µmol quanta m^{-2} s^{-1} (equivalent to 0.0003 % of surface PAR; Manske et al. 2005), based on observations of active GSB at more than 100 m depth in the Black Sea. In Kabuno Bay, GSB in the chemocline were sustained by 0.01-0.1 % of surface PAR (Llirós et al., 2015), however, absolute units were not given in that study.

Importantly, GSB may be present in stratified systems, but may not be very active if light has become too limiting. For example, Crowe et al. (2014a) noted that carbon fixation attributable to anoxygenic phototrophs in Lake Matano, although negligible to overall productivity in the lake, approached theoretical maximum values based on the light available (0.003 % of surface PAR or 0.12 µmol quanta m^{-2} s^{-1}). Their results indicated that light was the limiting factor determining growth of the population of anoxygenic phototrophs. It is unclear to

what extent such light-limited communities can persist and become active if and when light is again sufficient. For instance, *Chlorobium* sp. have been detected at 70 m in Lake Pavin and are implicated in sulfur-driven anoxygenic photosynthesis (Berg et al., 2019). The involvement of GSB in photoferrotrophy in Lake Pavin is thought to be negligible based on low relative abundances compared to GSB in Lake Matano and Lake La Cruz (Berg et al., 2019).

Canyon Lake in Michgan, USA also has a deep chemocline (16-17 m; defined by a sharp increase in specific conductance), but a seasonally variable oxycline, which causes the Fe^{2+}-oxygen redoxcline to overlie the chemocline (Lambrecht et al., 2018). The deepest depth at which light was detected, equivalent to 0.01 µmol quanta m^{-2} s^{-1}, was also seasonally variable, and generally occurred at or above the depth of the Fe^{2+}-oxygen redoxcline (**Figure 14**). However, very few 16S rRNA sequences related to anoxygenic photosynthetic bacteria were observed in that water column, with little evidence for an increased population at the Fe^{2+}-oxygen redoxcline (**Figure 14**). Notably, these sequences persisted throughout a summer. Although absolute light penetration depth is rarely quantified from lakes, this observation might imply that photoferrotrophy may not be a significant pathway in ferruginous lakes with deep Fe^{2+}-oxygen redoxclines.

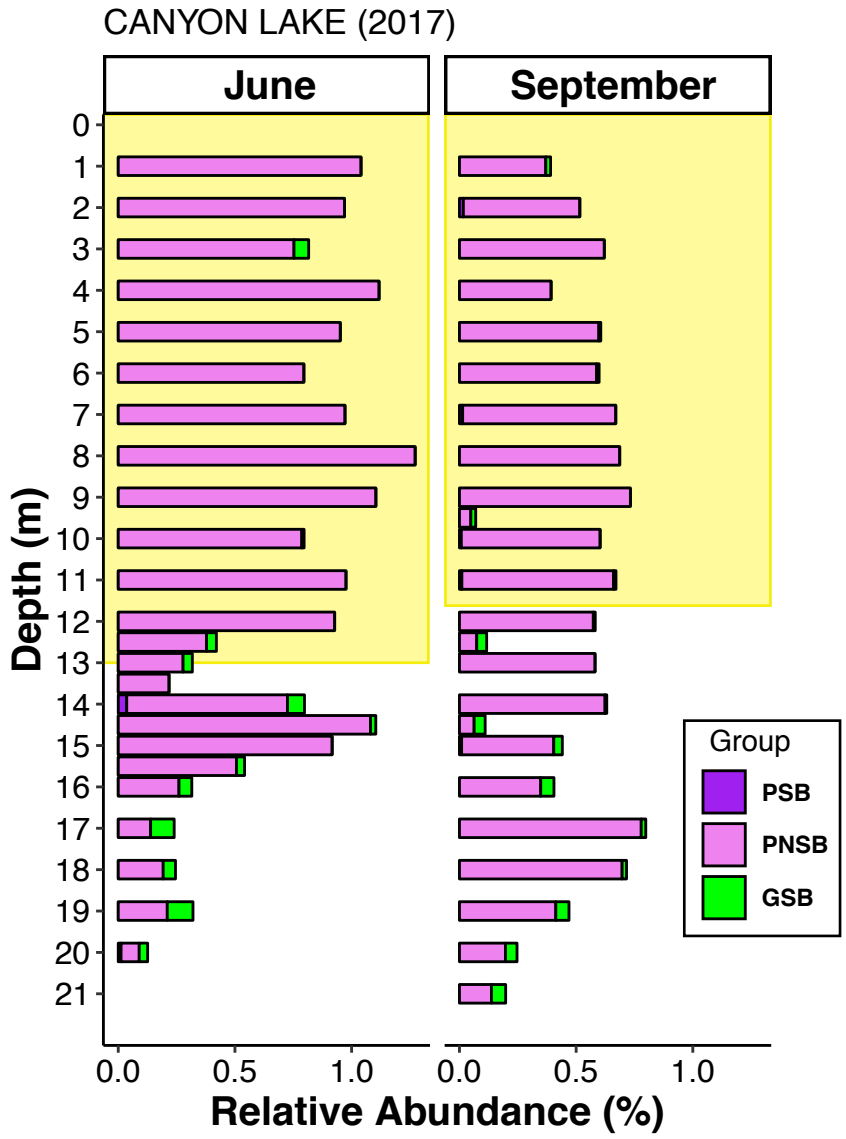

Figure 14. Abundance of anoxygenic phototrophic bacteria in the water column of Canyon Lake, Michigan in 2017. The yellow boxes denote the photic zone. The bottom of the photic zone represents 0.02 µmol quanta m^{-2} s^{-1} in June and 0.03 µmol quanta m^{-2} s^{-1} in September (~ 0.01 % surface irradiance). The Fe^{2+}-oxygen redoxcline occurred at 13 m in June and 10 m in September (Lambrecht et al., 2018). Sulfate concentrations are <5 µM in Canyon Lake, and free hydrogen sulfide was infrequently detected.

Methane

A notable feature of many ferruginous lakes studied to date is the abundance of methane below the chemocline (Hongve, 1980). Methane can be introduced to volcanic lakes through sublacustrine springs (Pasche et al., 2011), but the observation of large reservoirs of methane in the monimolimnion persists across non-volcanic ferruginous lakes (Camacho et al., 2017a; Lambrecht et al., 2020; Savvichev et al., 2017). For example, Brownie Lake and Canyon Lake have maximum methane concentrations of 1,050 and 1,980 µM, respectively (Lambrecht et al., 2018). Tropical Lake Matano and karstic Lake La Cruz have comparable maximum values of 1,400 and 2,200 µM, respectively (Crowe et al., 2011; Oswald et al., 2016). In addition, Lake Pavin, a volcanic crater lake, contains methane at >4,000 µM in the monimolimnion (Lopes et al., 2011; Michard et al., 1994).

Methanogenesis is likely to be the source of methane when $\delta^{13}C_{CH4}$ is -50 to -110 ‰ (Whiticar, 1999). Methanogenesis could be the major pathway for organic carbon degradation in ferruginous lakes due to the generally low availability of other electron acceptors for heterotrophic metabolisms (e.g. oxygen, nitrate, sulfate; Crowe et al., 2011; Hayes and Waldbauer, 2006). Other factors controlling the production of methane in lakes includes temperature and the type of organic carbon present as substrate for methanogenesis. Increasing freshwater sediment temperature generally correlates with an increased rate of methanogenesis (Bastviken, 2009 and references therein; Zeikus and Winfrey, 1976). Furthermore, methane production rates in lake sediment incubations have been observed to significantly increase when the source of organic carbon is phytoplankton-derived vs. terrestrial (West et al., 2012).

Methane is generally thought to be confined to the bottom waters due to efficient microbial oxidation pathways at the chemocline (Oswald et al., 2016). Oxidation occurs primarily by the activity of methanotrophic bacteria under suboxic conditions (Lambrecht et al., 2020; Oswald et al., 2016; Savvichev et al., 2017). However, AOM by archaea and even bacteria using electron acceptors such as nitrate, sulfate, or even $Fe^{3+}/Mn^{3+/4+}$ (oxyhydr)oxides has been proposed to occur in ferruginous lakes (Crowe et al., 2011; Lopes et al., 2011; Oswald et al., 2016). Recently, methane oxidation in the anoxic and ferruginous monimolimnion of Lake Matano was detected in incubations containing $^{14}CH_4$ (Sturm et al., 2018). Sulfate was a likely electron acceptor, and the authors also noted that methane assimilation was significant in the anoxic zone. This process may not be important in all ferruginous lakes, as AOM organisms were an insignificant portion of the microbial community and the metabolism had the process had marginal energetics in comparison to oxygen-dependent bacterial methanotrophy in Brownie and Canyon Lakes (Lambrecht et al., 2020).

Evidence for active methane oxidation and mitigation of dissolved methane in the water column have been taken as evidence that fluxes of methane to the atmosphere out of ferruginous lakes are negligible (Oswald et al., 2016; Sturm et al., 2018). However, most of these studies base these inferences on concentration profiles of methane, representing a diffusional flux. Several other emission pathways besides diffusion are at play in lakes and can be much more significant, especially in shallower lakes, at releasing methane to the atmosphere (Bastviken et al., 2004). Direct measurements of the methane flux from Brownie and Canyon Lakes indicated that non-diffusional pathways make up the majority of methane emissions (Lambrecht et al., 2020). Non-diffusional pathways can include bubbling of methane

from the sediment to the atmosphere (i.e. ebullition), release of methane stored in anoxic bottom waters upon seasonal mixing, transport through root systems of littoral plants (Bastviken et al., 2004), and lateral transport from littoral areas (Lambrecht et al., 2020).

Other element and nutrient cycles

Koeksoy et al. (2015) point out that aquatic settings where Fe^{2+} and sulfide co-exist are rare, but are necessary to understand Proterozoic oceans, which record an increasing reservoir of sulfate and transitions between ferruginous and euxinic conditions (sec. 2). Free bisulfide (HS^-), the predominant species at circumneutral pH, is likely to be in low abundance due to rapid precipitation of iron monosulfides with Fe^{2+} (e.g. FeS). The activities of Fe^{2+} and HS^- in equilibrium with mackinawite (FeS) are governed by their solubility product (K_{sp}; Morse and Arakaki, 1993):

$$K_{sp} = \frac{a_{Fe2+} * a_{HS-}}{a_{H+}} = 10^{-3.64} \quad \text{(eq. 4)}$$

Approximating concentration as activity (a reasonable assumption for dilute waters), at a pH of 8, 1.5 µM of both Fe^{2+} and HS^- could coexist. Higher concentrations may be permissible if aqueous complexes or organic ligands are present. For instance, in meromictic Lake Malawi, up to 4 µM HS^- are detected, indicating weakly sulfidic conditions that likely scavenge Fe^{2+}. Yet sedimentary accumulations of iron indicate that this lake may switch between being sulfidic and ferruginous (J. Li et al., 2018). Low concentrations of Fe^{2+} and HS^- may also occur near the chemocline of ferruginous and/or sulfidic lakes, allowing for cryptic microbial cycling of these elements. For instance, 10 µM Fe^{2+} co-occurred with 2 µM HS^- in Lake Svetloe (Savvichev et al., 2017). Four µM HS^- was observed in the presence of tens of µM Fe^{2+} in Lake Matano, and could

provide a niche for sulfide-oxidizing anoxygenic phototrophs in ferruginous lakes (Crowe et al., 2014a). Conversely, the presence of 1-2 µM Fe^{2+} above sulfidic deepwaters can support Fe^{2+}-based anoxygenic photosynthesis (Berg et al., 2019). In ferruginous meromictic lakes, microbial sulfate reduction rates increase below the oxycline (Crowe et al., 2014a; Savvichev et al., 2017). Sulfate-reducing bacteria may be as active as Fe^{3+}-reducing bacteria at the chemocline of Lake Pavin despite substrate limitation (<20 µM sulfate; Berg et al., 2019), and sulfate reduction rates are highest near the oxycline (Busigny et al., 2014).

While iron monosulfides can be saturated in the water column of ferruginous lakes, the role of sulfide in precipitation of iron from ferruginous lakes may also be more complicated than represented by eq. 4. Iron monosulfides were suggested to be in the sediments of Lake Pavin based on the extractability of this phase (Busigny et al., 2014). Pyrite is present in sediments, but not at their surface (Cosmidis et al., 2014; Viollier et al., 1997). Within the water column, aqueous or colloidal FeS_{aq} clusters, detected with voltammetric microelectrodes, are the predominant particulate form of reduced sulfur (Bura-Nakić et al., 2009). It has been suggested that the formation of FeS_{aq} clusters prevents formation of pyrite in ferruginous lakes (Luther et al., 2003). However, these species were not detected by X-ray absorption spectroscopy (XAS) in Lake Pavin (Cosmidis et al., 2014). While the total amount of iron increased in particulate matter with depth in Lake Pavin, phyllosilicates and Fe^{3+} (oxyhydr)oxides dominated the iron speciation above the chemocline, Fe^{3+}-phosphates formed at the chemocline, and Fe^{2+}-bearing phosphates (e.g. vivianite) predominated in the deepest waters and sediments (Cosmidis et al., 2014). The mineralogy of authigenic water column precipitates has not been intensely investigated in many ferruginous lakes, as poorly crystalline

2062 iron minerals are both difficult to preserve upon collection, and difficult to detect with
2063 traditional methods such as XRD. However, the solubility of different iron minerals will depend
2064 on the availability of iron and other mineral-forming anions in the environment. In Lake
2065 Matano, which is extremely phosphate-limited, green rust forms in the chemocline, as detected
2066 by transmission electron microscopy and synchrotron-based X-ray techniques on particulate
2067 matter (Zegeye et al., 2012). Green rust can contain hydroxyl, carbonate, sulfate, and/or
2068 chloride ions, and so the specific iron minerals forming likely reflect which anions exceed
2069 solubility of their respective iron mineral phases.

2070 The persistence of Fe^{3+} (oxyhydr)oxides below the chemocline of ferruginous waters has
2071 been documented, but such phases are absent in sediments of Lake Pavin, having already
2072 undergone transformation to vivianite (Cosmidis et al., 2014). Lake Matano sediments contain
2073 40-60 % Fe^{3+} (oxyhydr)oxides (Crowe et al., 2004), which are detritally sourced from lateritic
2074 soils (Crowe et al., 2008b). Neighboring Lake Towuti contains amorphous Fe^{3+} (oxyhydr)oxides
2075 in sediments, which are associated with carbonate green rusts and siderite (Vuillemin et al.,
2076 2019b). Both lakes also contain magnetite (Bauer et al., 2020). The reasons that Fe^{3+}
2077 (oxyhydr)oxides sediment in some lakes and not others may be due to limited organic carbon
2078 availability for microbial Fe^{3+} reduction, competition of methanogenesis with Fe^{3+} reduction
2079 (Roden and Wetzel, 2003), or aging or passivation of the mineral surfaces in ferruginous waters,
2080 making them inaccessible for further microbial reduction (Bray et al., 2017; Roden and Urrutia,
2081 2002). Therefore any effect on nutrient removal from ferruginous waters by adsorption to Fe^{3+}
2082 (oxyhydr)oxides (Bjerrum and Canfield, 2002; Konhauser et al., 2007) may depend on whether
2083 they survived the journey through the water column. While iron phosphate minerals provide a

2084 sedimentation path for removal of phosphate in ferruginous waters (Cosmidis et al., 2014),
2085 green rusts also potentially scavenge micronutrients, such as nickel (Zegeye et al., 2012).
2086 Microbes play a key role in mediating diagenetic reactions that transform iron and
2087 nutrients or other redox-active elements to forms that can precipitate as iron-bearing minerals
2088 in sediments. Enrichments of Lake Matano sediments yielded active microbial Fe^{3+} reduction,
2089 but only when provided with ferrihydrite (Bray et al., 2017). More crystalline forms of Fe^{3+}
2090 (oxyhydr)oxides such as goethite resulted in less Fe^{3+} reduction but did stimulate
2091 methanogenesis. The authors ascribed this to the lower energy yield of Fe^{3+} reduction with
2092 more crystalline minerals, with organic and H_2 substrates rather being used by methanogens. In
2093 Lake Towuti, sulfate-reducing bacteria were active in ferruginous sediments, despite low sulfate
2094 concentrations (usually <20 μM) (Vuillemin et al., 2016).
2095 The cycles of iron and phosphate are intimately linked in ferruginous lakes, as
2096 phosphate adsorbs strongly to Fe^{3+} (oxyhydr)oxides. Therefore, phosphate concentrations often
2097 increase dramatically in the bottom waters of ferruginous lakes. The concentrations of
2098 phosphate in ferruginous lakes vary widely, however, and likely depend on the trophic status of
2099 the lake. Microbes likely play an active role in phosphorus cycling within ferruginous lakes.
2100 Biological pathways for sedimentation of nutrients, specifically phosphate, could also prove
2101 important for sequestration in sediments. For instance, abundant intracellular polyphosphate
2102 was observed in microbes within Lake Pavin sediments, and vivianite was the predominant iron
2103 mineral in sediments (Cosmidis et al., 2014). Numerous other microbial pathways exist for
2104 sequestering nutrients intracellularly, especially in anaerobes. For instance, nitrate,
2105 polyphosphate and polysulfide are stored in vacuoles of the benthic sulfide-oxidizing bacteria

2106 *Beggiatoa* (Schulz-Vogt, 2011), indicating that intracellular nutrient storage could be an
2107 important pathway for delivering nutrients in sediments. Recently, vivianite nodules were
2108 reported from ferruginous Lake Towuti (A Vuillemin et al. 2019), formed through diagenetic
2109 processes involving microbial Fe^{3+} and sulfate reduction (Vuillemin et al., 2018).
2110 In Kabuno Bay of Lake Kivu, ammonium was the predominant form of nitrogen below
2111 the chemocline, with fixed nitrogen virtually absent in overlying water (Michiels et al., 2017).
2112 Reduction of nitrate (NO_3^-) to N_2 was extremely rapid at the chemocline, but a significant
2113 portion of nitrate was reduced to ammonium, which was retained as fixed nitrogen and
2114 available for subsequent assimilation. Ferrous iron amendments stimulated nitrate reduction to
2115 both N_2 and ammonium (Michiels et al., 2017). Most other ferruginous meromictic lakes
2116 investigated to date have abundant ammonium below the chemocline as was observed in
2117 Kabuno Bay (Lambrecht et al., 2018; Sibert et al., 2015), likely resulting from remineralization of
2118 organic nitrogen. In meromictic Lake Malawi, which is currently sulfidic but has been
2119 ferruginous in the past (sec. 4), ammonium oxidation and nitrification at the oxycline followed
2120 by denitrification explain the reaction zone for ammonium, more abundant in deep waters, and
2121 nitrate, more abundant in oxic waters (J. Li et al., 2018). In Lake Pavin, nitrate was more
2122 abundant than ammonium throughout the epilimnion, and supported primary production in
2123 phytoplankton who first reduced nitrate to ammonium (Mallet et al., 1998). Many other
2124 microbial nitrogen transformations could contribute to the nitrogen cycle in ferruginous lakes,
2125 including anaerobic nitrate reduction coupled to Fe^{2+} oxidation and/or chemodenitrification
2126 (Stanton et al., 2018), or Fe^{3+} reduction coupled to ammonium oxidation (Busigny et al., 2013).
2127 In Brownie Lake, the chemocline and Fe^{2+}-oxygen redoxcline co-occur with a minimum N:P,

indicating potential nitrogen limitation (**Figure 15**). Further work could explore whether N_2-fixation is active at this depth, and if Cyanobacteria or GSB are involved (Halm et al., 2009).

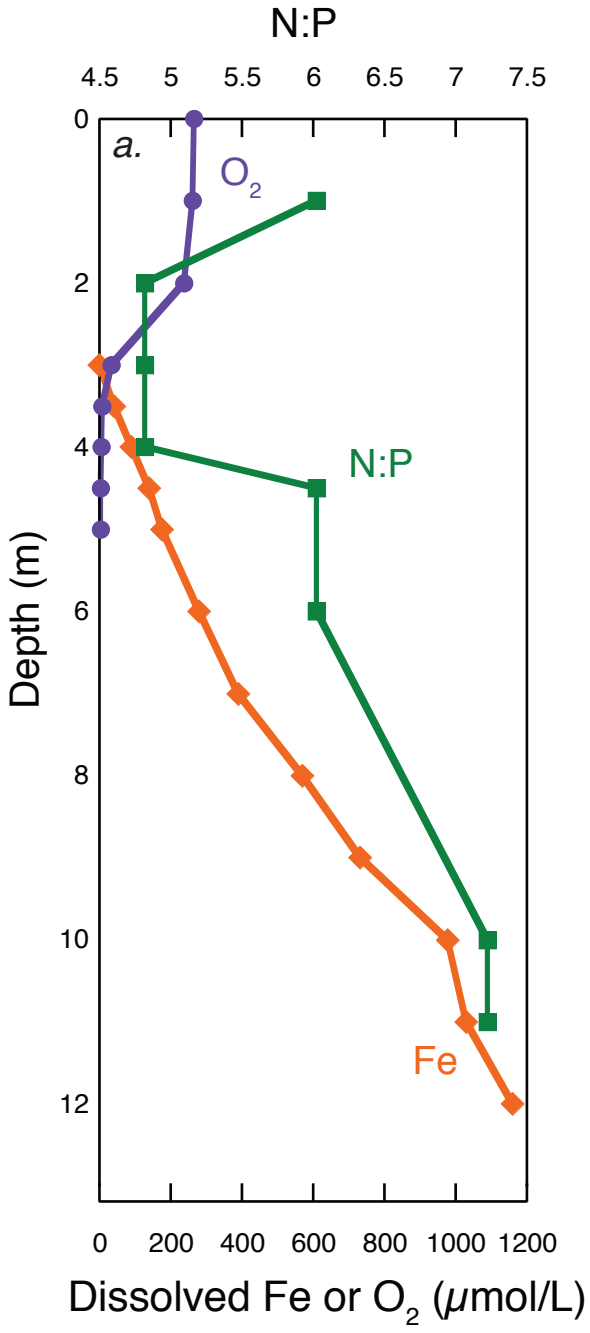

Figure 15. An N:P minimum in Brownie Lake occurs at the Fe^{2+}-oxygen redoxcline, which could be a site of N-limitation and/or N_2-fixation.

An active cycle between ferrous and ferric iron has been recognized to turnover iron rapidly across the oxycline of stratified waters. Microbes capable of non-photosynthetically oxidizing Fe^{2+} have been detected at the oxycline of ferruginous lakes by microscopic observation (Gorlenko et al., 1980). Magnetotactic bacteria, who perform non-metabolic redox transformations of iron and are detectable through magnetic techniques, are in greatest abundance at the oxycline of Brownie Lake, and occur in the anoxic sediments (Lascu et al., 2010). Non-photosynthetic Fe^{2+}-oxidizing and Fe^{3+}-reducing bacteria, detected by 16S rRNA and culturing efforts, were more abundant than photosynthetic Fe^{2+}-oxidizing bacteria within the chemocline of Lake Pavin (Berg et al., 2019; Lehours et al., 2009).

From study of past ocean sediments, several observations regarding the iron isotope budget of ferruginous oceans have been made, which can be informed by work in modern systems. In meromictic ferruginous lakes, dissolved iron $\delta^{56}Fe$ is heavy deep in the water column, but becomes lighter as dissolved iron concentrations diminish upward in the water column, toward the Fe^{2+}-oxygen redoxcline (Busigny et al., 2014; Malinovsky et al., 2005; Teutsch et al., 2009). This is interpreted to reflect distillation of heavy isotopes into Fe^{3+} (oxyhdyr)oxides following Fe^{2+} oxidation at the Fe^{2+}-oxygen redoxcline. A similar trend in dissolved $\delta^{56}Fe$ occurs at the chemocline of sulfidic meromictic Lake Cadagno (Ellwood et al., 2019). These examples corroborate interpretation of iron isotope data within a Neoarchean setting (Czaja et al., 2012; Eroglu et al., 2018).

2154 Iron isotope trends are also influenced by iron sulfide precipitation under anoxic
2155 conditions. In Lake Pavin the residual light $\delta^{56}Fe$ of dissolved iron also co-occurs with an FeS_{aq}
2156 species, a possible precursor for pyrite, leading to the suggestion that pyrite is a sink for
2157 residual light dissolved iron at the Fe^{2+}-oxygen redoxcline (Bura-Nakić et al., 2009; Busigny et
2158 al., 2014). In the Black Sea basin, dissolved iron occurs in a wedge above the euxinic bottom
2159 waters, and the $\delta^{56}Fe$ of dissolved iron increases by 3‰ into the sulfidic water (Rolison et al.,
2160 2018). The authors suggested that isotopically light iron is directly scavenged into sulfides at the
2161 base of the ferruginous layer (Rolison et al., 2018). These examples provide evidence within an
2162 Fe^{2+}-oxygen redoxcline and a ferruginous-sulfidic transition zone to support pyrite as a sink for
2163 light iron (i.e. Rouxel et al., 2005).
2164 Iron isotope systematics above ferruginous chemoclines remain underexplored,
2165 however. At Lake Cadagno, residual dissolved iron trended lighter upward into the oxycline, but
2166 underwent a 1 ‰ increase in $\delta^{56}Fe$ above the oxycline before returning to near 0 ‰ in the
2167 epilimnion (Ellwood et al., 2019). The authors attributed this excursion to the activity of
2168 photoferrotrophs at this depth (cf. Berg et al., 2016). However, no explanation was given for
2169 how photoferrotrophy would produce this heavy $\delta^{56}Fe$ in dissolved iron, as experimental
2170 determination of iron isotope fractionation during oxidation by these organisms always leaves
2171 residual dissolved iron isotopically lighter than the precipitated Fe^{3+} (oxyhydr)oxides (Croal et
2172 al., 2004; Swanner et al., 2015c; Wu et al., 2017). Heavier dissolved iron in oxic waters could
2173 also result from iron's complex role as a nutrient, particle, colloid, and ligand-bound element in
2174 the photic zone of lakes and the ocean (Conway and John, 2015; Lotfi-Kalahroodi et al., 2019;

2175 Mulholland et al., 2015; Sun and Wang, 2018). Further explorations of this oxic iron cycle and
2176 could be explored as indicators of oxygenic photosynthesis (e.g. Swanner et al., 2018).
2177 Molybdenum cycling has been investigated in euxinic meromictic lakes to validate its
2178 utility as a redox proxy, particularly for euxinic conditions (Dahl et al., 2013; Dahl and Wirth,
2179 2017). However, similar work has not been done in low-sulfate ferruginous lakes, despite
2180 application of the Mo proxy to sediments inferred to have been deposited under ferruginous
2181 conditions (Czaja et al., 2012; Kurzweil et al., 2015). The utility of Mo as a paleo-redox proxy is
2182 dependent on its affinity for sulfide, which causes Mo enrichments in sediments deposited from
2183 euxinic water columns (Algeo and Rowe, 2012; Scott et al., 2008). Thiomolybdate formation,
2184 where sulfur progressively replaces oxygen, seems to be a primary mechanism for Mo
2185 sulfidation (Helz et al., 1996; Wagner et al., 2017). An iron sulfide pathway has also been
2186 suggested (Vorlicek et al., 2018), which could be relevant to ferruginous lakes where FeS
2187 colloids are forming, e.g. Lake Pavin (Bura-Nakić et al., 2009). Pyrite, however, does not seem to
2188 be the main mineral host of Mo in anoxic sediments (Chappaz et al., 2014). Molybdenum does
2189 have significant interactions with organic carbon in anoxic sediments (Dahl et al., 2017; Wagner
2190 et al., 2017), which could be relevant for ferruginous systems. Scavenging of molybdenum onto
2191 Fe^{3+} and $Mn^{3+/4+}$ (oxyhydr)oxides, which imparts a distinct isotopic fractionation (Barling and
2192 Anbar, 2004; Poulson et al., 2006), might also be important under anoxic but not euxinic
2193 conditions (Rico et al., 2019).
2194 Uranium isotopes have been have emerged as a sensitive tracer of marine redox
2195 conditions, particularly in their ability to parse anoxic vs. oxic seafloor area when coupled to an
2196 isotope mass balance (Brennecka et al., 2011a; Kendall et al., 2015; Lau et al., 2019). However,

2197 there is little constraint on the fractionations expected under anoxic and ferruginous conditions
2198 (Gilleaudeau et al., 2019; Hood et al., 2016), limiting the applicability of the uranium isotope
2199 mass balance approach in the Precambrian. Recently, $\delta^{238}U$ values were determined from
2200 water column samples of Brownie Lake, and water column and sediment samples of Brownie
2201 Lake and Lake Pavin (Cole et al., 2020). Although heavy $\delta^{238}U$ is preferentially buried in anoxic
2202 settings, the average $\delta^{238}U$ of sediments deposited from oxic and ferruginous waters were
2203 statistically indistinguishable in these lakes. However, the range of $\delta^{238}U$ was larger from
2204 ferruginous samples (Cole et al., 2020). This may reflect the variety of potential processes for
2205 soluble U^{6+} under ferruginous conditions: microbial (Stylo et al., 2015), abiotic by Fe^{2+} (Brown et
2206 al., 2018), and reduction with FeS (Hua and Deng, 2008), each with a distinct fractionation
2207 factor. Adsorption to Fe^{3+} or $Mn^{3+/4+}$ (oxyhydr)oxides (Brennecka et al., 2011b), incorporation
2208 into organic matter (Chappaz et al., 2010), complexation by carbonate (Chen et al., 2017), or
2209 precipitation with phosphate (Dang et al., 2016) are all relevant pathways in ferruginous lakes
2210 as well.

2211 The mercury cycle has not been greatly explored in ferruginous meromictic lakes but
2212 may be worth investigating. Atmospheric deposition of mercury has increased globally since
2213 industrialization, with many records of enhanced mercury deposition from lakes (Fitzgerald et
2214 al., 1998; Swain et al., 1992). Mercury methylation, which converts inorganic mercury into a
2215 form that can bioaccumulate, has generally been attributed to sulfate-reducing bacteria
2216 (Compeau and Barth, 985; Gilmour et al., 1998; Jeremiason et al., 2006). However, recent work
2217 has documented that Fe^{3+} reducing bacteria such as *Geobacteraceae* can also methylate
2218 mercury (Bravo et al., 2018; Kerin et al., 2006; Si et al., 2015). Furthermore, a variety of

anoxygenic photosynthetic bacteria have recently been shown to mediate Hg^{2+} reduction under anoxic conditions (Grégoire et al., 2018; Grégoire and Poulain, 2016; Lavoie et al., 2020). Therefore, ferruginous environments may also have significant mercury methylation or other mercury redox transformations. Lake Pavin shows increases in methymercury concentrations below the thermocline, and sharp peaks in particulate mercury, both inorganic and methylmercury, at the chemocline (Cossa et al., 1994). Mercury may be shuttled across the chemocline in association with particulate iron or manganese.

7. Conclusions

While absent from the marine waters today, ferruginous conditions were a feature of oceans throughout the Precambrian, and re-occur in the Phanerozoic. While the major source of dissolved iron in oceans that deposited IFs likely came from hydrothermal input, the sedimentation of iron-rich clastic sediments throughout the Proterozoic indicates ferruginous conditions may have been controlled by multiple processes. Emerging questions on the temporal and spatial extent of ferruginous conditions include: What caused transitions from ferruginous to euxinic and/or oxic conditions? Why did transitions occur transiently or repeatedly in some basins? Where such transitions global in nature? And what is the tipping point in basins that fluctuate between ferruginous to sulfidic or oxic, or vice versa?

While ferruginous meromictic lakes all have Fe^{2+}-oxygen redoxclines, there is much variation in their chemistry. Ferruginous meromictic lakes introduced here may provide analogues to several of the depositional settings and mineral formation pathways in ferruginous oceans (**Figure 16**). Investigation of paleoferruginous lakes that transitioned

between ferruginous, euxinic, and/or oxic conditions, such as Lake Malawi or Otter Lake, can provide insights to the physical and chemical triggers that initiate the onset of new redox regimes. The supply of iron, water level fluctuations, and the ratio of iron to sulfur have all emerged as controls on, or indicators of, shifting redox conditions. Translating the lessons from lakes to oceans requires a careful accounting for the different scales of physical processes, such as mixing dynamics (e.g. seiches vs. ocean currents). The very act of articulating these differences, however, might yield new insights about the way in which physical processes influence redox dynamics. For example, Lake Malawi's fluctuations in response to mega-droughts are temporally linked to non-ferruginous intervals. Do sea-level fluctuations, or oceanic basin restrictions also correspond to changing redox conditions and changing sedimentation? Would re-organization of ocean currents or river systems change the supply of iron in a way that affects the redox conditions within a depositional basin?

While paleoferruginous basins can help understand transitions, modern euxinic and ferruginous basins can help us elucidate the extent of active iron and sulfur cycling. Examples include cryptic iron cycling in euxinic Lake Cadagno mediated by photoferrotrophs, and iron oxidation and distillation processes in a ferruginous depth interval of the Black Sea. In ferruginous Lake Pavin, both pyrite and vivianite are sinks for iron in sediments, and pyrite captures the light residual dissolved iron that in turn reflects iron oxidation near the Fe^{2+}-oxygen redoxcline. In eutrophic ferruginous Brownie Lake, sufficient sulfate (50-100 µM) is present for a significant sulfur cycle, similar to Lake Pavin. Productive ferruginous systems that deposit pyrite may be analogous to basins that deposited ferruginous shales (**Figure 16**).

In lakes, the sources of iron are controlled by regional geology. Aside from atmospheric deposition, dissolved iron comes from runoff, streamflow, shallow recharge, groundwater seepage, or the solid iron phases in sediments. The iron sources in the oceans include terrestrial runoff, glacial sources, groundwater, atmospheric deposition, (hydrothermal) alteration of seafloor, and mobilization from sediments. As the impact of each marine source varies regionally with such factors as distance from shore or restriction, different types of lakes may provide partial analogies. Could volcanic lakes (e.g. Lake Kivu, Lake Pavin) that receive their iron through temporally variable sub-lacustrine springs echo the waxing and waning intervals of high hydrothermal iron supply to the Precambrian oceans? The groundwater inputs of iron to post-glacial lakes may fluctuate with the water table, e.g. as in Lake Nordbytjernet. Can studying the magnitudes of these fluctuations give insights to how sea-level fluctuations might have re-organized the continental iron supply?

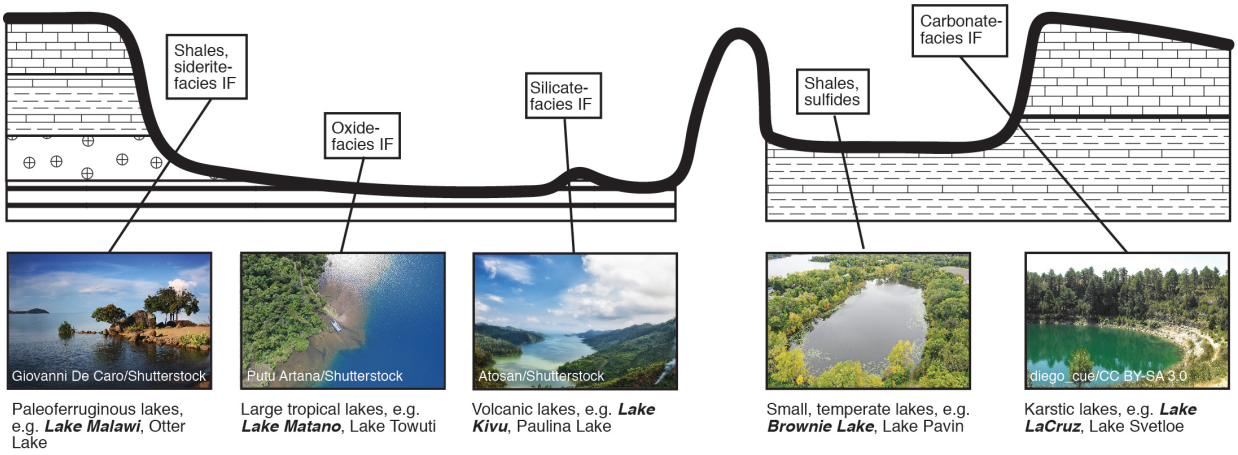

Figure 16. The depositional setting for different IF facies and other ferruginous sediment types. Images show different types of ferruginous lakes and examples discussed in text that have some analogy to the depositional environments encompassed in the top panel.

A key indicator of ferruginous intervals in paleoferruginous lakes is the deposition of siderite, but also vivianite. Higher water levels are interpreted to raise the carbonate compensation depth, resulting in dissolution of calcite, permitting siderite precipitation. Paleoferruginous lakes such as Otter Lakes can be useful in exploring controls on primary or early diagenetic formation of such carbonates and their preservation. Paleoferruginous lakes (e.g. Lake Towuti, Lake Malawi) offer insights into diagenetic controls on siderite formation. Constraining the $\delta^{13}C$ and $\delta^{18}O$ signatures that siderite or other Fe- and Mn-bearing carbonates formed via multiple pathways in ferruginous lakes will aid in the interpretation of pathways invoked in ancient systems.

The enigma of the primary iron precipitate to form IF may not have a single answer. Different IF facies may have formed under different depositional and chemical conditions, which resulted in different minerals. Oligotrophic Lake Matano's catchment is lateritic soils, and sediments record preservation of detrital Fe^{3+} (oxyhydr)oxides within a reducing water column. This system may analogous to open marine conditions, with low export of organic carbon, forming oxide-facies IF. Ferruginous volcanic lakes that support the cycling of hydrothermally-derived silica as well as iron may be appropriate analogues for silicate-facies IF forming closer to hydrothermal iron sources (e.g. Paulina Lake; Lefkowitz et al., 2017; Lake Kivu; Pasche et al., 2012), although disentangling contribution of Si-requiring phytoplankton (e.g. diatoms) to the silica cycle will be challenging.

Some of the major outstanding questions about the evolution of the Earth's surface environment revolve around primary productivity and oxygen production. Their levels could be

regulated by nutrients, or some other chemical or physical attributes of the oceans could have affected either the productivity or carbon preservation. Iron-replete conditions would have been the backdrop for marine primary productivity in the Precambrian, yet our understanding of primary productivity in the oxic ocean is galvanized by the paradigm of iron limitation (Martin, 1990). Studies from Lake Matano, Kabuno Bay of Lake Kivu, and Lake La Cruz have helped to identify the contributions of anoxygenic photosynthesis to primary productivity, and also delineate the controls on whether sulfide or Fe^{2+} is used as an electron donor. But subsurface Chl *a* maxima within Brownie Lake and Lake Svetloe highlight how oxygenic photosynthesis at an Fe^{2+}-oxygen chemocline might yet be an important part of Precambrian primary productivity. If subsurface chlorophyll maxima layers are so important to new productivity in diverse ocean regions today, why wouldn't they have been when chemical stratification was even more pronounced? If so, how did the presence of an Fe^{2+}-oxygen redoxcline affect primary productivity?

These questions are guideposts along the intertwined paths of the study of past ferruginous oceans and modern and paleo- ferruginous lakes. As our understanding of ferruginous ocean increases, new questions will emerge, ready to be informed by the lessons from ferruginous lakes. The increasing body of knowledge on ferruginous lakes will help to expose the relevant questions. As more ferruginous lakes are discovered, the lakes themselves might be elevated from curious limnological footnotes to important examples of how ferruginous conditions have played a central role in Earth's biogeochemistry not only in the past, but also in the present.

Acknowledgments

Iowa State University subject librarian Jesse Garrison gave assistance in identifying the origin and historical usage of the word “ferruginous”. Anna Nesterovich provided assistance with data extraction from limnology papers in Russian. Sharon Koenig from the Minnesota Pollution Control Agency provided the well geochemistry data. Erik T. Brown generously provided XRF core scan Fe/Ti data from Lake Malawi. Annete von der Handt guided EPMA analysis. The University of Minnesota Continental Scientific Drilling and Coordination Office (LacCore, NSF-1338322) provided access to Lake Malawi and Otter Lake cores. This work was supported by the National Science Foundation (NSF) collaborative research grant (EAR-1660691 to E. D. S., EAR-1660761 to C.W., and EAR-1660873 to S. K.) The Huron Mountain Wildlife Foundation (HMWF) provided housing and access to Canyon Lake. The Minneapolis Parks and Recreation Board provided access to Brownie Lake.

References

Ader, M., Macouin, M., Trindade, R.I.F., Hadrien, M.-H., Yang, Z., Sun, Z., Besse, J., 2009. A multilayered water column in the Ediacaran Yangtze platform? Insights from carbonate and organic matter paired δ13C. Earth Planet. Sci. Lett. 288, 213–227. https://doi.org/https://doi.org/10.1016/j.epsl.2009.09.024

Aeschbach-Hertig, W., Hofer, M., Schmid, M., Kipfer, R., Imboden, D.M., 2002. The physical structure and dynamics of a deep, meromictic crater lake (Lac Pavin, France). Hydrobiologia 487, 111–136. https://doi.org/10.1023/A:1022942226198

Ahm, A.-S.C., Maloof, A.C., Macdonald, F.A., Hoffman, P.F., Bjerrum, C.J., Bold, U., Rose, C. V,

Strauss, J. V, Higgins, J.A., 2019. An early diagenetic deglacial origin for basal Ediacaran "cap dolostones." Earth Planet. Sci. Lett. 506, 292–307. https://doi.org/https://doi.org/10.1016/j.epsl.2018.10.046

Ahn, J.H., Buseck, P.R., 1990. Hematite Nanospheres of Possible Colloidal Origin from a Precambrian Banded Iron Formation. Science (80-.). 250, 111 LP – 113. https://doi.org/10.1126/science.250.4977.111

Alcocer, J., 2017. Mexican Meromictic Lakes: What We Know So Far BT - Ecology of Meromictic Lakes, in: Gulati, R.D., Zadereev, E.S., Degermendzhi, A.G. (Eds.), . Springer International Publishing, Cham, pp. 353–375. https://doi.org/10.1007/978-3-319-49143-1_12

Alexander, B.W., Bau, M., Andersson, P., Dulski, P., 2008. Continentally-derived solutes in shallow Archean seawater: Rare earth element and Nd isotope evidence in iron formation from the 2.9Ga Pongola Supergroup, South Africa. Geochim. Cosmochim. Acta 72, 378–394. https://doi.org/https://doi.org/10.1016/j.gca.2007.10.028

Algeo, T.J., 2004. Can marine anoxic events draw down the trace element inventory of seawater? Geology 32, 1057–1060. https://doi.org/10.1130/g20896.1

Algeo, T.J., Liu, J., 2020. A re-assessment of elemental proxies for paleoredox analysis. Chem. Geol. 540, 119549. https://doi.org/https://doi.org/10.1016/j.chemgeo.2020.119549

Algeo, T.J., Rowe, H., 2012. Paleoceanographic applications of trace-metal concentration data. Chem. Geol. 324–325, 6–18. https://doi.org/https://doi.org/10.1016/j.chemgeo.2011.09.002

Algeo, T.J., Tribovillard, N., 2009. Environmental analysis of paleoceanographic systems based on molybdenum–uranium covariation. Chem. Geol. 268, 211–225.

https://doi.org/https://doi.org/10.1016/j.chemgeo.2009.09.001

Anbar, A.D., Duan, Y., Lyons, T.W., Arnold, G.L., Kendall, B., Creaser, R.A., Kaufman, A.J., Gordon, G.W., Scott, C., Garvin, J., Buick, R., 2007. A Whiff of Oxygen Before the Great Oxidation Event? Science (80-.). 317, 1903–1906. https://doi.org/10.1126/science.1140325

Anbar, A.D., Knoll, A.H., 2002. Proterozoic ocean chemistry and evolution: a bioinorganic bridge? Science (80-.). 297.

Anbar, A.D., Rouxel, O., 2007. Metal Stable Isotopes in Paleoceanography. Annu. Rev. Earth Planet. Sci. 35, 717–746. https://doi.org/doi:10.1146/annurev.earth.34.031405.125029

Andersen, M.B., Romaniello, S., Vance, D., Little, S.H., Herdman, R., Lyons, T.W., 2014. A modern framework for the interpretation of 238U/235U in studies of ancient ocean redox. Earth Planet. Sci. Lett. 400, 184–194. https://doi.org/https://doi.org/10.1016/j.epsl.2014.05.051

Anderson, R.Y., Dean, W.E., Bradbury, J.P., Love, D., 1985. Meromictic Lakes and Varved Lake Sediments in North America.

Anthony, R.S., 1977. Iron-rich rhythmically laminated sediments in Lake of the Clouds, northeastern Minnesota1. Limnol. Oceanogr. 22, 45–54. https://doi.org/10.4319/lo.1977.22.1.0045

Arnold, G.L., Anbar, A.D., Barling, J., Lyons, T.W., 2004. Molybdenum Isotope Evidence for Widespread Anoxia in Mid-Proterozoic Oceans. Science (80-.). 304, 87–90. https://doi.org/10.1126/science.1091785

Asael, D., Tissot, F.L.H., Reinhard, C.T., Rouxel, O., Dauphas, N., Lyons, T.W., Ponzevera, E.,

Liorzou, C., Chéron, S., 2013. Coupled molybdenum, iron and uranium stable isotopes as oceanic paleoredox proxies during the Paleoproterozoic Shunga Event. Chem. Geol. 362, 193–210. https://doi.org/https://doi.org/10.1016/j.chemgeo.2013.08.003

Assayag, N., Jezequel, D., Ader, M., Viollier, E., Michard, G., Prevot, F., Agrinier, P., 2008. Hydrological budget, carbon sources and biogeochemical processes in Lac Pavin (France): Constraints from δ18O of water and δ13C of dissolved inorganic carbon. Appl. Geochemistry 23, 2800–2816.

Ayres, D.E., 1972. Genesis of Iron-bearing Minerals in Banded Iron Formation Mesobands in The Dales Gorge Member, Hamersley Group, Western Australia. Econ. Geol. 67, 1214–1233. https://doi.org/10.2113/gsecongeo.67.8.1214

Babechuk, M., Weimar, N., Kleinhanns, I., Eroglu, S., Swanner, E.D., Kenny, G., Kamber, B., Schoenberg, R., 2019. Pervasively anoxic surface conditions at the onset of the Great Oxidation Event: new multi-proxy constraints from the Cooper Lake paleosol. Precambrian Res. 323, 126–163. https://doi.org/10.1016/j.precamres.2018.12.029

Bahrig, B., 1988. Paleo-environment information from deep water siderite (Lake of Laach, West Germany). Geol. Soc. London, Spec. Publ. 40, 153–158.

Baker, A., Brook, A., 1971. Optical density profiles as an aid to the study of microstratified phytoplankton populations in lakes. Arch. für Hydrobiol. 69, 214–233.

Barghoorn, E.S., Tyler, S.A., 1965. Microorganisms from the Gunflint Chert. Science (80-.). 147, 563 LP – 575. https://doi.org/10.1126/science.147.3658.563

Barley, M.E., Pickard, A.L., Sylvester, P.J., 1997. Emplacement of a large igneous province as a possible cause of banded iron formation 2.45 billion years ago. Nature 385, 55–58.

Barling, J., Anbar, A.D., 2004. Molybdenum isotope fractionation during adsorption by manganese oxides. Earth Planet. Sci. Lett. 217, 315–329. https://doi.org/http://dx.doi.org/10.1016/S0012-821X(03)00608-3

Barnes, N.A., Kehew, A.E., Krishnamurthy, R. V, Koretsky, C.M., 2011. Redox evolution in glacial drift aquifers: role of diamicton units in reduction of Fe(III). Environ. Earth Sci. 62, 1027–1038. https://doi.org/10.1007/s12665-010-0590-7

Bartley, J.K., Kah, L.C., 2004. Marine carbon reservoir, Corg-Ccarb coupling, and the evolution of the Proterozoic carbon cycle. Geology 32, 129–132. https://doi.org/10.1130/g19939.1

Bastviken, D., 2009. Methane, in: Encyclopedia of Inland Waters. Elsevier, Stockholm University, Sweden, pp. 783–805. https://doi.org/10.1016/B978-012370626-3.00117-4

Bastviken, D., Cole, J., Pace, M., Tranvik, L., 2004. Methane emissions from lakes: Dependence of lake characteristics, two regional assessments, and a global estimate. Global Biogeochem. Cycles 18. https://doi.org/10.1029/2004GB002238

Bau, M., Moeller, P., 1993. Rare earth element systematics of the chemically precipitated component in Early Precambrian iron formations and the evolution of the terrestrial atmosphere-hydrosphere-lithosphere system. Geochim. Cosmochim. Acta 57, 2239–2249.

Bauer, K.W., Byrne, J.M., Kenward, P., Simister, R.L., Michiels, C.C., Friese, A., Vuillemin, A., Henny, C., Nomosatryo, S., Kallmeyer, J., Kappler, A., Smit, M.A., Francois, R., Crowe, S.A., 2020. Magnetite biomineralization in ferruginous waters and early Earth evolution. Earth Planet. Sci. Lett. 549, 116495. https://doi.org/https://doi.org/10.1016/j.epsl.2020.116495

Beaumont, V., Robert, F., 1999. Nitrogen isotope ratios of kerogens in Precambrian cherts: a record of the evolution of atmosphere chemistry? Precambrian Res. 96, 63–82.

Becker, R.H., Clayton, R.N., 1976. Oxygen isotope study of a Precambrian banded iron-formation, Hamersley Range, Western Australia. Geochim. Cosmochim. Acta 40, 1153–1165. https://doi.org/https://doi.org/10.1016/0016-7037(76)90151-4

Beghin, J., Guilbaud, R., Poulton, S.W., Gueneli, N., Brocks, J.J., Storme, J.-Y., Blanpied, C., Javaux, E.J., 2017. A palaeoecological model for the late Mesoproterozoic – early Neoproterozoic Atar/El Mreïti Group, Taoudeni Basin, Mauritania, northwestern Africa. Precambrian Res. 299, 1–14. https://doi.org/https://doi.org/10.1016/j.precamres.2017.07.016

Bekker, A., Kaufman, A.J., 2007. Oxidative forcing of global climate change: A biogeochemical record across the oldest Paleoproterozoic ice age in North America. Earth Planet. Sci. Lett. 258, 486–499.

Bekker, A., Planavsky, N.J., Krapež, B., Rasmussen, B., Hofmann, A., Slack, J.F., Rouxel, O.J., Konhauser, K.O., 2014. 9.18 - Iron Formations: Their Origins and Implications for Ancient Seawater Chemistry, in: Holland, H.D., Turekian, K.K.B.T.-T. on G. (Second E. (Eds.), . Elsevier, Oxford, pp. 561–628. https://doi.org/https://doi.org/10.1016/B978-0-08-095975-7.00719-1

Bekker, A., Slack, J.F., Planavsky, N.J., Krapez, B., Hofmann, A., Konhauser, K.O., Rouxel, O.J., 2010. Iron Formation: The Sedimentary Product of a Complex Interplay among Mantle, Tectonic, Oceanic, and Biospheric Processes. Econ. Geol. 105, 467–508.

Benkovitz, A., Matthews, A., Teutsch, N., Poulton, S.W., Bar-Matthews, M., Almogi-Labin, A., 2020. Tracing water column euxinia in Eastern Mediterranean Sapropels S5 and S7. Chem. Geol. 545, 119627. https://doi.org/https://doi.org/10.1016/j.chemgeo.2020.119627

Berg, J.S., Jézéquel, D., Duverger, A., Lamy, D., Laberty-Robert, C., Miot, J., 2019. Microbial diversity involved in iron and cryptic sulfur cycling in the ferruginous, low-sulfate waters of Lake Pavin. PLoS One 14, e0212787.

Berg, J.S., Michellod, D., Pjevac, P., Martinez-Perez, C., Buckner, C.R.T., Hach, P.F., Schubert, C.J., Milucka, J., Kuypers, M.M.M., 2016. Intensive cryptic microbial iron cycling in the low iron water column of the meromictic Lake Cadagno. Environ. Microbiol. 18, 5288–5302. https://doi.org/10.1111/1462-2920.13587

Berner, R.A., 1970. Sedimentary pyrite formation. Am. J. Sci. 286, 1–23.

Beukes, N.J., Gutzmer, J., 2008. Origin and paleoenvironmental significance of major iron formations at the Archean-Paleoproterozoic boundary. SEG Rev. 15, 5–47.

Beukes, N.J., Klein, C., 1992. Models for iron-formation deposition, in: Schopf, J.W., Klein, C. (Eds.), The Proterozoic Biosphere: A Multidisciplinary Study. Cambridge University Press, New York, pp. 147–151.

Beukes, N.J., Klein, C., 1990. Geochemistry and sedimentology of a facies transition -- from microbanded to granular iron-formation -- in the early Proterozoic Transvaal Supergroup, South Africa. Precambrian Res. 47, 99–139.

Beukes, N.J., Klein, C., Kaufman, A.J., Hayes, J.M., 1990. Carbonate petrography, kerogen distribution, and carbon and oxygen isotope variations in an early Proterozoic transition from limestone to iron-formation deposition, Transvaal Supergroup, South Africa. Econ. Geol. 85, 663–690. https://doi.org/10.2113/gsecongeo.85.4.663

Bishop, J.L., Louris, S.K., Rogoff, D.A., Rothschild, L.J., 2006. Nanophase iron oxide as a key ultraviolet sunscreen for ancient photosynthetic microbes. Int. J. Astrobiol. 5, 1–12.

Bjerrum, C.J., Canfield, D.E., 2002. Ocean productivity before about 1.9 Gyr ago limited by phosphorus adsorption onto iron oxides. Nature 417, 159–162.

Blamey, N.J.F., Brand, U., Parnell, J., Spear, N., Lécuyer, C., Benison, K., Meng, F., Ni, P., 2016. Paradigm shift in determining Neoproterozoic atmospheric oxygen. Geology 44, 651–654. https://doi.org/10.1130/G37937.1

Boehrer, B., Dietz, S., Rohden, C. von, Kiwel, U., Jöhnk, K.D., Naujoks, S., Ilmberger, J., Lessmann, D., 2009. Double-diffusive deep water circulation in an iron-meromictic lake. Geochemistry, Geophys. Geosystems 10. https://doi.org/10.1029/2009GC002389

Boehrer, B., Schultze, M., 2008. Stratification of lakes. Rev. Geophys. 46. https://doi.org/10.1029/2006RG000210

Boehrer, B., von Rohden, C., Schultze, M., 2017. Physical Features of Meromictic Lakes: Stratification and Circulation, in: Gulati, R.D., Zadereev, E.S., Degermendzhi, A.G. (Eds.), Ecology of Meromictic Lakes. Springer International Publishing, Cham, pp. 15–34. https://doi.org/10.1007/978-3-319-49143-1_2

Boesen, C., Postma, D., 1988. Pyrite formation in anoxic environments of the Baltic. Am. J. Sci. 288, 575–603.

Boyd, E.S., Anbar, A.D., Miller, S., Hamilton, T.L., Lavin, M., Peters, J.W., 2011. A late methanogen origin for molybdenum-dependent nitrogenase. Geobiology 9, 221–232. https://doi.org/10.1111/j.1472-4669.2011.00278.x

Boyle, E.A., Edmond, J.M., Sholkovitz, E.R., 1977. The mechanism of iron removal in estuaries. Geochim. Cosmochim. Acta 41, 1313–1324. https://doi.org/https://doi.org/10.1016/0016-7037(77)90075-8

2498 Brauer, A., Haug, G.H., Dulski, P., Sigman, D.M., Negendank, J.F.W., 2008. An abrupt wind shift
2499 in western Europe at the onset of the Younger Dryas cold period. Nat. Geosci. 1, 520–523.
2500 https://doi.org/10.1038/ngeo263
2501 Bravo, A.G., Zopfi, J., Buck, M., Xu, J., Bertilsson, S., Schaefer, J.K., Poté, J., Cosio, C., 2018.
2502 Geobacteraceae are important members of mercury-methylating microbial communities
2503 of sediments impacted by waste water releases. ISME J. 12, 802–812.
2504 https://doi.org/10.1038/s41396-017-0007-7
2505 Bray, M.S., Wu, J., Reed, B.C., Kretz, C.B., Belli, K.M., Simister, R.L., Henny, C., Stewart, F.J.,
2506 DiChristina, T.J., Brandes, J.A., Fowle, D.A., Crowe, S.A., Glass, J.B., 2017. Shifting microbial
2507 communities sustain multiyear iron reduction and methanogenesis in ferruginous
2508 sediment incubations. Geobiology 15, 678–689. https://doi.org/10.1111/gbi.12239
2509 Brennecka, G.A., Herrmann, A.D., Algeo, T.J., Anbar, A.D., 2011a. Rapid expansion of oceanic
2510 anoxia immediately before the end-Permian mass extinction. Proc. Natl. Acad. Sci.
2511 https://doi.org/10.1073/pnas.1106039108
2512 Brennecka, G.A., Wasylenki, L.E., Bargar, J.R., Weyer, S., Anbar, A.D., 2011b. Uranium Isotope
2513 Fractionation during Adsorption to Mn-Oxyhydroxides. Environ. Sci. Technol. 45, 1370–
2514 1375. https://doi.org/10.1021/es103061v
2515 Brocks, J.J., Love, G.D., Summons, R.E., Knoll, A.H., Logan, G.A., Bowden, S.A., 2005. Biomarker
2516 evidence for green and purple sulphur bacteria in a stratified Palaeoproterozoic sea.
2517 Nature 437, 866–870.
2518 https://doi.org/http://www.nature.com/nature/journal/v437/n7060/suppinfo/nature040
2519 68_S1.html

Brocks, J.J., Schaeffer, P., 2008. Okenane, a biomarker for purple sulfur bacteria (Chromatiaceae), and other new carotenoid derivatives from the 1640 Ma Barney Creek Formation. Geochim. Cosmochim. Acta 72, 1396–1414. https://doi.org/http://dx.doi.org/10.1016/j.gca.2007.12.006

Brown, E.T., 2011. Lake Malawi's response to "megadrought" terminations: Sedimentary records of flooding, weathering and erosion. Palaeogeogr. Palaeoclimatol. Palaeoecol. 303, 120–125. https://doi.org/https://doi.org/10.1016/j.palaeo.2010.01.038

Brown, S.T., Basu, A., Ding, X., Christensen, J.N., DePaolo, D.J., 2018. Uranium isotope fractionation by abiotic reductive precipitation. Proc. Natl. Acad. Sci. 115, 8688 LP – 8693. https://doi.org/10.1073/pnas.1805234115

Bura-Nakić, E., Viollier, E., Jezequel, D., Thiam A., Ciglenečki, I., 2009. Reduced sulfur and iron species in anoxic water column of meromictic crater Lake Pavin (Massif Central, France). Chem. Geol. 266, 311–317. https://doi.org/10.1016/j.chemgeo.2009.06.020

Burnett, L., Moorhead, D., Hawes, I., Howard-Williams, C., 2006. Environmental Factors Associated with Deep Chlorophyll Maxima in Dry Valley Lakes, South Victoria Land, Antarctica. Arctic, Antarct. Alp. Res. 38, 179–189. https://doi.org/10.1657/1523-0430(2006)38[179:EFAWDC]2.0.CO;2

Busigny, V., Lebeau, O., Ader, M., Krapež, B., Bekker, A., 2013. Nitrogen cycle in the Late Archean ferruginous ocean. Chem. Geol. 362, 115–130. https://doi.org/https://doi.org/10.1016/j.chemgeo.2013.06.023

Busigny, V., Planavsky, N.J., Jézéquel, D., Crowe, S., Louvat, P., Moureau, J., Viollier, E., Lyons, T.W., 2014. Iron isotopes in an Archean ocean analogue. Geochim. Cosmochim. Acta 133,

443–462. https://doi.org/http://dx.doi.org/10.1016/j.gca.2014.03.004

Cairns-Smith, A.G., 1978. Precambrian solution photochemistry, inverse segregation, and banded iron formations. Nature 76, 807–808.

Camacho, A., Miracle, M.R., Romero-Viana, L., Picazo, A., Vicente, E., 2017a. Lake La Cruz, an Iron-Rich Karstic Meromictic Lake in Central Spain BT - Ecology of Meromictic Lakes, in: Gulati, R.D., Zadereev, E.S., Degermendzhi, A.G. (Eds.), . Springer International Publishing, Cham, pp. 187–233. https://doi.org/10.1007/978-3-319-49143-1_8

Camacho, A., Walter, X.A., Picazo, A., Zopfi, J., 2017b. Photoferrotrophy: Remains of an Ancient Photosynthesis in Modern Environments . Front. Microbiol. .

Campbell, P., Torgersen, T., 1980. Maintenance of Iron Meromixis by Iron Redeposition in a Rapidly Flushed Monimolimnion. Can. J. Fish. Aquat. Sci. 37, 1303–1313. https://doi.org/10.1139/f80-166

Canfield, D.E., 2005. The early history of atmospheric oxygen: homage to Robert M. Garrels. Annu. Rev. Earth Planet. Sci. 33, 1–36. https://doi.org/doi:10.1146/annurev.earth.33.092203.122711

Canfield, D.E., 1998. A new model for Proterozoic ocean chemistry. Nature 396, 450–453.

Canfield, D.E., 1989. Reactive iron in marine sediments. Geochim. Cosmochim. Acta 53, 619–632. https://doi.org/https://doi.org/10.1016/0016-7037(89)90005-7

Canfield, D.E., Farquhar, J., 2009. Animal evolution, bioturbation, and the sulfate concentration of the oceans. Proc Natl Acad Sci U S A 106, 8123–8127.

Canfield, D.E., Poulton, S.W., Knoll, A.H., Narbonne, G.M., Ross, G., Goldberg, T., Strauss, H., 2008. Ferruginous Conditions Dominated Later Neoproterozoic Deep-Water Chemistry.

Science (80-.). 321, 949 LP – 952. https://doi.org/10.1126/science.1154499

Canfield, D.E., Rosing, M.T., Bjerrum, C., 2006. Early anaerobic metabolisms. Philos. Trans. R. Soc. B Biol. Sci. 361, 1819–1836. https://doi.org/10.1098/rstb.2006.1906

Canfield, D.E., Thamdrup, B., 2009. Towards a consistent classification scheme for geochemical environments, or, why we with the term “suboxic” would go away. Geobiology 7, 385–392.

Canfield, D.E., Zhang, S., Wang, H., Wang, X., Zhao, W., Su, J., Bjerrum, C.J., Haxen, E.R., Hammarlund, E.U., 2018. A Mesoproterozoic iron formation. Proc. Natl. Acad. Sci. 115, E3895 LP-E3904. https://doi.org/10.1073/pnas.1720529115

Carothers, W.W., Adami, L.H., Rosenbauer, R.J., 1988. Experimental oxygen isotope fractionation between siderite-water and phosphoric acid liberated CO2-siderite. Geochim. Cosmochim. Acta 52, 2445–2450. https://doi.org/https://doi.org/10.1016/0016-7037(88)90302-X

Carrigan, W.J., Cameron, E.M., 1991. Petrological and stable isotope studies of carbonate and sulfide minerals from the Gunflint Formation, Ontario: evidence for the origin of early Proterozoic iron-formation. Precambrian Res. 52, 347–380. https://doi.org/https://doi.org/10.1016/0301-9268(91)90088-R

Castañeda, I.S., Schouten, S., 2011. A review of molecular organic proxies for examining modern and ancient lacustrine environments. Quat. Sci. Rev. 30, 2851–2891. https://doi.org/https://doi.org/10.1016/j.quascirev.2011.07.009

Catling, D.C., Claire, M.W., 2005. How Earth’s atmosphere evolved to an oxic state: A status report. Earth Planet. Sci. Lett. 237, 1–20.

Catling, D.C., Zahnle, K.J., 2020. The Archean atmosphere. Sci. Adv. 6, eaax1420.

https://doi.org/10.1126/sciadv.aax1420

Chan, C.S., De Stasio, G., Welch, S.A., Girasole, M., Frazer, B.H., Nesterova, M. V, Fakra, S.C., Banfield, J.F., 2004. Microbial Polysaccharides Template Assembly of Nanocrystal Fibers. Science (80-.). 303, 1656–1658. https://doi.org/10.1126/science.1092098

Chappaz, A., Gobeil, C., Tessier, A., 2010. Controls on uranium distribution in lake sediments. Geochim. Cosmochim. Acta 74, 203–214. https://doi.org/https://doi.org/10.1016/j.gca.2009.09.026

Chappaz, A., Lyons, T.W., Gregory, D.D., Reinhard, C.T., Gill, B.C., Li, C., Large, R.R., 2014. Does pyrite act as an important host for molybdenum in modern and ancient euxinic sediments? Geochim. Cosmochim. Acta 126, 112–122. https://doi.org/http://dx.doi.org/10.1016/j.gca.2013.10.028

Chen, X., Romaniello, S.J., Anbar, A.D., 2017. Uranium isotope fractionation induced by aqueous speciation: Implications for U isotopes in marine CaCO3 as a paleoredox proxy. Geochim. Cosmochim. Acta 215, 162–172. https://doi.org/https://doi.org/10.1016/j.gca.2017.08.006

Ciglenečki, I., Ljubešić, Z., Janeković, I., Batistić, M., 2017. Rogoznica Lake, a Euxinic Marine Lake on the Adriatic Coast (Croatia) that Fluctuates Between Anoxic Holomictic and Meromictic Conditions BT - Ecology of Meromictic Lakes, in: Gulati, R.D., Zadereev, E.S., Degermendzhi, A.G. (Eds.), . Springer International Publishing, Cham, pp. 125–154. https://doi.org/10.1007/978-3-319-49143-1_6

Claire, M.W., Catling, D.C., Zahnle, K.J., 2006. Biogeochemical modelling of the rise in atmospheric oxygen. Geobiology 4, 239–269.

Clarkson, M.O., Poulton, S.W., Guilbaud, R., Wood, R.A., 2014. Assessing the utility of Fe/Al and

Fe-speciation to record water column redox conditions in carbonate-rich sediments. Chem. Geol. 382, 111–122. https://doi.org/https://doi.org/10.1016/j.chemgeo.2014.05.031

Clarkson, M.O., Wood, R.A., Poulton, S.W., Richoz, S., Newton, R.J., Kasemann, S.A., Bowyer, F., Krystyn, L., 2016. Dynamic anoxic ferruginous conditions during the end-Permian mass extinction and recovery. Nat. Commun. 7, 12236. https://doi.org/10.1038/ncomms12236

Cloud Jr., P.E., 1968. Atmospheric and hydrospheric evolution on the primitive Earth: both secular accretion and biological and geochemical processes have affected earth's volatile envelope. Science (80-.). 160, 729–736. https://doi.org/10.1126/science.160.3829.729

Cloud, P.E., 1965. Significance of Gunflint (Precambrian) Microflora. Science (80-.). 148, 27–35.

Cockell, C.S., 2000. Ultraviolet Radiation and the Photobiology of Earth's Early Oceans. Orig. life Evol. Biosph. 30, 467–500. https://doi.org/10.1023/A:1006765405786

Codispoti, L.A., Christensen, J.P., 1985. Nitrification, denitrification and nitrous oxide cycling in the eastern tropical South Pacific ocean. Mar. Chem. 16, 277–300. https://doi.org/https://doi.org/10.1016/0304-4203(85)90051-9

Cohen, Y., Jorgensen, B.B., Padan, E., Shilo, M., 1975. Sulphide-dependent anoxygenic photosynthesis in the cyanobacterium Oscillatoria limnetica. Nature 257, 489–492.

Cole, D.B., Planavsky, N.J., Longley, M., Böning, P., Wilkes, D., Wang, X., Swanner, E.D., Wittkop, C., Loydell, D.K., Busigny, V., Knudsen, A.C., Sperling, E.A., 2020. Uranium Isotope Fractionation in Non-sulfidic Anoxic Settings and the Global Uranium Isotope Mass Balance. Global Biogeochem. Cycles 34, e2020GB006649. https://doi.org/10.1029/2020GB006649

Cole, D.B., Reinhard, C.T., Wang, X., Gueguen, B., Halverson, G.P., Gibson, T., Hodgskiss, M.S.W.,

McKenzie, N.R., Lyons, T.W., Planavsky, N.J., 2016. A shale-hosted Cr isotope record of low atmospheric oxygen during the Proterozoic. Geology 44, 555–558. https://doi.org/10.1130/G37787.1

Cole, D.B., Zhang, S., Planavsky, N.J., 2017. A new estimate of detrital redox-sensitive metal concentrations and variability in fluxes to marine sediments. Geochim. Cosmochim. Acta 215, 337–353. https://doi.org/https://doi.org/10.1016/j.gca.2017.08.004

Compeau, G.C., Barth, R., 985. Sulfate-reducing bacteria: principal methylators of mercury in anoxic estuarine sediment. Appl Env. Microbiol1 50, 498–502.

Conway, T.M., John, S.G., 2015. The cycling of iron, zinc and cadmium in the North East Pacific Ocean – Insights from stable isotopes. Geochim. Cosmochim. Acta 164, 262–283. https://doi.org/https://doi.org/10.1016/j.gca.2015.05.023

Cosmidis, J., Benzerara, K., Morin, G., Busigny, V., Lebeau, O., Jézéquel, D., Noël, V., Dublet, G., Othmane, G., 2014. Biomineralization of iron-phosphates in the water column of Lake Pavin (Massif Central, France). Geochim. Cosmochim. Acta 126, 78–96. https://doi.org/http://dx.doi.org/10.1016/j.gca.2013.10.037

Cossa, D., Mason, R.P., Fitzgerald, W.F., 1994. Chemical speciation of mercury in a meromictic lake, in: Watras, C.J., Huckabee, J.W. (Eds.), Mercury Pollution: Integration and Synthesis. pp. 57–67.

Costa, K.M., Russell, J.M., Vogel, H., Bijaksana, S., 2015. Hydrological connectivity and mixing of Lake Towuti, Indonesia in response to paleoclimatic changes over the last 60,000years. Palaeogeogr. Palaeoclimatol. Palaeoecol. 417, 467–475. https://doi.org/https://doi.org/10.1016/j.palaeo.2014.10.009

Cox, G.M., Halverson, G.P., Minarik, W.G., Le Heron, D.P., Macdonald, F.A., Bellefroid, E.J., Strauss, J. V, 2013. Neoproterozoic iron formation: An evaluation of its temporal, environmental and tectonic significance. Chem. Geol. 362, 232–249. https://doi.org/http://dx.doi.org/10.1016/j.chemgeo.2013.08.002

Croal, L.R., Johnson, C.M., Beard, B.L., Newman, D.K., 2004. Iron isotope fractionation by Fe(II)-oxidizing photoautotrophic bacteria. Geochim. Cosmochim. Acta 68, 1227–1242.

Crockford, P.W., Hayles, J.A., Bao, H., Planavsky, N.J., Bekker, A., Fralick, P.W., Halverson, G.P., Bui, T.H., Peng, Y., Wing, B.A., 2018. Triple oxygen isotope evidence for limited mid-Proterozoic primary productivity. Nature 559, 613–616. https://doi.org/10.1038/s41586-018-0349-y

Crowe, S.A., Hahn, A.S., Morgan-Lang, C., Thompson, K.J., Simister, R.L., Llirós, M., Hirst, M., Hallam, S.J., 2017. Draft Genome Sequence of the Pelagic Photoferrotroph Chlorobium phaeoferrooxidans. Genome Announc. 5, e01584-16. https://doi.org/10.1128/genomeA.01584-16

Crowe, S.A., Jones, C., Katsev, S., Magen, C., O'Neill, A.H., Sturm, A., Canfield, D., Haffner, G.D., Mucci, A., Sundby, B., Fowle, D.A., 2008a. Photoferrotrophs thrive in an Archean Ocean analogue. Proc. Natl. Acad. Sci. 105, 15938–15943. https://doi.org/10.1073/pnas.0805313105

Crowe, S.A., Katsev, S., Leslie, K., Sturm, A., Magen, C., Nomosatryo, S., Pack, M.A., Kessler, J.D., Reeburgh, W.S., Roberts, J.A., GonzÁLez, L., Douglas Haffner, G., Mucci, A., Sundby, B., Fowle, D.A., 2011. The methane cycle in ferruginous Lake Matano. Geobiology 9, 61–78. https://doi.org/10.1111/j.1472-4669.2010.00257.x

2674 Crowe, S.A., Maresca, J.A., Jones, C., Sturm, A., Henny, C., Fowle, D.A., Cox, R.P., Delong, E.F.,
2675 Canfield, D.E., 2014a. Deep-water anoxygenic photosynthesis in a ferruginous chemocline.
2676 Geobiology 12, 322–339. https://doi.org/10.1111/gbi.12089
2677 Crowe, S.A., O'Neill, A.H., Katsev, S., Hehanussa, P., Haffner, D.G., Sundby, B., Mucci, A., Fowle,
2678 D.A., 2008b. The biogeochemistry of tropical lakes: A case study from Lake Matano,
2679 Indonesia. Limnol. Oceanogr. 53, 319–331. https://doi.org/10.4319/lo.2008.53.1.0319
2680 Crowe, S.A., Pannalal, S.J., Fowle, D.A., Cioppa, M.T., Symons, D.T.A., Haffner, G.D., Fryer, B.J.,
2681 McNeely, R., Sundby, B., Hehanussa, P.E., 2004. Biogoechemical cycling in Fe-rich
2682 sediments from Lake Matano, Indonesia, in: 11th International Symposium on Water-Rock
2683 Interaction. pp. 1185–1189.
2684 Crowe, S.A., Paris, G., Katsev, S., Jones, C., Kim, S., Zerkle, A.L., Nomosatryo, S., Fowle, D.A.,
2685 Adkins, J.F., Sessions, A.L., Farquhar, J., Canfield, D.E., 2014b. Sulfate was a trace
2686 constituent of Archean seawater. Science (80-.). 346, 735–739.
2687 https://doi.org/10.1126/science.1258966
2688 Cullen, J.J., 2015. Subsurface Chlorophyll Maximum Layers: Enduring Enigma or Mystery
2689 Solved? Ann. Rev. Mar. Sci. 7, 207–239. https://doi.org/10.1146/annurev-marine-010213-
2690 135111
2691 Cullen, J.J., 1982. The Deep Chlorophyll Maximum: Comparing Vertical Profiles of Chlorophyll a.
2692 Can. J. Fish. Aquat. Sci. 39, 791–803.
2693 Cullen, J.J., Eppley, R.W., 1981. Chlorophyll maximum layers of the Southern California Bight
2694 and possible mechanisms of their formation and maintenance. Oceanol. Acta 4, 23–32.
2695 Culver, D.A., 1977. Biogenic meromixis and stability in a soft-water lake. Limnol. Ocean. 22,

667–686.

Cumming, V.M., Poulton, S.W., Rooney, A.D., Selby, D., 2013. Anoxia in the terrestrial environment during the late Mesoproterozoic. Geology 41, 583–586. https://doi.org/10.1130/G34299.1

Czaja, A.D., Johnson, C.M., Roden, E.E., Beard, B.L., Vogelin, A.R., Nägler, T.F., Beukes, N.J., Wille, M., 2012. Evidence for free oxygen in the Neoarchean ocean based on coupled iron-molybdenum isotope fractionation. Geochim. Cosmochim. Acta 86, 118–137.

Dahl, T.W., Chappaz, A., Fitts, J.P., Lyons, T.W., 2013. Molybdenum reduction in a sulfidic lake: Evidence from X-ray absorption fine-structure spectroscopy and implications for the Mo paleoproxy. Geochim. Cosmochim. Acta 103, 213–231. https://doi.org/http://dx.doi.org/10.1016/j.gca.2012.10.058

Dahl, T.W., Chappaz, A., Hoek, J., McKenzie, C.J., Svane, S., Canfield, D.E., 2017. Evidence of molybdenum association with particulate organic matter under sulfidic conditions. Geobiology 15, 311–323. https://doi.org/10.1111/gbi.12220

Dahl, T.W., Wirth, S.B., 2017. Molybdenum isotope fractionation and speciation in a euxinic lake—Testing ways to discern isotope fractionation processes in a sulfidic setting. Chem. Geol. 460, 84–92. https://doi.org/https://doi.org/10.1016/j.chemgeo.2017.04.018

Dalsgaard, T., Thamdrup, B., Farías, L., Revsbech, N.P., 2012. Anammox and denitrification in the oxygen minimum zone of the eastern South Pacific. Limnol. Oceanogr. 57, 1331–1346. https://doi.org/10.4319/lo.2012.57.5.1331

Dang, D.H., Novotnik, B., Wang, W., Georg, R.B., Evans, R.D., 2016. Uranium Isotope Fractionation during Adsorption, (Co)precipitation, and Biotic Reduction. Environ. Sci.

Technol. 50, 12695–12704. https://doi.org/10.1021/acs.est.6b01459

Dauphas, N., Kasting, J.F., 2011. Low pCO2 in the pore water, not in the Archean air. Nature 474, E1–E1.

Davison, W., 1993. Iron and manganese in lakes. Earth-Science Rev. 34, 119–163. https://doi.org/http://dx.doi.org/10.1016/0012-8252(93)90029-7

Dean, W.E., Bradbury, J.P., Anderson, R.Y., Barnosky, C.W., 1984. The Variability of Holocene Climate Change: Evidence from Varved Lake Sediments. Science (80-.). 226, 1191–1194.

Dean, W.E., Neff, B.P., Rosenberry, D.O., Winter, T.C., Parkhurst, R., 2006. The Significance of Ground Water to the Accumulation of Iron and Manganese in the Sediments of Two Hydrologically Distinct Lakes in North-Central Minnesota: A Geological Perspective. Groundwater 41, 951–963. https://doi.org/10.1111/j.1745-6584.2003.tb02437.x

Degens, E.T., Stoffers, P., 1976. Stratified waters as a key to the past. Nature 263, 22–27. https://doi.org/10.1038/263022a0

Demidov, I.N., Houmark-Nielsen, M., Kjær, K.H., Funder, S., Larsen, E., Lyså, A., Lunkka, J.-P., Saarnisto, M., 2004. Valdaian glacial maxima in the Arkhangelsk district of northwestern Russia, in: Ehlers, J., Gibbard, P.L.B.T.-D. in Q.S. (Eds.), Quaternary Glaciations Extent and Chronology. Elsevier, pp. 321–336. https://doi.org/https://doi.org/10.1016/S1571-0866(04)80082-4

Derry, L.A., 2015. Causes and consequences of mid-Proterozoic anoxia. Geophys. Res. Lett. 42, 8538–8546. https://doi.org/10.1002/2015GL065333

Des Marais, D.J., Strauss, H., Summons, R.E., Hayes, J.M., 1992. Carbon isotope evidence for the stepwise oxidation of the Proterozoic environment. Nature 359, 605–609.

Deuser, W.G., 1970. Carbon-13 in Black Sea Waters and Implications for the Origin of Hydrogen Sulfide. Science (80-.). 168, 1575–1577.

Dickinson, K.A., 1988. Paleolimnology of Lake Tubutulik, an iron-meromictic Eocene Lake, eastern Seward Peninsula, Alaska. Sediment. Geol. 54, 303–320. https://doi.org/https://doi.org/10.1016/0037-0738(88)90038-3

Dickman, M., Ouellet, M., 1987. Limnology of Garrow Lake, NWT, Canada. Polar Rec. (Gr. Brit). 23, 531–549.

Dijkstra, N., Slomp, C.P., Behrends, T., 2016. Vivianite is a key sink for phosphorus in sediments of the Landsort Deep, an intermittently anoxic deep basin in the Baltic Sea. Chem. Geol. 438, 58–72. https://doi.org/https://doi.org/10.1016/j.chemgeo.2016.05.025

Doyle, K.A., Poulton, S.W., Newton, R.J., Podkovyrov, V.N., Bekker, A., 2018. Shallow water anoxia in the Mesoproterozoic ocean: Evidence from the Bashkir Meganticlinorium, Southern Urals. Precambrian Res. 317, 196–210. https://doi.org/https://doi.org/10.1016/j.precamres.2018.09.001

Dupuis, D., Sprague, E., Docherty, K.M., Koretsky, C.M., 2019. The influence of road salt on seasonal mixing, redox stratification and methane concentrations in urban kettle lakes. Sci. Total Environ. 661, 514–521. https://doi.org/https://doi.org/10.1016/j.scitotenv.2019.01.191

Ehrenreich, A., Widdel, F., 1994. Anaerobic oxidation of ferrous iron by purple bacteria, a new type of phototrophic metabolism. Appl Env. Microbiol 60, 1526–4517.

Ellwood, M.J., Hassler, C., Moisset, S., Pascal, L., Danza, F., Peduzzi, S., Tonolla, M., Vance, D., 2019. Iron isotope transformations in the meromictic Lake Cadagno. Geochim.

Cosmochim. Acta 255, 205–221. https://doi.org/https://doi.org/10.1016/j.gca.2019.04.007

Erickson, M.L., Barnes, R.J., 2005. Glacial Sediment Causing Regional-Scale Elevated Arsenic in Drinking Water. Ground Water 43, 796–805. https://doi.org/10.1111/j.1745-6584.2005.00053.x

Erickson, M.L., Elliott, S.M., Christenson, C.A., Krall, A.L., 2018. Predicting geogenic Arsenic in Drinking Water Wells in Glacial Aquifers, North-Central USA: Accounting for Depth-Dependent Features. Water Resour. Res. 54, 10,110-172,187. https://doi.org/10.1029/2018WR023106

Eroglu, S., Schoenberg, R., Pascarelli, S., Beukes, N.J., Kleinhanns, I.C., Swanner, E.D., 2018. Open ocean vs. continentally-derived iron cycles along the Neoarchean Campbellrand-Malmani Carbonate platform, South Africa. Am. J. Sci. 318, 367–408. https://doi.org/10.2475/04.2018.01

Eugster, H.P., Chou, I.-M., 1973. The Depositional Environments of Precambrian Banded Iron-Formations. Econ. Geol. 68, 1144–1168. https://doi.org/10.2113/gsecongeo.68.7.1144

Ewers, W.E., 1983. Chemical factors in the deposition and diagenesis of Banded Iron-Formation, in: Trendall, A.F., Morris, R.C. (Eds.), Iron-Formation: Facts and Problems. Elsevier Science Publishers B. V., pp. 491–512.

Ewers, W.E., 1980. Chemical conditions for the precipitation of banded iron-formations., in: P. A. Trudinger, M.R.W. and B.J.R. (Ed.), Biogeochemistry of Ancient and Modern Environments. Springer-Verlag, Berlin, pp. 83–92.

Fakhraee, M., Hancisse, O., Canfield, D.E., Crowe, S.A., Katsev, S., 2019. Proterozoic seawater sulfate scarcity and the evolution of ocean–atmosphere chemistry. Nat. Geosci. 12, 375–

380. https://doi.org/10.1038/s41561-019-0351-5

Felder, M., Gaupp, R., 2006. The δ13C and δ18O signatures of siderite - a tool to discriminate mixis patterns in ancient lakes. Zeitschrift für der Dtsch. Gesellschaft für Geowissenschaften 157, 387–410.

Fennel, K., Follows, M., Falkowski, P.G., 2005. The co-evolution of the nitrogen, carbon and oxygen cycles in the Proterozoic Ocean. Am. J. Sci. 305, 526–545.

Fernandez, A., van Dijk, J., Müller, I.A., Bernasconi, S.M., 2016. Siderite acid fractionation factors for sealed and open vessel digestions at 70°C and 100°C. Chem. Geol. 444, 180–186. https://doi.org/https://doi.org/10.1016/j.chemgeo.2016.10.015

Ferrera, I., Sarmento, H., Priscu, J.C., Chiuchiolo, A., González, J.M., Grossart, H.-P., 2017. Diversity and Distribution of Freshwater Aerobic Anoxygenic Phototrophic Bacteria across a Wide Latitudinal Gradient. Front. Microbiol. 8, 175. https://doi.org/10.3389/fmicb.2017.00175

Feulner, G., 2012. The faint young Sun problem. Rev. Geophys. 50. https://doi.org/10.1029/2011RG000375

Fischer, W.W., Schroeder, S., Lacassie, J.P., Beukes, N.J., Goldberg, T., Strauss, H., Horstmann, U.E., Schrag, D.P., Knoll, A.H., 2009. Isotopic constraints on the Late Archean carbon cycle from the Transvaal Supergroup along the western margin of the Kaapvaal Craton, South Africa. Precambrian Res. 169, 15–27.

Fitzgerald, W.F., Engstrom, D.R., Mason, R.P., Nater, E.A., 1998. The Case for Atmospheric Mercury Contamination in Remote Areas. Environ. Sci. Technol. 32, 1–7. https://doi.org/10.1021/es970284w

Flament, N., Coltice, N., Rey, P.F., 2008. A case for late-Archaean continental emergence from thermal evolution models and hypsometry. Earth Planet. Sci. Lett. 275, 326–336. https://doi.org/https://doi.org/10.1016/j.epsl.2008.08.029

Flannery, D.T., Allwood, A.C., Van Kranendonk, M.J., 2016. Lacustrine facies dependence of highly 13C-depleted organic matter during the global age of methanotrophy. Precambrian Res. 285, 216–241. https://doi.org/https://doi.org/10.1016/j.precamres.2016.09.021

Froelich, P.N., Klinkhammer, G.P., Bender, M.L., Luedtke, N.A., Heath, G.R., Cullen, D., Dauphin, P., Hammond, D., Hartman, B., Maynard, V., 1979. Early oxidation of organic matter in pelagic sediments of the eastern equatorial Atlantic: suboxic diagenesis. Geochim. Cosmochim. Acta 43, 1075–1090. https://doi.org/http://dx.doi.org/10.1016/0016-7037(79)90095-4

Fry, B., Jannasch, H.W., Molyneaux, S.J., Wirsen, C.O., Muramoto, J.A., King, S., 1991. Stable isotope studies of the carbon, nitrogen and sulfur cycles in the Black Sea and the Cariaco Trench. Deep Sea Res. Part A. Oceanogr. Res. Pap. 38, S1003–S1019. https://doi.org/https://doi.org/10.1016/S0198-0149(10)80021-4

Gäb, F., Ballhaus, C., Siemens, J., Heuser, A., Lissner, M., Geisler, T., Garbe-Schönberg, D., 2017. Siderite cannot be used as CO2 sensor for Archaean atmospheres. Geochim. Cosmochim. Acta 214, 209–225. https://doi.org/https://doi.org/10.1016/j.gca.2017.07.027

Galili, N., Shemesh, A., Yam, R., Brailovsky, I., Sela-Adler, M., Schuster, E.M., Collom, C., Bekker, A., Planavsky, N., Macdonald, F.A., Préat, A., Rudmin, M., Trela, W., Sturesson, U., Heikoop, J.M., Aurell, M., Ramajo, J., Halevy, I., 2019. The geologic history of seawater oxygen isotopes from marine iron oxides. Science (80-.). 365, 469 LP – 473.

https://doi.org/10.1126/science.aaw9247

Gauger, T., Konhauser, K., Kappler, A., 2015. Protection of phototrophic iron(II)-oxidizing bacteria from UV irradiation by biogenic iron(III) minerals: Implications for early Archean banded iron formation. Geology 43, 1067–1070. https://doi.org/10.1130/G37095.1

Gilleaudeau, G.J., Kah, L.C., 2015. Heterogeneous redox conditions and a shallow chemocline in the Mesoproterozoic ocean: Evidence from carbon–sulfur–iron relationships. Precambrian Res. 257, 94–108. https://doi.org/https://doi.org/10.1016/j.precamres.2014.11.030

Gilleaudeau, G.J., Romaniello, S.J., Luo, G., Kaufman, A.J., Zhang, F., Klaebe, R.M., Kah, L.C., Azmy, K., Bartley, J.K., Zheng, W., Knoll, A.H., Anbar, A.D., 2019. Uranium isotope evidence for limited euxinia in mid-Proterozoic oceans. Earth Planet. Sci. Lett. 521, 150–157. https://doi.org/https://doi.org/10.1016/j.epsl.2019.06.012

Gilmour, C.C., Riedel, G.S., Ederington, M.C., Bell, J.T., Gill, G.A., Stordal, M.C., 1998. Methylmercury concentrations and production rates across a trophic gradient in the northern Everglades. Biogeochemistry 40, 327–345. https://doi.org/10.1023/A:1005972708616

Glass, J.B., Wolfe-Simon, F., Anbar, A.D., 2009. Coevolution of metal availability and nitrogen assimilation in cyanobacteria and algae. Geobiology 7, 100–123.

Godfrey, L. V, Falkowski, P.G., 2009. The cycling and redox state of nitrogen in the Archaean ocean. Nat. Geosci. 2, 725–729.

Godfrey, L. V, Poulton, S.W., Bebout, G.E., Fralick, P.W., 2013. Stability of the nitrogen cycle during development of sulfidic water in the redox-stratified late Paleoproterozoic Ocean. Geology 41, 655–658. https://doi.org/10.1130/g33930.1

2850 Goldberg, T., Strauss, H., Guo, Q., Liu, C., 2007. Reconstructing marine redox conditions for the
2851 Early Cambrian Yangtze Platform: Evidence from biogenic sulphur and organic carbon
2852 isotopes. Palaeogeogr. Palaeoclimatol. Palaeoecol. 254, 175–193.
2853 https://doi.org/https://doi.org/10.1016/j.palaeo.2007.03.015
2854 Goldblatt, C., Lenton, T.M., Watson, A.J., 2006. Bistability of atmospheric oxygen and the Great
2855 Oxidation. Nature 443, 683–686.
2856 https://doi.org/http://www.nature.com/nature/journal/v443/n7112/suppinfo/nature051
2857 69_S1.html
2858 Gordon, G.W., Lyons, T.W., Arnold, G.L., Roe, J., Sageman, B.B., Anbar, A.D., 2009. When do
2859 black shales tell molybdenum isotope tales? Geology 37, 535–538.
2860 https://doi.org/10.1130/G25186A.1
2861 Gorham, E., 1957. The Development of Peat Lands. Q. Rev. Biol. 32, 145–166.
2862 Gorham, E., Boyce, F.M., 1989. Influence of lake surface area and depth upon thermal
2863 stratification and the depth of the summer thermocline. J Gt. Lakes Res 15, 233–245.
2864 Gorham, E., Dean, W.E., Sanger, J.E., 1983. The chemical composition of lakes in the north-
2865 central United States. Limnol. Ocean. 28, 287–301.
2866 Gorlenko, V.M., Vainstein, M.B., Kachalkin, V.I., 1978. Microbiological characteristic of lake
2867 Mogilnoye. Arch. für Hydrobiol. 81, 475–492.
2868 Gorlenko, V.M., Vainstein, M. V., Chebotarev, E.N., 1980. Bacteria involved in turnover of sulfur
2869 and iron metabolism in meromictic Lake Kuznechikha with low sulfate content.
2870 Microbiology 49, 653–659.
2871 Goudge, T.A., Russell, J.M., Mustard, J.F., Head, J.W., Bijaksana, S., 2017. A 40,000 yr record of

clay mineralogy at Lake Towuti, Indonesia: Paleoclimate reconstruction from reflectance spectroscopy and perspectives on paleolakes on Mars. GSA Bull. 129, 806–819. https://doi.org/10.1130/B31569.1

Grégoire, D.S., Lavoie, N.C., Poulain, A.J., 2018. Heliobacteria Reveal Fermentation As a Key Pathway for Mercury Reduction in Anoxic Environments. Environ. Sci. Technol. 52, 4145–4153. https://doi.org/10.1021/acs.est.8b00320

Grégoire, D.S., Poulain, A.J., 2016. A physiological role for HgII during phototrophic growth. Nat. Geosci. 9, 121–125. https://doi.org/10.1038/ngeo2629

Guilbaud, R., Poulton, S.W., Butterfield, N.J., Zhu, M., Shields-Zhou, G.A., 2015. A global transition to ferruginous conditions in the early Neoproterozoic oceans. Nat. Geosci 8, 466–470. https://doi.org/10.1038/ngeo2434http://www.nature.com/ngeo/journal/v8/n6/abs/ngeo2434.html#supplementary-information

Habicht, K.S., Gade, M., Thamdrup, B., Berg, P., Canfield, D.E., 2002. Calibration of Sulfate Levels in the Archean Ocean. Science (80-.). 298, 2372–2374. https://doi.org/10.1126/science.1078265

Hakala, A., 2004. Meromixis as a part of lake evolution - observations and a revised classification of true meromictic lakes in Finland. Boreal Environ. Res. 9, 37–53.

Halama, M., Swanner, E.D., Konhauser, K.O., Kappler, A., 2016. Evaluation of siderite and magnetite formation in BIFs by pressure–temperature experiments of Fe(III) minerals and microbial biomass. Earth Planet. Sci. Lett. 450, 243–253. https://doi.org/10.1016/j.epsl.2016.06.032

2894 Halevy, I., Alesker, M., Schuster, E.M., Popovitz-Biro, R., Feldman, Y., 2017. A key role for green
2895 rust in the Precambrian oceans and the genesis of iron formations. Nat. Geosci. 10, 135.
2896 Hall, K., Northcote, T., 2012. Meromictic Lakes, in: Bengtsson, L., Herschy, R., Fairbridge, R.
2897 (Eds.), Encyclopedia of Lakes and Reservoirs. pp. 519–524.
2898 Halm, H., Musat, N., Lam, P., Langlois, R., Musat, F., Peduzzi, S., Lavik, G., Schubert, C.J., Singha,
2899 B., LaRoche, J., Kuypers, M.M.M., 2009. Co-occurrence of denitrification and nitrogen
2900 fixation in a meromictic lake, Lake Cadagno (Switzerland). Environ. Microbiol. 11, 1945–
2901 1958. https://doi.org/10.1111/j.1462-2920.2009.01917.x
2902 Hamilton, T.L., Klatt, J.M., de Beer, D., Macalady, J.L., 2018. Cyanobacterial photosynthesis
2903 under sulfidic conditions: insights from the isolate Leptolyngbya sp. strain hensonii. Isme J.
2904 12, 568.
2905 Hand, R.M., Burton, H.R., 1981. 25. Microbial ecology of an Antarctic saline meromictic lake.
2906 Hydrobiologia 81, 363–374. https://doi.org/10.1007/BF00048725
2907 Hasberg, A.K.M., Bijaksana, S., Held, P., Just, J., Melles, M., Morlock, M.A., Opitz, S., Russell,
2908 J.M., Vogel, H., Wennrich, V., 2019. Modern sedimentation processes in Lake Towuti,
2909 Indonesia, revealed by the composition of surface sediments. Sedimentology 66, 675–698.
2910 https://doi.org/10.1111/sed.12503
2911 Havig, J.R., Hamilton, T.L., Bachan, A., Kump, L.R., 2017. Sulfur and carbon isotopic evidence for
2912 metabolic pathway evolution and a four-stepped Earth system progression across the
2913 Archean and Paleoproterozoic. Earth-Science Rev. 174, 1–21.
2914 https://doi.org/https://doi.org/10.1016/j.earscirev.2017.06.014
2915 Hawkings, J.R., Wadham, J.L., Tranter, M., Raiswell, R., Benning, L.G., Statham, P.J., Tedstone,

2916 A., Nienow, P., Lee, K., Telling, J., 2014. Ice sheets as a significant source of highly reactive
2917 nanoparticulate iron to the oceans. Nat. Commun. 5, 3929.
2918 https://doi.org/10.1038/ncomms4929
2919 Hayes, J.M., 1994. Global methanotrophy at the Archean-Proterozoic transition, in: Bengston, S.
2920 (Ed.), Early Life on Earth. Nobel Symposium. Columbia University Press, New York.
2921 Hayes, J.M., Waldbauer, J.R., 2006. The carbon cycle and associated redox processes through
2922 time. Philos. Trans. R. Soc. B Biol. Sci. 361, 931–950.
2923 https://doi.org/10.1098/rstb.2006.1840
2924 Hegler, F., Posth, N.R., Jiang, J., Kappler, A., 2008. Physiology of phototrophic iron(II)-oxidizing
2925 bacteria: implications for modern and ancient environments. FEMS Microbiol. Ecol. 66,
2926 250–260.
2927 Heimann, A., Johnson, C.M., Beard, B.L., Valley, J.W., Roden, E.E., Spicuzza, M.J., Beukes, N.J.,
2928 2010. Fe, C, and O isotope compositions of banded iron formation carbonates
2929 demonstrate a major role for dissimilatory iron reduction in ~2.5Ga marine environments.
2930 Earth Planet. Sci. Lett. 294, 8–18.
2931 https://doi.org/https://doi.org/10.1016/j.epsl.2010.02.015
2932 Heising, S., Richter, L., Ludwig, W., Schink, B., 1999. Chlorobium ferrooxidans sp. nov., a
2933 phototrophic green sulfur bacterium that oxidizes ferrous iron in coculture with a
2934 “Geospirillum” sp. strain. Arch. Microbiol. 172, 116–124.
2935 https://doi.org/10.1007/s002030050748
2936 Heising, S., Schink, B., 1998. Phototrophic oxidation of ferrous iron by a Rhodomicrobium
2937 vannielii strain. Microbiology 144, 2263–2269.

Helz, G.R., Miller, C. V, Charnock, J.M., Mosselmans, J.F.W., Pattrick, R.A.D., Garner, C.D., Vaughan, D.J., 1996. Mechanism of molybdenum removal from the sea and its concentration in black shales: EXAFS evidence. Geochim. Cosmochim. Acta 60, 3631–3642. https://doi.org/10.1016/0016-7037(96)00195-0

Hiatt, E.E., Pufahl, P.K., Guimarães da Silva, L., 2020. Iron and phosphorus biochemical systems and the Cryogenian-Ediacaran transition, Jacadigo basin, Brazil: Implications for the Neoproterozoic oxygenation event. Precambrian Res. 337, 105533. https://doi.org/https://doi.org/10.1016/j.precamres.2019.105533

Hinrichs, K.-U., 2002. Microbial fixation of methane carbon at 2.7 Ga: Was an anaerobic mechanism possible? Geochemistry, Geophys. Geosystems 3, 1–10. https://doi.org/10.1029/2001GC000286

Hogle, S.L., Dupont, C.L., Hopkinson, B.M., King, A.L., Buck, K.N., Roe, K.L., Stuart, R.K., Allen, A.E., Mann, E.L., Johnson, Z.I., Barbeau, K.A., 2018. Pervasive iron limitation at subsurface chlorophyll maxima of the California Current. Proc. Natl. Acad. Sci. 115, 13300 LP – 13305. https://doi.org/10.1073/pnas.1813192115

Holland, H.D., 2007. 6.21 - The Geologic History of Seawater, in: Turekian, H.D.H.K. (Ed.), Treatise on Geochemistry. Pergamon, Oxford, pp. 1–46. https://doi.org/http://dx.doi.org/10.1016/B0-08-043751-6/06122-3

Holland, H.D., 1984. The Chemical Evolution of the Atmosphere and Oceans. Princeton University Press, Princeton, NJ.

Holland, H.D., 1973. The Oceans: a possible source for iron in iron-formations. Econ. Geol. 68, 1169–1172.

Hongve, D., 2002. Seasonal Mixing and Genesis of Endogenic Meromixis in Small Lakes in Southeast Norway. Hydrol. Res. 33, 189 LP – 206.

Hongve, D., 1999. Long-term Variation in the Stability of the Meromictic Lake Nordbytjernet Caused by Groundwater Fluctuations. Nord. Hydrol. 30, 21–38.

Hongve, D., 1980. Chemical stratification and stability of meromictic lakes in the Upper Romerike district. Schweiz Z. Hydrol. 42, 171–195.

Hongve, D., 1977. The ionic composition of lakes fed by ground water and precipitation in the Upper Romerike District. Nord. Hydrol. 8, 141–162.

Hongve, D., 1974. Hydrological features of Nordbytjernet, a manganese-rich meromictic lake in SE Norway. Arch. für Hydrobiol. 74, 227–246.

Hood, A. v. S., Planavsky, N.J., Wallace, M.W., Wang, X., Bellefroid, E.J., Gueguen, B., Cole, D.B., 2016. Integrated geochemical-petrographic insights from component-selective δ238U of Cryogenian marine carbonates. Geology 44, 935–938. https://doi.org/10.1130/G38533.1

Hood, A.V.S., Wallace, M.W., 2014. Marine cements reveal the structure of an anoxic, ferruginous Neoproterozoic ocean. J. Geol. Soc. London. 171, 741 LP – 744. https://doi.org/10.1144/jgs2013-099

Hopkinson, B.M., Barbeau, K.A., 2012. Iron transporters in marine prokaryotic genomes and metagenomes. Environ. Microbiol. 14, 114–128. https://doi.org/10.1111/j.1462-2920.2011.02539.x

Hopkinson, B.M., Barbeau, K.A., 2008. Interactive influences of iron and light limitation on phytoplankton at subsurface chlorophyll maxima in the eastern North Pacific. Limnol. Oceanogr. 53, 1303–1318. https://doi.org/10.4319/lo.2008.53.4.1303

Hua, B., Deng, B., 2008. Reductive Immobilization of Uranium(VI) by Amorphous Iron Sulfide. Environ. Sci. Technol. 42, 8703–8708. https://doi.org/10.1021/es801225z

Huang, J.-H., Huang, F., Evans, L., Glasauer, S., 2015. Vanadium: Global (bio)geochemistry. Chem. Geol. 417, 68–89. https://doi.org/https://doi.org/10.1016/j.chemgeo.2015.09.019

Isley, A.E., 1995. Hydrothermal plumes and the delivery of iron to Banded Iron Formations. J. Geol. 103, 169–185.

Isley, A.E., Abbott, D.H., 1999. Plume-related mafic volcanism and the deposition of banded iron formation. J. Geophys. Res. 104.

Jaffrés, J.B.D., Shields, G.A., Wallmann, K., 2007. The oxygen isotope evolution of seawater: A critical review of a long-standing controversy and an improved geological water cycle model for the past 3.4 billion years. Earth-Science Rev. 83, 83–122. https://doi.org/https://doi.org/10.1016/j.earscirev.2007.04.002

James, H.L., 1954. Sedimentary facies of iron-formation. Econ. Geol. 49, 253–293.

Jeremiason, J.D., Engstrom, D.R., Swain, E.B., Nater, E.A., Johnson, B.M., Almendinger, J.E., Monson, B.A., Kolka, R.K., 2006. Sulfate Addition Increases Methylmercury Production in an Experimental Wetland. Environ. Sci. Technol. 40, 3800–3806. https://doi.org/10.1021/es0524144

Jiang, C.Z., Tosca, N.J., 2020. Growth kinetics of siderite at 298.15 K and 1 bar. Geochim. Cosmochim. Acta 274, 97–117. https://doi.org/https://doi.org/10.1016/j.gca.2020.01.047

Jiang, C.Z., Tosca, N.J., 2019. Fe(II)-carbonate precipitation kinetics and the chemistry of anoxic ferruginous seawater. Earth Planet. Sci. Lett. 506, 231–242. https://doi.org/https://doi.org/10.1016/j.epsl.2018.11.010

3004 Jiao, Y., Kappler, A., Croal, L.R., Newman, D.K., 2005. Isolation and characterization of a
3005 genetically tractable photoautotrophic Fe(II)-oxidizing bacterium Rhodopseudomonas
3006 palustris strain TIE-1. Appl. Envir. Microbiol. 71, 4487–4496.
3007 Jimenez-Lopez, C., Romanek, C.S., 2004. Precipitation kinetics and carbon isotope partitioning
3008 of inorganic siderite at 25°C and 1 atm 1. Geochim. Cosmochim. Acta 68, 557–571.
3009 https://doi.org/https://doi.org/10.1016/S0016-7037(03)00460-5
3010 Jirsa, F., Neubauer, E., Kittinger, R., Hofmann, T., Krachler, R., von der Kammer, F., Keppler, B.K.,
3011 2013. Natural organic matter and iron export from the Tanner Moor, Austria. Limnologica
3012 43, 239–244. https://doi.org/https://doi.org/10.1016/j.limno.2012.09.006
3013 Johnson, B.W., Wing, B.A., 2020. Limited Archaean continental emergence reflected in an early
3014 Archaean 18O-enriched ocean. Nat. Geosci. 13, 243–248. https://doi.org/10.1038/s41561-
3015 020-0538-9
3016 Johnson, C.M., Beard, B.L., Beukes, N.J., Klein, C., O'Leary, J.M., 2003. Ancient geochemical
3017 cycling in the Earth as inferred from Fe isotope studies of banded iron formations from the
3018 Transvaal Craton. Contrib. to Mineral. Petrol. 144, 523–547.
3019 Johnson, C.M., Beard, B.L., Klein, C., Beukes, N.J., Roden, E.E., 2008a. Iron isotopes constrain
3020 biologic and abiologic processes in banded iron formation genesis. Geochim. Cosmochim.
3021 Acta 72, 151–169.
3022 Johnson, C.M., Beard, B.L., Roden, E.E., 2008b. The Iron Isotope Fingerprints of Redox and
3023 Biogeochemical Cycling in Modern and Ancient Earth. Annu. Rev. Earth Planet. Sci. 36,
3024 457–493. https://doi.org/doi:10.1146/annurev.earth.36.031207.124139
3025 Johnson, C.M., Ludois, J.M., Beard, B.L., Beukes, N.J., Heimann, A., 2013. Iron formation

carbonates: Paleoceanographic proxy or recorder of microbial diagenesis? Geology 41, 1147–1150.

Johnson, C.M., Roden, E.E., Welch, S.A., L., B.B., 2005. Experimental constraints on Fe isotope fractionation during magnetite and Fe carbonate formation coupled to dissimilatory hydrous ferric oxide reduction. Geochim. Cosmochim. Acta 69, 963–993.

Johnson, J.E., Molnar, P.H., 2019. Widespread and Persistent Deposition of Iron Formations for Two Billion Years. Geophys. Res. Lett. 46, 3327–3339. https://doi.org/10.1029/2019GL081970

Johnson, J.E., Muhling, J.R., Cosmidis, J., Rasmussen, B., Templeton, A.S., 2018. Low-Fe(III) Greenalite Was a Primary Mineral From Neoarchean Oceans. Geophys. Res. Lett. 45, 3182–3192. https://doi.org/10.1002/2017GL076311

Johnson, M.D., Adams, R.S., Gowan, A.S., Harris, K.L., Hobbs, H.C., Jennings, C.E., Knaeble, A.R., Lusardi, B.A., Meyer, G.N., 2016. RI-86 Quaternary Lithostratigraphic Units of Minnesota.

Johnson, T.C., Brown, E.T., Shi, J., 2011. Biogenic silica deposition in Lake Malawi, East Africa over the past 150,000years. Palaeogeogr. Palaeoclimatol. Palaeoecol. 303, 103–109. https://doi.org/https://doi.org/10.1016/j.palaeo.2010.01.024

Johnston, D.T., Poulton, S.W., Dehler, C., Porter, S., Husson, J., Canfield, D.E., Knoll, A.H., 2010. An emerging picture of Neoproterozoic ocean chemistry: Insights from the Chuar Group, Grand Canyon, USA. Earth Planet. Sci. Lett. 290, 64–73. https://doi.org/https://doi.org/10.1016/j.epsl.2009.11.059

Johnston, D.T., Wolfe-Simon, F., Pearson, A., Knoll, A.H., 2009. Anoxygenic photosynthesis modulated Proterozoic oxygen and sustained Earth's middle age. Proc. Natl. Acad. Sci. 106,

16925–16929. https://doi.org/10.1073/pnas.0909248106

Jones, C., Nomosatryo, S., Crowe, S.A., Bjerrum, C.J., Canfield, D.E., 2015. Iron oxides, divalent cations, silica, and the early earth phosphorus crisis. Geology 43, 135–138. https://doi.org/10.1130/G36044.1

Jones, P.M., Trost, J.J., Rosenberry, D.O., Jackson, P.R., Bode, J.A., O'Grady, R.M., 2013. Groundwater and Surface-Water Interactions near White Bear Lake, Minnesota, through 2011, U.S. Geological Survey Scientific Investigations Report 2013-5044.

Jungkunst, H.F., Krüger, J.P., Heitkamp, F., Erasmi, S., Fiedler, S., Glatzel, S., Lal, R., 2012. Accounting More Precisely for Peat and Other Soil Carbon Resources BT - Recarbonization of the Biosphere: Ecosystems and the Global Carbon Cycle, in: Lal, R., Lorenz, K., Hüttl, R.F., Schneider, B.U., von Braun, J. (Eds.), . Springer Netherlands, Dordrecht, pp. 127–157. https://doi.org/10.1007/978-94-007-4159-1_7

Kah, L.C., Lyons, T.W., Frank, T.D., 2004. Low marine sulphate and protracted oxygenation of the Proterozoic biosphere. Nature 431, 834.

Kappler, A., Johnson, C.M., Crosby, H.A., Beard, B.L., Newman, D.K., 2010. Evidence for equilibrium iron isotope fractionation by nitrate-reducing iron(II)-oxidizing bacteria. Geochim. Cosmochim. Acta 74, 2826–2842.

Kappler, A., Newman, D.K., 2004. Formation of Fe(III)-minerals by Fe(II)-oxidizing photoautotrophic bacteria. Geochim. Cosmochim. Acta 68, 1217–1226.

Kappler, A., Pasquero, C., Konhauser, K.O., Newman, D.K., 2005. Deposition of banded iron formations by anoxygenic phototrophic Fe(II)-oxidizing bacteria. Geology 33, 865–868.

Kasting, J.F., 2013. What caused the rise of atmospheric O2? Chem. Geol. 362, 13–25.

https://doi.org/10.1016/j.chemgeo.2013.05.039

Katsev, S., Verburg, P., Llirós, M., Minor, E.C., Kruger, B.R., Li, J., 2017. Tropical Meromictic Lakes: Specifics of Meromixis and Case Studies of Lakes Tanganyika, Malawi, and Matano, in: Gulati, R.D., Zadereev, E.S., Degermendzhi, A.G. (Eds.), Ecology of Meromictic Lakes. Springer International Publishing, Cham, pp. 277–323. https://doi.org/10.1007/978-3-319-49143-1_10

Kaufman, A.J., Hayes, J.M., Klein, C., 1990. Primary and diagenetic controls of isotopic compositions of iron-formation carbonates. Geochim. Cosmochim. Acta 54, 3461–3473. https://doi.org/http://dx.doi.org/10.1016/0016-7037(90)90298-Y

Kendall, B., Creaser, R.A., Gordon, G.W., Anbar, A.D., 2009. Re/Os and Mo isotope systematics of black shales from the Middle Proterozoic Velkerri and Wollogorang Formations, McArthur Basin, northern Australia. Geochim. Cosmochim. Acta 73, 2534–2558. https://doi.org/10.1016/j.gca.2009.02.013

Kendall, B., Creaser, R.A., Reinhard, C.T., Lyons, T.W., Anbar, A.D., 2015. Transient episodes of mild environmental oxygenation and oxidative continental weathering during the late Archean. Sci. Adv. 1, e1500777. https://doi.org/10.1126/sciadv.1500777

Kendall, B., Gordon, G.W., Poulton, S.W., Anbar, A.D., 2011. Molybdenum isotope constraints on the extent of late Paleoproterozoic ocean euxinia. Earth Planet. Sci. Lett. 307, 450–460. https://doi.org/https://doi.org/10.1016/j.epsl.2011.05.019

Kendall, B., Reinhard, C.T., Lyons, T.W., Kaufman, A.J., Poulton, S.W., Anbar, A.D., 2010. Pervasive oxygenation along late Archean ocean margins. Nat. Geosci. 3, 647–652.

Kerin, E.J., Gilmour, C.C., Roden, E., Suzuki, M.T., Coates, J.D., Mason, R.P., 2006. Mercury

methylation by dissimilatory iron-reducing bacteria. Appl. Environ. Microbiol. 72, 7919–7921. https://doi.org/10.1128/AEM.01602-06

Kharecha, P., Kasting, J.F., Siefert, J., 2005. A coupled atmospheric-ecosystem model of the early Archean Earth. Geobiology 3, 53–76.

Kim, S.-T., Kang, J.O., Yun, S.-T., O'Neil, J.R., Mucci, A., 2009. Experimental studies of oxygen isotope fractionation between rhodochrosite (MnCO3) and water at low temperatures. Geochim. Cosmochim. Acta 73, 4400–4408. https://doi.org/https://doi.org/10.1016/j.gca.2009.04.018

Kipp, M.A., Stüeken, E.E., Bekker, A., Buick, R., 2017. Selenium isotopes record extensive marine suboxia during the Great Oxidation Event. Proc. Natl. Acad. Sci. 114, 875 LP – 880. https://doi.org/10.1073/pnas.1615867114

Kipp, M.A., Stüeken, E.E., Yun, M., Bekker, A., Buick, R., 2018. Pervasive aerobic nitrogen cycling in the surface ocean across the Paleoproterozoic Era. Earth Planet. Sci. Lett. 500, 117–126. https://doi.org/https://doi.org/10.1016/j.epsl.2018.08.007

Kirillin, G., Shatwell, T., 2016. Generalized scaling of seasonal thermal stratification in lakes. Earth-Science Rev. 161, 179–190. https://doi.org/https://doi.org/10.1016/j.earscirev.2016.08.008

Kjensmo, J., 1967. The development and some main features of "iron-meromictic" soft water lakes. Arch. Hydrobiol. 32, 137–312.

Kjensmo, J., 1962. Some extreme features of the iron metabolism in lakes. Schweizerische Zeitschrift für Hydrol. 24, 244–252. https://doi.org/10.1007/BF02503040

Klein, C., 2005. Some Precambrian banded iron-formations (BIFs) from around the world: Their

age, geologic setting, mineralogy, metamorphism, geochemistry, and origins. Am. Mineral. 90, 1473–1499. https://doi.org/10.2138/am.2005.1871

Klein, C., Beukes, N.J., 1992. Time Distribution, Stratigraphy, and Sedimentologic Setting, and Geochemistry of Precambrian Iron-Formation, in: Schopf, J.W., Klein, C. (Eds.), The Proterozoic Bioshpere: A Multidisciplinary Biosphere. Cambridge University Press, New York, NY, pp. 139–146.

Klein, D.H., 1975. Fluxes, residence times, and sources of some elements to Lake Michigan. Water. Air. Soil Pollut. 4, 3–8. https://doi.org/10.1007/BF01794127

Knauth, L.P., Kennedy, M.J., 2009. The late Precambrian greening of the Earth. Nature 460, 728–732. https://doi.org/10.1038/nature08213

Knoll, A.H., 2003. Life on a Young Planet, REV-Revi. ed. Princeton University Press.

Koehler, I., Konhauser, K., Kappler, A., 2010. Role of Microorganisms in Banded Iron Formations BT - Geomicrobiology: Molecular and Environmental Perspective, in: Barton, L.L., Mandl, M., Loy, A. (Eds.), . Springer Netherlands, Dordrecht, pp. 309–324. https://doi.org/10.1007/978-90-481-9204-5_14

Koeksoy, E., Halama, M., Konhauser, K.O., Kappler, A., 2015. Using modern ferruginous habitats to interpret Precambrian banded iron formation deposition. Int. J. Astrobiol. FirstView, 1–13. https://doi.org/doi:10.1017/S1473550415000373

Köhler, I., Konhauser, K.O., Papineau, D., Bekker, A., Kappler, A., 2013. Biological carbon precursor to diagenetic siderite with spherical structures in iron formations. Nat Commun 4, 1741. https://doi.org/10.1038/ncomms2770

Kolber, Z.S., Gerald, F., Plumley, Lang, A.S., Beatty, J.T., Blankenship, R.E., VanDover, C.L.,

Vetriani, C., Koblizek, M., Rathgeber, C., Falkowski, P.G., 2001. Contribution of Aerobic Photoheterotrophic Bacteria to the Carbon Cycle in the Ocean. Science (80-.). 292, 2492–2495. https://doi.org/10.1126/science.1059707

Kolber, Z.S., Van Dover, C.L., Niederman, R.A., Falkowski, P.G., 2000. Bacterial photosynthesis in surface waters of the open ocean. Nature 407, 177–179.

Konhauser, K.O., Hamade, T., Raiswell, R., Morris, R.C., Grant Ferris, F., Southam, G., Canfield, D.E., 2002. Could bacteria have formed the Precambrian banded iron formations? Geology 30, 1079–1082.

Konhauser, K.O., Lalonde, S. V, Amskold, L., Holland, H.D., 2007. Was There Really an Archean Phosphate Crisis? Science (80-.). 315, 1234. https://doi.org/10.1126/science.1136328

Konhauser, K.O., Newman, D.K., Kappler, A., 2005. The potential significance of microbial Fe(III) reduction during deposition of Precambrian banded iron formations. Geobiology 3, 167–177. https://doi.org/doi:10.1111/j.1472-4669.2005.00055.x

Konhauser, K.O., Planavsky, N.J., Hardisty, D.S., Robbins, L.J., Warchola, T.J., Haugaard, R., Lalonde, S. V, Partin, C.A., Oonk, P.B.H., Tsikos, H., Lyons, T.W., Bekker, A., Johnson, C.M., 2017. Iron formations: A global record of Neoarchaean to Palaeoproterozoic environmental history. Earth-Science Rev. 172, 140–177. https://doi.org/https://doi.org/10.1016/j.earscirev.2017.06.012

Kononen, K., Hällfors, S., Kokkonen, M., Kuosa, H., Laanemets, J., Pavelson, J., Autio, R., 1998. Development of a subsurface chlorophyll maximum at the entrance to the Gulf of Finland, Baltic Sea. Limnol. Oceanogr. 43, 1089–1106. https://doi.org/10.4319/lo.1998.43.6.1089

Kopf, S.H., Newman, D.K., 2012. Photomixotrophic growth of Rhodobacter capsulatus SB1003

on ferrous iron. Geobiology 10, 216–222. https://doi.org/10.1111/j.1472-4669.2011.00313.x

Koretsky, C.M., MacLeod, A., Sibert, R.J., Snyder, C., 2012. Redox Stratification and Salinization of Three Kettle Lakes in Southwest Michigan, USA. Water, Air, Soil Pollut. 223, 1415–1427. https://doi.org/10.1007/s11270-011-0954-y

Krachler, R., Krachler, R.F., Wallner, G., Steier, P., El Abiead, Y., Wiesinger, H., Jirsa, F., Keppler, B.K., 2016. Sphagnum-dominated bog systems are highly effective yet variable sources of bio-available iron to marine waters. Sci. Total Environ. 556, 53–62. https://doi.org/https://doi.org/10.1016/j.scitotenv.2016.03.012

Krissansen-Totton, J., Arney, G.N., Catling, D.C., 2018. Constraining the climate and ocean pH of the early Earth with a geological carbon cycle model. Proc. Natl. Acad. Sci. 115, 4105 LP – 4110. https://doi.org/10.1073/pnas.1721296115

Kump, L.R., Arthur, M.A., 1999. Interpreting carbon-isotope excursions: carbonates and organic matter. Chem. Geol. 161, 181–198. https://doi.org/https://doi.org/10.1016/S0009-2541(99)00086-8

Kump, L.R., Seyfried Jr, W.E., 2005. Hydrothermal Fe fluxes during the Precambrian: Effect of low oceanic sulfate concentrations and low hydrostatic pressure on the composition of black smokers. Earth Planet. Sci. Lett. 235, 654–662.

Kunoh, T., Matsumoto, S., Nagaoka, N., Kanashima, S., Hino, K., Uchida, T., Tamura, K., Kunoh, H., Takada, J., 2017. Amino group in Leptothrix sheath skeleton is responsible for direct deposition of Fe(III) minerals onto the sheaths. Sci. Rep. 7, 6498. https://doi.org/10.1038/s41598-017-06644-8

Kunzmann, M., Halverson, G.P., Scott, C., Minarik, W.G., Wing, B.A., 2015. Geochemistry of Neoproterozoic black shales from Svalbard: Implications for oceanic redox conditions spanning Cryogenian glaciations. Chem. Geol. 417, 383–393. https://doi.org/https://doi.org/10.1016/j.chemgeo.2015.10.022

Kurzweil, F., Wille, M., Schoenberg, R., Taubald, H., Van Kranendonk, M.J., 2015. Continuously increasing δ98Mo values in Neoarchean black shales and iron formations from the Hamersley Basin. Geochim. Cosmochim. Acta 164, 523–542. https://doi.org/https://doi.org/10.1016/j.gca.2015.05.009

Kuznetsov, S.I., 1968. RECENT STUDIES ON THE ROLE OF MICROORGANISMS IN THE CYCLING OF SUBSTANCES IN LAKES1. Limnol. Oceanogr. 13, 211–224. https://doi.org/doi:10.4319/lo.1968.13.2.0211

Laakso, T.A., Schrag, D.P., 2019. Methane in the Precambrian atmosphere. Earth Planet. Sci. Lett. 522, 48–54. https://doi.org/https://doi.org/10.1016/j.epsl.2019.06.022

Lambrecht, N.L., Wittkop, C., Katsev, S., Fakhraee, M., Swanner, E.D., 2018. Geochemical characterization of two ferruginous meromictic lakes in the Upper Midwest, U. S. A. J. Geophys. Res. Biogeosciences 123, 3403–3422. https://doi.org/10.1029/2018JG004587

Lambrecht, N.L., Wittkop, C., Katsev, S., Sheik, C., Fakhraee, M., Hall, S.J., Swanner, E.D., 2020. Biogeochemical and physical controls on methane fluxes from two meromictic ferruginous lakes. Geobiology 18, 54–69. https://doi.org/10.1111/gbi.12365

Land, L.S., 1998. Failure to Precipitate Dolomite at 25 °C fromDilute Solution Despite 1000-Fold Oversaturation after32 Years. Aquat. Geochemistry 4, 361–368. https://doi.org/10.1023/A:1009688315854

Lane, C.S., Chorn, B.T., Johnson, T.C., 2013. Ash from the Toba supereruption in Lake Malawi shows no volcanic winter in East Africa at 75 ka. Proc. Natl. Acad. Sci. 110, 8025 LP – 8029. https://doi.org/10.1073/pnas.1301474110

Large, R.R., Mukherjee, I., Gregory, D., Steadman, J., Corkrey, R., Danyushevsky, L. V, 2019. Atmosphere oxygen cycling through the Proterozoic and Phanerozoic. Miner. Depos. 54, 485–506.

Lascu, I., Banerjee, S.K., Berquó, T.S., 2010. Quantifying the concentration of ferrimagnetic particles in sediments using rock magnetic methods. Geochemistry, Geophys. Geosystems 11, n/a-n/a. https://doi.org/10.1029/2010GC003182

Lau, K. V, Romaniello, S.J., Zhang, F., 2019. The Uranium Isotope Paleoredox Proxy, Elements in Geochemical Tracers in Earth System Science, Elements in Geochemical Tracers in Earth System Science. Cambridge University Press, Cambridge. https://doi.org/DOI: 10.1017/9781108584142

Laufer, K., Niemeyer, A., Nikeleit, V., Halama, M., Byrne, J.M., Kappler, A., 2017. Physiological characterization of a halotolerant anoxygenic phototrophic Fe(II)-oxidizing green-sulfur bacterium isolated from a marine sediment. FEMS Microbiol. Ecol. 93, fix054–fix054.

Lavoie, N.C., Grégoire, D.S., Stenzler, B.R., Poulain, A.J., 2020. Reduced sulphur sources favour HgII reduction during anoxygenic photosynthesis by Heliobacteria. Geobiology 18, 70–79. https://doi.org/10.1111/gbi.12364

Lebeau, O., Busigny, V., Chaduteau, C., Ader, M., 2014. Organic matter removal for the analysis of carbon and oxygen isotope compositions of siderite. Chem. Geol. 372, 54–61. https://doi.org/https://doi.org/10.1016/j.chemgeo.2014.02.020

Lefkowitz, J.N., Varekamp, J.C., Reynolds, R.W., Thomas, E., 2017. A tale of two lakes: the Newberry Volcano twin crater lakes, Oregon, USA. Geol. Soc. London, Spec. Publ. 437, 253 LP – 288. https://doi.org/10.1144/SP437.15

Lehours, A.-C., Batisson, I., Guedon, A., Mailhot, G., Fonty, G., 2009. Diversity of Culturable Bacteria, from the Anaerobic Zone of the Meromictic Lake Pavin, Able to Perform Dissimilatory-Iron Reduction in Different in Vitro Conditions. Geomicrobiol. J. 26, 212–223.

Lehours, A.-C., Evans, P., Bardot, C., Joblin, K., Gérard, F., 2007. Phylogenetic diversity of archaea and bacteria in the anoxic zone of a meromictic lake (Lake Pavin, France). Appl. Environ. Microbiol. 73, 2016–2019. https://doi.org/10.1128/AEM.01490-06

Lepot, K., Addad, A., Knoll, A.H., Wang, J., Troadec, D., Béché, A., Javaux, E.J., 2017. Iron minerals within specific microfossil morphospecies of the 1.88 Ga Gunflint Formation. Nat. Commun. 8, 14890. https://doi.org/10.1038/ncomms14890 https://www.nature.com/articles/ncomms14890#supplementary-information

Lepot, K., Williford, K.H., Philippot, P., Thomazo, C., Ushikubo, T., Kitajima, K., Mostefaoui, S., Valley, J.W., 2019. Extreme 13C-depletions and organic sulfur content argue for S-fueled anaerobic methane oxidation in 2.72 Ga old stromatolites. Geochim. Cosmochim. Acta 244, 522–547. https://doi.org/https://doi.org/10.1016/j.gca.2018.10.014

Lewis Jr., W.M., 1996. Tropical lakes: how latitude makes a difference. Perpsectives Trop. Limnol. 43–64.

Li, C., Love, G.D., Lyons, T.W., Fike, D.A., Sessions, A.L., Chu, X., 2010. A Stratified Redox Model for the Ediacaran Ocean. Science (80-.). 328, 80–83. https://doi.org/10.1126/science.1182369

Li, J., Brown, E.T., Crowe, S.A., Katsev, S., 2018. Sediment geochemistry and contributions to carbon and nutrient cycling in a deep meromictic tropical lake: Lake Malawi (East Africa). J. Great Lakes Res. 44, 1221–1234. https://doi.org/https://doi.org/10.1016/j.jglr.2017.12.001

Li, W., Beard, B.L., Johnson, C.M., 2015. Biologically recycled continental iron is a major component in banded iron formations. Proc. Natl. Acad. Sci. 201505515. https://doi.org/10.1073/pnas.1505515112

Li, W., Huberty, J.M., Beard, B.L., Kita, N.T., Valley, J.W., Johnson, C.M., 2013. Contrasting behavior of oxygen and iron isotopes in banded iron formations revealed by in situ isotopic analysis. Earth Planet. Sci. Lett. 384, 132–143. https://doi.org/https://doi.org/10.1016/j.epsl.2013.10.014

Li, Y.-L., Konhauser, K.O., Zhai, M., 2017. The formation of magnetite in the early Archean oceans. Earth Planet. Sci. Lett. 466, 103–114. https://doi.org/https://doi.org/10.1016/j.epsl.2017.03.013

Li, Z.-Q., Zhang, L.-C., Xue, C.-J., Zheng, M.-T., Zhu, M.-T., Robbins, L.J., Slack, J.F., Planavsky, N.J., Konhauser, K.O., 2018. Earth's youngest banded iron formation implies ferruginous conditions in the Early Cambrian ocean. Sci. Rep. 8, 9970. https://doi.org/10.1038/s41598-018-28187-2

Lin, C.Y., Turchyn, A. V, Krylov, A., Antler, G., 2020. The microbially driven formation of siderite in salt marsh sediments. Geobiology 18, 207–224. https://doi.org/10.1111/gbi.12371

Liu, J., Izon, G., Wang, J., Antler, G., Wang, Z., Zhao, J., Egger, M., 2018. Vivianite formation in methane-rich deep-sea sediments from the South China Sea. Biogeosciences 15, 6329–

6348. https://doi.org/10.5194/bg-15-6329-2018

Llirós, M., García–Armisen, T., Darchambeau, F., Morana, C., Triadó–Margarit, X., Inceoğlu, Ö., Borrego, C.M., Bouillon, S., Servais, P., Borges, A. V, Descy, J., Canfield, D.E., Crowe, S.A., 2015. Pelagic photoferrotrophy and iron cycling in a modern ferruginous basin. Sci. Rep. 5, 13803. https://doi.org/10.1038/srep13803http://www.nature.com/articles/srep13803#supplementary-information

Lopes, F., Viollier, E., Thiam, A., Michard, G., Abril, G., Groleau, A., Prevot, F., Carrias, J.-F., Alberic, P., Jezequel, D., 2011. Biogeochemical modelling of anaerobic vs. aerobic methane oxidation in a meromictic crater lake (Lake Pavin, France). Appl. Geochemistry 26, 1919–1932. https://doi.org/10.1016/j.apgeochem.2011.06.021

Lotfi-Kalahroodi, E., Pierson-Wickmann, A.-C., Guénet, H., Rouxel, O., Ponzevera, E., Bouhnik-Le Coz, M., Vantelon, D., Dia, A., Davranche, M., 2019. Iron isotope fractionation in iron-organic matter associations: Experimental evidence using filtration and ultrafiltration. Geochim. Cosmochim. Acta 250, 98–116. https://doi.org/https://doi.org/10.1016/j.gca.2019.01.036

Ludlam, S.D., 1996. The comparative limnology of high arctic, coastal, meromictic lakes. J. Paleolimnol. 16, 111–131.

Lunina, O.N., Savvichev, A.S., Kuznetsov, B.B., Pimenov, N. V, Gorlenko, V.M., 2013. Anoxygenic phototrophic bacteria of the Kislo-Sladkoe stratified lake (White Sea, Kandalaksha Bay). Microbiology 82, 815–832. https://doi.org/10.1134/S0026261714010081

Luo, G., Junium, C.K., Izon, G., Ono, S., Beukes, N.J., Algeo, T.J., Cui, Y., Xie, S., Summons, R.E.,

2018. Nitrogen fixation sustained productivity in the wake of the Palaeoproterozoic Great Oxygenation Event. Nat. Commun. 9, 978. https://doi.org/10.1038/s41467-018-03361-2

Luo, G., Ono, S., Beukes, N.J., Wang, D.T., Xie, S., Summons, R.E., 2016. Rapid oxygenation of Earth's atmosphere 2.33 billion years ago. Sci. Adv. 2. https://doi.org/10.1126/sciadv.1600134

Luther, G.W., Glazer, B., Ma, S., Trouwborst, R., Shultz, B.R., Druschel, G., Kraiya, C., 2003. Iron and Sulfur Chemistry in a Stratified Lake: Evidence for Iron-Rich Sulfide Complexes. Aquat. Geochemistry 9, 87–110. https://doi.org/10.1023/B:AQUA.0000019466.62564.94

Lyons, T.W., Reinhard, C.T., Planavsky, N.J., 2014. The rise of oxygen in Earth's early ocean and atmosphere. Nature 506, 307–315. https://doi.org/10.1038/nature13068

Lyons, T.W., Severmann, S., 2006. A critical look at iron paleoredox proxies: New insights from modern euxinic marine basins. Geochim. Cosmochim. Acta 70, 5698–5722. https://doi.org/10.1016/j.gca.2006.08.021

Lyons, T.W., Werne, J.P., Hollander, D.J., Murray, R.W., 2003. Contrasting sulfur geochemistry and Fe/Al and Mo/Al ratios across the last oxic-to-anoxic transition in the Cariaco Basin, Venezuela. Chem. Geol. 195, 131–157.

Mahowald, N.M., Baker, A.R., Bergametti, G., Brooks, N., Duce, R.A., Jickells, T.D., Kubilay, N., Prospero, J.M., Tegen, I., 2005. Atmospheric global dust cycle and iron inputs to the ocean. Global Biogeochem. Cycles 19. https://doi.org/10.1029/2004GB002402

Malinovsky, D.N., Rodyushkin, I. V., Shcherbakova, E.P., Ponter, C., Öhlander, B., Ingri, J., 2005. Fraction of Fe Isotopes as a result of redox processes in a basin. Geochemistry Int. 43, 878–885.

Mallet, C., Charpin, M.F., Devaux, J., 1998. Nitrate reductase activity of phytoplankton populations in eutrophic Lake Aydat and meso-oligotrophic Lake Pavin: a comparison. Hydrobiologia 373, 135–148. https://doi.org/10.1023/A:1017087825545

Mallorquí, N., Arellano, J.B., Borrego, C.M., Garcia-Gil, L.J., 2005. Signature pigments of green sulfur bacteria in lower Pleistocene deposits from the Banyoles lacustrine area (Spain). J. Paleolimnol. 34, 271–280. https://doi.org/10.1007/s10933-005-3731-3

Manske, A.K., Glaeser, J., Kuypers, M.M.M., Overmann, J., 2005. Physiology and phylogeny of green sulfur bacteria forming a monospecific phototrophic assemblage at a depth of 100 meters in the Black Sea. Appl. Environ. Microbiol. 71, 8049–8060. https://doi.org/10.1128/aem.71.12.8049-8060.2005

Martin, J.H., 1990. Glacial-interglacial CO2 change: the Iron Hypothesis. Paleoceanography 5, 1–13.

März, C., Poulton, S.W., Beckmann, B., Küster, K., Wagner, T., Kasten, S., 2008. Redox sensitivity of P cycling during marine black shale formation: Dynamics of sulfidic and anoxic, non-sulfidic bottom waters. Geochim. Cosmochim. Acta 72, 3703–3717. https://doi.org/https://doi.org/10.1016/j.gca.2008.04.025

Maynard, J.B., 2010. The Chemistry of Manganese Ores through Time: A Signal of Increasing Diversity of Earth-Surface Environments. Econ. Geol. 105, 535–552. https://doi.org/10.2113/gsecongeo.105.3.535

Mazumder, A., Taylor, W.D., 1994. Thermal structure of lakes varying in size and water clarity. Limnol. Oceanogr. 39, 968–976. https://doi.org/10.4319/lo.1994.39.4.0968

Megard, R.O., Bradbury, J.P., Dean, W.E., 1993. Climatic and limnologic setting of Elk Lake, in:

Bradbury, J. P., Dean, W.E. (Eds.), Elk Lake, Minnesota: Evidence for Rapid Climate Change in the North-Central United States. The Geological Society of America.

Mel'nik, Y.P., 1973. Physical and chemical conditions of genesis of Precambrian ferruginous quartzites. Akad Nauk Ukr. S.S.R., Inst. Geokhim. Fiz. Mineral., Kiev.

Meriläinen, J., 1970. On the limnology of the meromictic Lake Valkiajärvi, in the Finnish Lake District. Ann. Bot. Fenn. 7, 29–51.

Michard, G., Viollier, E., Jézéquel, D., Sarazin, G., 1994. Geochemical study of a crater lake: Pavin Lake, France — Identification, location and quantification of the chemical reactions in the lake. Chem. Geol. 115, 103–115. https://doi.org/https://doi.org/10.1016/0009-2541(94)90147-3

Michiels, C.C., Darchambeau, F., Roland, F.A.E., Morana, C., Llirós, M., García-Armisen, T., Thamdrup, B., Borges, A. V, Canfield, D.E., Servais, P., Descy, J.-P., Crowe, S.A., 2017. Iron-dependent nitrogen cycling in a ferruginous lake and the nutrient status of Proterozoic oceans. Nat. Geosci. 10, 217.

Mloszewska, A.M., Cole, D.B., Planavsky, N.J., Kappler, A., Whitford, D.S., Owttrim, G.W., Konhauser, K.O., 2018. UV radiation limited the expansion of cyanobacteria in early marine photic environments. Nat. Commun. 9, 3088. https://doi.org/10.1038/s41467-018-05520-x

Molot, L.A., Dillon, P.J., Clark, B.J., Neary, B.P., 1992. Predicting End-of-Summer Oxygen Profiles in Stratified Lakes. Can. J. Fish. Aquat. Sci. 49, 2363–2372. https://doi.org/10.1139/f92-260

Morana, C., Roland, F.A.E., Crowe, S.A., Llirós, M., Borges, A. V., Darchambeau, F., Bouillon, S., 2016. Chemoautotrophy and anoxygenic photosynthesis within the water column of a large meromictic tropical lake (Lake Kivu, East Africa). Limnol. Oceanogr. 61, 1424–1437.

https://doi.org/10.1002/lno.10304

Mori, Y., Kataoka, T., Okamura, T., Kondo, R., 2013. Dominance of green sulfur bacteria in the chemocline of the meromictic Lake Suigetsu, Japan, as revealed by dissimilatory sulfite reductase gene analysis. Arch. Microbiol. 195, 303–312. https://doi.org/10.1007/s00203-013-0879-5

Morris, R.C., 2012. Genesis of iron ore in Banded Iron-Formation by supergene and supergene-metamorphic processes - a conceptual model, in: Luisa, B.G. (Ed.), Regional Studies and Specific Deposits. Elsevier.

Morris, R.C., 1993. Genetic modelling for banded iron-formation of the Hamersley Group, Pilbara Craton, Western Australia. Precambrian Res. 60, 243–286. https://doi.org/10.1016/0301-9268(93)90051-3

Morse, J.W., Arakaki, T., 1993. Adsorption and coprecipitation of divalent metals with mackinawite (FeS). Geochim. Cosmochim. Acta 57, 3635–3640.

Muehlenbachs, K., 1998. The oxygen isotopic composition of the oceans, sediments and the seafloor. Chem. Geol. 145, 263–273. https://doi.org/https://doi.org/10.1016/S0009-2541(97)00147-2

Mulholland, D.S., Poitrasson, F., Shirokova, L.S., González, A.G., Pokrovsky, O.S., Boaventura, G.R., Vieira, L.C., 2015. Iron isotope fractionation during Fe(II) and Fe(III) adsorption on cyanobacteria. Chem. Geol. 400, 24–33. https://doi.org/http://dx.doi.org/10.1016/j.chemgeo.2015.01.017

Myrbo, A., 2008. Sedimentary and historical context of eutrophication and remediation in urban Lake McCarrons (Roseville, MN). Lake Reserv. Manag. 24, 349–360.

Myrbo, A., Shapley, M.D., 2006. Seasonal water-column dynamics of dissolved inorganic carbon stable isotopic compositions (δ13CDIC) in small hardwater lakes in Minnesota and Montana. Geochim. Cosmochim. Acta 70, 2699–2714. https://doi.org/http://dx.doi.org/10.1016/j.gca.2006.02.010

Novotny, E. V, Murphy, D., Stefan, H.G., 2008. Increase of urban lake salinity by road deicing salt. Sci. Total Environ. 406, 131–144. https://doi.org/https://doi.org/10.1016/j.scitotenv.2008.07.037

Nürnberg, G.K., Dillon, P.J., 1993. Iron Budgets in Temperate Lakes. Can. J. Fish. Aquat. Sci. 50, 1728–1737. https://doi.org/10.1139/f93-194

Oehlerich, M., Baumer, M., Lücke, A., Mayr, C., 2013. Effects of organic matter on carbonate stable isotope ratios (δ13C, δ18O values) – implications for analyses of bulk sediments. Rapid Commun. Mass Spectrom. 27, 707–712. https://doi.org/10.1002/rcm.6492

Ohmoto, H., Watanabe, Y., Yamaguchi, K.E., Naraoka, H., Haruna, M., Kakegawa, T., Hayashi, K., Kato, Y., 2006. Chemical and biological evolution of early Earth: Constraints from banded iron formations, in: Kesler, S.E., Ohmoto, H. (Eds.), Evolution of Early Earth's Atmosphere, Hydrosphere, and Biosphere - Constraints from Ore Deposits. Geological Society of America, p. 0. https://doi.org/10.1130/2006.1198(17)

Ojala, A.E.K., Saarnisto, M., 1999. Comparative varve counting and magnetic properties of the 8400-yr sequence of an annually laminated sediment in Lake Valkiajärvi, Central Finland. J. Paleolimnol. 22, 335–348. https://doi.org/10.1023/A:1008064613031

Olson, S.L., Kump, L.R., Kasting, J.F., 2013. Quantifying the areal extent and dissolved oxygen concentrations of Archean oxygen oases. Chem. Geol. 362, 35–43.

Ordoñez, L., Vogel, H., Sebag, D., Ariztegui, D., Adatte, T., Russell, J.M., Kallmeyer, J., Vuillemin, A., Friese, A., Crowe, S.A., Bauer, K.W., Simister, R., Henny, C., Nomosatryo, S., Bijaksana, S., 2019. Empowering conventional Rock-Eval pyrolysis for organic matter characterization of the siderite-rich sediments of Lake Towuti (Indonesia) using End-Member Analysis. Org. Geochem. 134, 32–44. https://doi.org/https://doi.org/10.1016/j.orggeochem.2019.05.002

Oren, A., 2011. 12 - Characterization of Pigments of Prokaryotes and Their Use in Taxonomy and Classification, in: Rainey, F., Oren, A.B.T.-M. in M. (Eds.), Taxonomy of Prokaryotes. Academic Press, pp. 261–282. https://doi.org/https://doi.org/10.1016/B978-0-12-387730-7.00012-7

Orihel, D.M., Schindler, D.W., Ballard, N.C., Graham, M.D., O'Connell, D.W., Wilson, L.R., Vinebrooke, R.D., 2015. The "nutrient pump:" Iron-poor sediments fuel low nitrogen-to-phosphorus ratios and cyanobacterial blooms in polymictic lakes. Limnol. Oceanogr. 60, 856–871. https://doi.org/10.1002/lno.10076

Ossa Ossa, F., Hofmann, A., Spangenberg, J.E., Poulton, S.W., Stüeken, E.E., Schoenberg, R., Eickmann, B., Wille, M., Butler, M., Bekker, A., 2019. Limited oxygen production in the Mesoarchean ocean. Proc. Natl. Acad. Sci. 201818762. https://doi.org/10.1073/pnas.1818762116

Oswald, K., Jegge, C., Tischer, J., Berg, J., Brand, A., Miracle, M.R., Soria, X., Vicente, E., Lehmann, M.F., Zopfi, J., Schubert, C.J., 2016. Methanotrophy under Versatile Conditions in the Water Column of the Ferruginous Meromictic Lake La Cruz (Spain). Front. Microbiol. 7. https://doi.org/10.3389/fmicb.2016.01762

Overmann, J., Cypionka, H., Pfenning, N., 1992. An extremely low-light-adapted phototrophic

sulfur bacterium from the Black Sea. Limnol. Ocean. 37, 150–154.

Overmann, J., Garcia-Pichel, F., 2013. The Phototrophic Way of Life BT - The Prokaryotes: Prokaryotic Communities and Ecophysiology, in: Rosenberg, E., DeLong, E.F., Lory, S., Stackebrandt, E., Thompson, F. (Eds.), The Prokaryotes. Springer Berlin Heidelberg, Berlin, Heidelberg, pp. 203–257. https://doi.org/10.1007/978-3-642-30123-0_51

Ozaki, K., Tajika, E., Hong, P.K., Nakagawa, Y., Reinhard, C.T., 2018. Effects of primitive photosynthesis on Earth's early climate system. Nat. Geosci. 11, 55–59. https://doi.org/10.1038/s41561-017-0031-2

Papineau, D., She, Z., Dodd, M.S., 2017. Chemically-oscillating reactions during the diagenetic oxidation of organic matter and in the formation of granules in late Palaeoproterozoic chert from Lake Superior. Chem. Geol. 470, 33–54. https://doi.org/https://doi.org/10.1016/j.chemgeo.2017.08.021

Parkin, T.B., Brock, T.D., 1980. Photosynthetic bacterial production in lakes: The effects of light intensity. Limnol. Oceanogr. 25, 711–718. https://doi.org/10.4319/lo.1980.25.4.0711

Partin, C.A., Lalonde, S. V, Planavsky, N.J., Bekker, A., Rouxel, O.J., Lyons, T.W., Konhauser, K.O., 2013. Uranium in iron formations and the rise of atmospheric oxygen. Chem. Geol. 362, 82–90. https://doi.org/http://dx.doi.org/10.1016/j.chemgeo.2013.09.005

Pasche, N., Muvundja, F.A., Schmid, M., Wüest, A., Müller, B., 2012. Nutrient cycling in Lake Kivu, in: Descy, J.-P., Darchambeau, F., Schmid, M. (Eds.), Lake Kivu: Limnology and Biogeochemistry of a Tropical Great Lake. pp. 31–46.

Pasche, N., Schmid, M., Vazquez, F., Schubert, C.J., Wüest, A., Kessler, J.D., Pack, M.A., Reeburgh, W.S., Bürgmann, H., 2011. Methane sources and sinks in Lake Kivu. J. Geophys.

Res. Biogeosciences 116. https://doi.org/10.1029/2011JG001690

Pavlov, A.A., Hurtgen, M.T., Kasting, J.F., Arthur, M.A., 2003. Methane-rich Proterozoic atmosphere. Geology 31, 87–90.

Perry, E.C., Tan, F.C., Morey, G.B., 1973. Geology and Stable Isotope Geochemistry of the Biwabik Iron Formation, Northern Minnesota. Econ. Geol. 68, 1110–1125.

Picard, A., Kappler, A., Schmid, G., Quaroni, L., Obst, M., 2015. Experimental diagenesis of organo-mineral structures formed by microaerophilic Fe(II)-oxidizing bacteria. Nat Commun 6, Article number 6277. https://doi.org/10.1038/ncomms7277

Piper, D.Z., Calvert, S.E., 2009. A marine biogeochemical perspective on black shale deposition. Earth-Science Rev. 95, 63–96. https://doi.org/10.1016/j.earscirev.2009.03.001

Planavsky, N.J., Asael, D., Hofmann, A., Reinhard, C.T., Lalonde, S. V, Knudsen, A., Wang, X., Ossa Ossa, F., Pecoits, E., Smith, A.J.B., Beukes, N.J., Bekker, A., Johnson, T.M., Konhauser, K.O., Lyons, T.W., Rouxel, O.J., 2014a. Evidence for oxygenic photosynthesis half a billion years before the Great Oxidation Event. Nat. Geosci. 7, 283–286. https://doi.org/10.1038/ngeo2122http://www.nature.com/ngeo/journal/vaop/ncurrent/abs/ngeo2122.html#supplementary-information

Planavsky, N.J., Cole, D.B., Reinhard, C.T., Diamond, C., Love, G.D., Luo, G., Zhang, S., Konhauser, K.O., Lyons, T.W., 2016. No evidence for high atmospheric oxygen levels 1,400 million years ago. Proc. Natl. Acad. Sci. 113, E2550 LP-E2551. https://doi.org/10.1073/pnas.1601925113

Planavsky, N.J., McGoldrick, P., Scott, C.T., Li, C., Reinhard, C.T., Kelly, A.E., Chu, X., Bekker, A., Love, G.D., Lyons, T.W., 2011. Widespread iron-rich conditions in the mid-Proterozoic

ocean. Nature 477, 448–451. https://doi.org/http://www.nature.com/nature/journal/v477/n7365/abs/nature10327.html#supplementary-information

Planavsky, N.J., Reinhard, C.T., Wang, X., Thomson, D., McGoldrick, P., Rainbird, R.H., Johnson, T., Fischer, W.W., Lyons, T.W., 2014b. Low Mid-Proterozoic atmospheric oxygen levels and the delayed rise of animals. Science (80-.). 346, 635–638. https://doi.org/10.1126/science.1258410

Planavsky, N.J., Robbins, L.J., Kamber, B.S., Schoenberg, R., 2020. Weathering, alteration and reconstructing Earth's oxygenation. Interface Focus 10, 20190140. https://doi.org/10.1098/rsfs.2019.0140

Planavsky, N.J., Rouxel, O.J., Bekker, A., Lalonde, S. V, Konhauser, K.O., Reinhard, C.T., Lyons, T.W., 2010. The evolution of the marine phosphate reservoir. Nature 467, 1088–1090. https://doi.org/http://www.nature.com/nature/journal/v467/n7319/abs/10.1038-nature09485-unlocked.html#supplementary-information

Planavsky, N.J., Rouxel, O.J., Bekker, A., Shapiro, R., Fralick, P.W., Knudsen, A., 2009. Iron-oxidizing microbial ecosystems thrived in late Paleoproterozoic redox-stratified oceans. Earth Planet. Sci. Lett. 286, 230–242.

Planavsky, N.J., Slack, J.F., Cannon, W.F., O'Connell, B., Isson, T.T., Asael, D., Jackson, J.C., Hardisty, D.S., Lyons, T.W., Bekker, A., 2018. Evidence for episodic oxygenation in a weakly redox-buffered deep mid-Proterozoic ocean. Chem. Geol. 483, 581–594. https://doi.org/https://doi.org/10.1016/j.chemgeo.2018.03.028

Posth, N.R., Köhler, I., D. Swanner, E., Schröder, C., Wellmann, E., Binder, B., Konhauser, K.O.,

Neumann, U., Berthold, C., Nowak, M., Kappler, A., 2013a. Simulating Precambrian banded iron formation diagenesis. Chem. Geol. 362, 66–73. https://doi.org/10.1016/j.chemgeo.2013.05.031

Posth, N.R., Konhauser, K.O., Kappler, A., 2013b. Microbiological processes in banded iron formation deposition. Sedimentology 60, 1733–1754. https://doi.org/10.1111/sed.12051

Poulain, A.J., Newman, D.K., 2009. Rhodobacter capsulatus Catalyzes Light-Dependent Fe(II) Oxidation under Anaerobic Conditions as a Potential Detoxification Mechanism. Appl. Environ. Microbiol. 75, 6639–6646. https://doi.org/10.1128/aem.00054-09

Poulson, R.L., Siebert, C., McManus, J., Berelson, W.M., 2006. Authigenic molybdenum isotope signatures in marine sediments. Geology 34, 617–620. https://doi.org/10.1130/g22485.1

Poulton, S.W., Canfield, D.E., 2011. Ferruginous Conditions: A Dominant Feature of the Ocean through Earth's History. Elements 7, 107–112. https://doi.org/10.2113/gselements.7.2.107

Poulton, S.W., Canfield, D.E., 2005. Development of a sequential extraction procedure for iron: implications for iron partitioning in continentally derived particulates. Chem. Geol. 214, 209–221.

Poulton, S.W., Fralick, P.W., Canfield, D.E., 2010. Spatial variability in oceanic redox structure 1.8 billion years ago. Nat. Geosci 3, 486–490.

Poulton, S.W., Fralick, P.W., Canfield, D.E., 2004a. The transition to a sulphidic ocean ~1.84 billion years ago. Nature 431, 173–177.

Poulton, S.W., Henkel, S., März, C., Urquhart, H., Flögel, S., Kasten, S., Sinninghe Damsté, J.S., Wagner, T., 2015. A continental-weathering control on orbitally driven redox-nutrient cycling during Cretaceous Oceanic Anoxic Event 2. Geology 43, 963–966.

https://doi.org/10.1130/G36837.1

Poulton, S.W., Krom, M.D., Raiswell, R., 2004b. A revised scheme for the reactivity of iron (oxyhydr)oxide minerals towards dissolved sulfide. Geochim. Cosmochim. Acta 68, 3703–3715.

Raiswell, R., 2006. An evaluation of diagenetic recycling as a source of iron for banded iron formations, in: Kesler, S.E., Ohmoto, H. (Eds.), Evolution of Early Earth's Atmosphere, Hydrosphere, and Biosphere - Constraints from Ore Deposits. Geological Society of America, p. 0. https://doi.org/10.1130/2006.1198(13)

Raiswell, R., Hardisty, D.S., Lyons, T.W., Canfield, D.E., Owens, J.D., Planavsky, N.J., Poulton, S.W., Reinhard, C.T., 2018. The iron paleoredox proxies: A guide to the pitfalls, problems and proper practice. Am. J. Sci. 318, 491–526. https://doi.org/10.2475/05.2018.03

Raiswell, R., Reinhard, C.T., Derkowski, A., Owens, J., Bottrell, S.H., Anbar, A.D., Lyons, T.W., 2011. Formation of syngenetic and early diagenetic iron minerals in the late Archean Mt. McRae Shale, Hamersley Basin, Australia: New insights on the patterns, controls and paleoenvironmental implications of authigenic mineral formation. Geochim. Cosmochim. Acta 75, 1072–1087. https://doi.org/10.1016/j.gca.2010.11.013

Rasmussen, B., Fletcher, I.R., Bekker, A., Muhling, J.R., Gregory, C.J., Thorne, A.M., 2012. Deposition of 1.88-billion-year-old iron formations as a consequence of rapid crustal growth. Nature 484, 498–501. https://doi.org/http://www.nature.com/nature/journal/v484/n7395/abs/nature11021.html#supplementary-information

Rasmussen, B., Krapež, B., Meier, D.B., 2014. Replacement origin for hematite in 2.5 Ga banded

iron formation: Evidence for postdepositional oxidation of iron-bearing minerals. Geol. Soc. Am. Bull. 126, 438–446. https://doi.org/10.1130/b30944.1

Rasmussen, B., Krapež, B., Muhling, J.R., Suvorova, A., 2015. Precipitation of iron silicate nanoparticles in early Precambrian oceans marks Earth's first iron age. Geology 43, 303–306. https://doi.org/10.1130/g36309.1

Rasmussen, B., Meier, D.B., Krapež, B., Muhling, J.R., 2013. Iron silicate microgranules as precursor sediments to 2.5-billion-year-old banded iron formations. Geology 41, 435–438. https://doi.org/10.1130/G33828.1

Rasmussen, B., Muhling, J.R., 2018. Making magnetite late again: Evidence for widespread magnetite growth by thermal decomposition of siderite in Hamersley banded iron formations. Precambrian Res. 306, 64–93. https://doi.org/https://doi.org/10.1016/j.precamres.2017.12.017

Rasmussen, B., Muhling, J.R., Suvorova, A., Krapež, B., 2017. Greenalite precipitation linked to the deposition of banded iron formations downslope from a late Archean carbonate platform. Precambrian Res. 290, 49–62. https://doi.org/https://doi.org/10.1016/j.precamres.2016.12.005

Raven, J.A., Kübler, J.E., Beardall, J., 2000. Put out the light, and then put out the light. J. Mar. Biol. Assoc. United Kingdom 80, 1–25. https://doi.org/DOI: 10.1017/S0025315499001526

Reinhard, C.T., Planavsky, N.J., 2011. Mineralogical constraints on Precambrian pCO2. Nature 474, E1–E1.

Reinhard, C.T., Planavsky, N.J., Gill, B.C., Ozaki, K., Robbins, L.J., Lyons, T.W., Fischer, W.W., Wang, C., Cole, D.B., Konhauser, K.O., 2016. Evolution of the global phosphorus cycle.

Nature 541, 386.

Reinhard, C.T., Planavsky, N.J., Robbins, L.J., Partin, C.A., Gill, B.C., Lalonde, S. V, Bekker, A., Konhauser, K.O., Lyons, T.W., 2013. Proterozoic ocean redox and biogeochemical stasis. Proc. Natl. Acad. Sci. https://doi.org/10.1073/pnas.1208622110

Rico, K.I., Sheldon, N.D., 2019. Nutrient and iron cycling in a modern analogue for the redoxcline of a Proterozoic ocean shelf. Chem. Geol. 511, 42–50. https://doi.org/https://doi.org/10.1016/j.chemgeo.2019.02.032

Rico, K.I., Sheldon, N.D., Gallagher, T.M., Chappaz, A., 2019. Redox Chemistry and Molybdenum Burial in a Mesoproterozoic Lake. Geophys. Res. Lett. 46, 5871–5878. https://doi.org/10.1029/2019GL083316

Robbins, E.I., LaBaugh, J.W., Merk, D.A., Parkhurst, L.J., Puckett, D.P., Rosenberry, D.O., Schuster, P.F., Shelito, P.A., 1997. Bacterial indicators of ground-water discharge-iron seeps in the Shingobee River and Crow Wing watersheds, in: Winter, T.C. (Ed.), Interdisciplinary Research Initiative: Hydrological and Biogeochemical Research in the Shingobee River Headwaters Area, North-Central Minnesota. United States Geological Survey Water Resources Investigations Research, pp. 177–186.

Robbins, L.J., Funk, S.P., Flynn, S.L., Warchola, T.J., Li, Z., Lalonde, S. V, Rostron, B.J., Smith, A.J.B., Beukes, N.J., de Kock, M.O., Heaman, L.M., Alessi, D.S., Konhauser, K.O., 2019. Hydrogeological constraints on the formation of Palaeoproterozoic banded iron formations. Nat. Geosci. 12, 558–563. https://doi.org/10.1038/s41561-019-0372-0

Robbins, L.J., Lalonde, S. V, Planavsky, N.J., Partin, C.A., Reinhard, C.T., Kendall, B., Scott, C., Hardisty, D.S., Gill, B.C., Alessi, D.S., Dupont, C.L., Saito, M.A., Crowe, S.A., Poulton, S.W.,

Bekker, A., Lyons, T.W., Konhauser, K.O., 2016. Trace elements at the intersection of marine biological and geochemical evolution. Earth-Science Rev. 163, 323–348. https://doi.org/https://doi.org/10.1016/j.earscirev.2016.10.013

Robbins, L.J., Lalonde, S. V, Saito, M.A., Planavsky, N.J., Mloszewska, A.M., Pecoits, E., Scott, C., Dupont, C.L., Kappler, A., Konhauser, K.O., 2013. Authigenic iron oxide proxies for marine zinc over geological time and implications for marine eukaryotic metallome evolution. Geobiology 11, 295–306.

Roden, E.E., Urrutia, M.M., 2002. Influence of Biogenic Fe(II) on Bacterial Crystalline Fe(III) Oxide Reduction. Geomicrobiol. J. 19, 209–251. https://doi.org/10.1080/01490450252864280

Roden, E.E., Wetzel, R.G., 2003. Competition between Fe(III)-Reducing and Methanogenic Bacteria for Acetate in Iron-Rich Freshwater Sediments. Microb. Ecol. 45, 252–258. https://doi.org/10.1007/s00248-002-1037-9

Rodrigo, M.A., Miracle, M.R., Vicente, E., 2001. The meromictic Lake La Cruz (Central Spain). Patterns of stratification. Aquat. Sci. 63, 406–416. https://doi.org/10.1007/s00027-001-8041-x

Rogozin, D.Y., Trusova, M.Y., Khromechek, E.B., Degermendzhy, A.G., 2010. Microbial community of the chemocline of the meromictic Lake Shunet (Khakassia, Russia) during summer stratification. Microbiology 79, 253–261. https://doi.org/10.1134/S0026261710020189

Rolison, J.M., Stirling, C.H., Middag, R., Gault-Ringold, M., George, E., Rijkenberg, M.J.A., 2018. Iron isotope fractionation during pyrite formation in a sulfidic Precambrian ocean

analogue. Earth Planet. Sci. Lett. 488, 1–13. https://doi.org/10.1016/j.epsl.2018.02.006

Rosenbaum, J., Sheppard, S.M.F., 1986. An isotopic study of siderites, dolomites and ankerites at high temperatures. Geochim. Cosmochim. Acta 50, 1147–1150. https://doi.org/https://doi.org/10.1016/0016-7037(86)90396-0

Rosing, M.T., Bird, D.K., Sleep, N.H., Bjerrum, C.J., 2010. No climate paradox under the faint early Sun. Nature 464, 744–747.

Ross, K.A., Gashugi, E., Gafasi, A., Wüest, A., Schmid, M., 2015. Characterisation of the Subaquatic Groundwater Discharge That Maintains the Permanent Stratification within Lake Kivu; East Africa. PLoS One 10, e0121217.

Rouxel, O.J., Bekker, A., Edwards, K.J., 2005. Iron Isotope Constraints on the Archean and Paleoproterozoic Ocean Redox State. Science (80-.). 307, 1088–1091. https://doi.org/10.1126/science.1105692

Roy, S., 2006. Sedimentary manganese metallogenesis in response to the evolution of the Earth system. Earth-Science Rev. 77, 273–305. https://doi.org/http://dx.doi.org/10.1016/j.earscirev.2006.03.004

Salonen, K., Arvola, L., Rask, M., 1983. Autumnal and vernal circulation of small forest lakes in Southern Finland. Verhandlungen Int. Vereinigung für Theor. und Angew. Limnol. 22, 103–107.

Savvichev, A.S., Kokryatskaya, N.M., Zabelina, S.A., Rusanov, I.I., Zakharova, E.E., Veslopolova, E.F., Lunina, O.N., Patutina, E.O., Bumazhkin, B.K., Gruzdev, D.S., Sigalevich, P.A., Pimenov, N. V, Kuznetsov, B.B., Gorlenko, V.M., 2017. Microbial processes of the carbon and sulfur cycles in an ice-covered, iron-rich meromictic lake Svetloe (Arkhangelsk region, Russia).

Environ. Microbiol. 19, 659–672. https://doi.org/10.1111/1462-2920.13591

Savvichev, A.S., Rusanov, I.I., Rogozin, D.Y., Zakharova, E.E., Lunina, O.N., Bryantseva, I.A., Yusupov, S.K., Pimenov, N. V, Degermendzhi, A.G., Ivanov, M. V, 2005. Microbiological and Isotopic-Geochemical Investigations of Meromictic Lakes in Khakasia in Winter. Microbiology 74, 477–485. https://doi.org/10.1007/s11021-005-0092-x

Schiff, S.L., Tsuji, J.M., Wu, L., Venkiteswaran, J.J., Molot, L.A., Elgood, R.J., Paterson, M.J., Neufeld, J.D., 2017. Millions of Boreal Shield Lakes can be used to Probe Archaean Ocean Biogeochemistry. Sci. Rep. 7, 46708.

Scholz, C.A., Cohen, A.S., Johnson, T.C., King, J., Talbot, M.R., Brown, E.T., 2011a. Scientific drilling in the Great Rift Valley: The 2005 Lake Malawi Scientific Drilling Project — An overview of the past 145,000years of climate variability in Southern Hemisphere East Africa. Palaeogeogr. Palaeoclimatol. Palaeoecol. 303, 3–19. https://doi.org/https://doi.org/10.1016/j.palaeo.2010.10.030

Scholz, C.A., Talbot, M.R., Brown, E.T., Lyons, R.P., 2011b. Lithostratigraphy, physical properties and organic matter variability in Lake Malawi Drillcore sediments over the past 145,000years. Palaeogeogr. Palaeoclimatol. Palaeoecol. 303, 38–50. https://doi.org/https://doi.org/10.1016/j.palaeo.2010.10.028

Scholz, F., 2018. Identifying oxygen minimum zone-type biogeochemical cycling in Earth history using inorganic geochemical proxies. Earth-Science Rev. 184, 29–45. https://doi.org/https://doi.org/10.1016/j.earscirev.2018.08.002

Schopf, J.W., Kitajima, K., Spicuzza, M.J., Kudryavtsev, A.B., Valley, J.W., 2018. SIMS analyses of the oldest known assemblage of microfossils document their taxon-correlated carbon

3642 isotope compositions. Proc. Natl. Acad. Sci. 115, 53 LP – 58.
3643 https://doi.org/10.1073/pnas.1718063115
3644 Schultze, M., Boehrer, B., Wendt-Potthoff, K., Katsev, S., Brown, E.T., 2017. Chemical Setting
3645 and Biogeochemical Reactions in Meromictic Lakes BT - Ecology of Meromictic Lakes, in:
3646 Gulati, R.D., Zadereev, E.S., Degermendzhi, A.G. (Eds.), . Springer International Publishing,
3647 Cham, pp. 35–59. https://doi.org/10.1007/978-3-319-49143-1_3
3648 Schulz-Vogt, H.N., 2011. Beggiatoa BT - Encyclopedia of Geobiology, in: Reitner, J., Thiel, V.
3649 (Eds.), . Springer Netherlands, Dordrecht, pp. 111–112. https://doi.org/10.1007/978-1-
3650 4020-9212-1_22
3651 Scott, C., Lyons, T.W., 2012. Contrasting molybdenum cycling and isotopic properties in euxinic
3652 versus non-euxinic sediments and sedimentary rocks: Refining the paleoproxies. Chem.
3653 Geol. 324–325, 19–27.
3654 Scott, C., Lyons, T.W., Bekker, A., Shen, Y., Poulton, S.W., Chu, X., Anbar, A.D., 2008. Tracing the
3655 stepwise oxygenation of the Proterozoic ocean. Nature 452, 456–459.
3656 Scott, C., Planavsky, N.J., Dupont, C.L., Kendall, B., Gill, B.C., Robbins, L.J., Husband, K.F., Arnold,
3657 G.L., Wing, B.A., Poulton, S.W., Bekker, A., Anbar, A.D., Konhauser, K.O., Lyons, T.W., 2012.
3658 Bioavalability of zinc in marine systems through time. Nat. Geosci. 6, 125–128.
3659 https://doi.org/DOI: 10.1038/NGEO1679
3660 Shanks III, W.C., 2001. Stable Isotopes in Seafloor Hydrothermal Systems: Vent fluids,
3661 hydrothermal deposits, hydrothermal alteration, and microbial processes. Rev. Mineral.
3662 Geochemistry 43, 469–525. https://doi.org/10.2138/gsrmg.43.1.469
3663 Shanks III, W.C., Böhlke, J.K., Seal II, R.R., 1995. Stable Isotopes in Mid-Ocean Ridge

Hydrothermal Systems: Interactions Between Fluids, Minerals, and Organisms. Seafloor Hydrothermal Syst. Phys. Chem. Biol. Geol. Interact., Geophysical Monograph Series. https://doi.org/doi:10.1029/GM091p0194

Shaporenko, S.I., Shil'krot, G.S., 2006. Stability and variations in hydrochemical characteristics of Lake Glubokoe under conditions of a natural reserve. Water Resour. 33, 421–435. https://doi.org/10.1134/S0097807806040087

Sheen, A.I., Kendall, B., Reinhard, C.T., Creaser, R.A., Lyons, T.W., Bekker, A., Poulton, S.W., Anbar, A.D., 2018. A model for the oceanic mass balance of rhenium and implications for the extent of Proterozoic ocean anoxia. Geochim. Cosmochim. Acta 227, 75–95. https://doi.org/https://doi.org/10.1016/j.gca.2018.01.036

Shen, Y., Canfield, D.E., Knoll, A.H., 2002. Middle Proterozoic ocean chemistry: Evidence from the McArthur Basin, northern Australia. Am. J. Sci. 302, 81–109. https://doi.org/10.2475/ajs.302.2.81

Shen, Y., Knoll, A.H., Walter, M.R., 2003. Evidence for low sulphate and anoxia in a mid-Proterozoic marine basin. Nature 423, 632–635. https://doi.org/http://www.nature.com/nature/journal/v423/n6940/suppinfo/nature01651_S1.html

Shields, G., Veizer, J., 2002. Precambrian marine carbonate isotope database: Version 1.1. Geochemistry, Geophys. Geosystems 3, 1 of 12–12 12. https://doi.org/10.1029/2001GC000266

Si, Y., Zou, Y., Liu, X., Si, X., Mao, J., 2015. Mercury methylation coupled to iron reduction by dissimilatory iron-reducing bacteria. Chemosphere 122, 206–212.

https://doi.org/https://doi.org/10.1016/j.chemosphere.2014.11.054

Sibert, R.J., Koretsky, C.M., Wyman, D.A., 2015. Cultural meromixis: Effects of road salt on the chemical stratification of an urban kettle lake. Chem. Geol. 395, 126–137.

Silsbe, G.M., Malkin, S.Y., 2016. Where Light and Nutrients Collide: The Global Distribution and Activity of Subsurface Chlorophyll Maximum Layers, in: Glibert, P.M., Kana, T.M. (Eds.), Aquatic Microbial Ecology and Biogeochemistry: A Dual Perspective. Springer International Publishing, Cham, pp. 141–152. https://doi.org/10.1007/978-3-319-30259-1_12

Simonson, B.M., 1985. Sedimentological constraints on the origins of Precambrian iron-formations. GSA Bull. 96, 244–252. https://doi.org/10.1130/0016-7606(1985)96<244:SCOTOO>2.0.CO;2

Simpkins, W.W., Parkin, T.B., 1993. Hydrogeology and Redox Geochemistry of CH4 in a Late Wisconsinan Till and Loess Sequence in Central Iowa. Water Resour. Reserach 29, 3643–3657.

Slotznick, S.P., Fischer, W.W., 2016. Examining Archean methanotrophy. Earth Planet. Sci. Lett. 441, 52–59. https://doi.org/https://doi.org/10.1016/j.epsl.2016.02.013

Slotznick, S.P., Swanson-Hysell, N.L., Sperling, E.A., 2018. Oxygenated Mesoproterozoic lake revealed through magnetic mineralogy. Proc. Natl. Acad. Sci. 115, 12938 LP – 12943. https://doi.org/10.1073/pnas.1813493115

Smith Jr., L.L., 1940. A Limnological Investigation of a Permanantly Stratified Lake in the Huron Mountain Region of Northern Michigan. Michigan Acad. Sci. Arts Lett.

Song, Haijun, Jiang, G., Poulton, S.W., Wignall, P.B., Tong, J., Song, Huyue, An, Z., Chu, D., Tian, L., She, Z., Wang, C., 2017. The onset of widespread marine red beds and the evolution of

ferruginous oceans. Nat. Commun. 8, 399. https://doi.org/10.1038/s41467-017-00502-x

Sperling, E.A., Rooney, A.D., Hays, L., Sergeev, V.N., Vorob'eva, N.G., Sergeeva, N.D., Selby, D., Johnston, D.T., Knoll, A.H., 2014. Redox heterogeneity of subsurface waters in the Mesoproterozoic ocean. Geobiology. https://doi.org/10.1111/gbi.12091

Sperling, E.A., Wolock, C.J., Morgan, A.S., Gill, B.C., Kunzmann, M., Halverson, G.P., Macdonald, F.A., Knoll, A.H., Johnston, D.T., 2015. Statistical analysis of iron geochemical data suggests limited late Proterozoic oxygenation. Nature 523, 451–454.

Stanton, C.L., Reinhard, C.T., Kasting, J.F., Ostrom, N.E., Haslun, J.A., Lyons, T.W., Glass, J.B., 2018. Nitrous oxide from chemodenitrification: A possible missing link in the Proterozoic greenhouse and the evolution of aerobic respiration. Geobiology 16, 597–609. https://doi.org/10.1111/gbi.12311

Steadman, J.A., Large, R.R., Blamey, N.J., Mukherjee, I., Corkrey, R., Danyushevsky, L. V, Maslennikov, V., Hollings, P., Garven, G., Brand, U., Lécuyer, C., 2020. Evidence for elevated and variable atmospheric oxygen in the Precambrian. Precambrian Res. 343, 105722. https://doi.org/https://doi.org/10.1016/j.precamres.2020.105722

Stewart, K., Maleng, K., Sager, P., 1965. Comparitive winter studies on dimictic and meromictic lakes. Interationale Vereinigung für Theor. und Angew. Limnol. Verhandlungen 16, 47–57.

Stewart, K.M., Walker, K.F., Likens, G.E., 2009. Meromictic Lakes, in: Likens, G.E.B.T.-E. of I.W. (Ed.), . Academic Press, Oxford, pp. 589–602. https://doi.org/https://doi.org/10.1016/B978-012370626-3.00027-2

Storelli, N., Peduzzi, S., Saad, M.M., Frigaard, N., Perret, X., Tonolla, M., 2013. CO2 assimilation in the chemocline of Lake Cadagno is dominated by a few types of phototrophic purple

3730 sulfur bacteria. FEMS Microbiol. Ecol. 84, 421–432. https://doi.org/10.1111/1574-
3731 6941.12074
3732 Straub, K.L., Rainey, F.R., Widdel, F., 1999. Rhodovulum iodosum sp. nov. and Rhodovulum
3733 robiginosum sp. nov., two new marine phototrophic ferrous-iron-oxidizing purple bacteria.
3734 Int. J. Syst. Bacteriol. 49, 729–735.
3735 Striegl, R.G., Michmerhuizen, C.M., 1998. Hydrologic influence on methane and carbon dioxide
3736 dynamics at two north-central Minnesota lakes. Limnol. Oceanogr. 43, 1519–1529.
3737 https://doi.org/10.4319/lo.1998.43.7.1519
3738 Stüeken, E.E., 2013. A test of the nitrogen-limitation hypothesis for retarded eukaryote
3739 radiation: Nitrogen isotopes across a Mesoproterozoic basinal profile. Geochim.
3740 Cosmochim. Acta 120, 121–139.
3741 https://doi.org/http://dx.doi.org/10.1016/j.gca.2013.06.002
3742 Stüeken, E.E., Buick, R., Anderson, R.E., Baross, J.A., Planavsky, N.J., Lyons, T.W., 2017.
3743 Environmental niches and metabolic diversity in Neoarchean lakes. Geobiology 15, 767–
3744 783. https://doi.org/10.1111/gbi.12251
3745 Stüeken, E.E., Buick, R., Guy, B.M., Koehler, M.C., 2015. Isotopic evidence for biological nitrogen
3746 fixation by molybdenum-nitrogenase from 3.2 Gyr. Nature 520, 666.
3747 Stüeken, E.E., Martinez, A., Love, G., Olsen, P.E., Bates, S., Lyons, T.W., 2019. Effects of pH on
3748 redox proxies in a Jurassic rift lake: Implications for interpreting environmental records in
3749 deep time. Geochim. Cosmochim. Acta 252, 240–267.
3750 https://doi.org/https://doi.org/10.1016/j.gca.2019.03.014
3751 Sturm, A., Fowle, D.A., Jones, C., Leslie, K., Nomosatryo, S., Henny, C., Canfield, D.E., Crowe,

S.A., 2018. Rates and pathways of CH4 oxidation in ferruginous Lake Matano, Indonesia. Geobiology 0. https://doi.org/10.1111/gbi.12325

Stylo, M., Neubert, N., Wang, Y., Monga, N., Romaniello, S.J., Weyer, S., Bernier-Latmani, R., 2015. Uranium isotopes fingerprint biotic reduction. Proc. Natl. Acad. Sci. 112, 5619 LP – 5624. https://doi.org/10.1073/pnas.1421841112

Summons, R.E., Powell, T.G., 1987. Identification of aryl isoprenoids in source rocks and crude oils: Biological markers for the green sulphur bacteria. Geochim. Cosmochim. Acta 51, 557–566. https://doi.org/https://doi.org/10.1016/0016-7037(87)90069-X

Summons, R.E., Powell, T.G., 1986. Chlorobiaceae in Palaeozoic seas revealed by biological markers, isotopes and geology. Nature 319, 763–765. https://doi.org/10.1038/319763a0

Sumner, D.Y., 1997. Carbonate precipitation and oxygen stratification in late Archean seawater as deduced from facies and stratigraphy of the Gamohaan and Frisco formations, Transvaal Supergroup, South Africa. Am. J. Sci. 297, 455–487. https://doi.org/10.2475/ajs.297.5.455

Sumner, D.Y., Grotzinger, J.P., 1996. Were kinetics of Archean calcium carbonate precipitation related to oxygen concentrations? Geology 24, 119–122.

Sun, J., Zhu, X., Li, Z., 2018. Confirmation and global significance of a large-scale early Neoproterozoic banded iron formation on Hainan Island, China. Precambrian Res. 307, 82–92. https://doi.org/https://doi.org/10.1016/j.precamres.2018.01.005

Sun, R., Wang, B., 2018. Iron isotope fractionation during uptake of ferrous ion by phytoplankton. Chem. Geol. 481, 65–73. https://doi.org/https://doi.org/10.1016/j.chemgeo.2018.01.031

Swain, E.B., 1984. The paucity of blue-green algae in meromictic Brownie Lake: iron limitation

or heavy-metal toxicity. University of Minnesota, Ann Arbor, MI.

Swain, E.B., Engstrom, D.R., Brigham, M.E., Henning, T.A., Brezonik, P.L., 1992. Increasing Rates of Atmospheric Mercury Deposition in Midcontinental North America. Science (80-.). 257, 784 LP – 787. https://doi.org/10.1126/science.257.5071.784

Swanner, E.D., Bayer, T., Wu, W., Hao, L., Obst, M., Sundman, A., Byrne, J.M., Michel, F.M., Kleinhanns, I.C., Kappler, A., Schoenberg, R., 2017. Iron Isotope Fractionation during Fe(II) Oxidation Mediated by the Oxygen-Producing Marine Cyanobacterium Synechococcus PCC 7002. Environ. Sci. Technol. 51, 4897–4906. https://doi.org/10.1021/acs.est.6b05833

Swanner, E.D., Maisch, M., Wu, W., Kappler, A., 2018. Oxic Fe(III) reduction could have generated Fe(II) in the photic zone of Precambrian seawater. Sci. Rep. 8, 4238. https://doi.org/10.1038/s41598-018-22694-y

Swanner, E.D., Mloszewska, A.M., Cirpka, O.A., Schoenberg, R., Konhauser, K.O., Kappler, A., 2015a. Modulation of oxygen production in Archaean oceans by episodes of Fe(II) toxicity. Nat. Geosci. 8, 126–130. https://doi.org/10.1038/ngeo2327

Swanner, E.D., Planavsky, N.J., Lalonde, S. V., Robbins, L.J., Bekker, A., Rouxel, O.J., Saito, M.A., Kappler, A., Mojzsis, S.J., Konhauser, K.O., 2014. Cobalt and marine redox evolution. Earth Planet. Sci. Lett. 390, 253–263. https://doi.org/10.1016/j.epsl.2014.01.001

Swanner, E.D., Wu, W., Hao, L., Wüstner, M.L., Obst, M., Moran, D.M., McIlvin, M.R., Saito, M.A., Kappler, A., 2015b. Physiology, Fe(II) oxidation, and Fe mineral formation by a marine planktonic cyanobacterium grown under ferruginous conditions. Front. Earth Sci. 3. https://doi.org/10.3389/feart.2015.00060

Swanner, E.D., Wu, W., Schoenberg, R., Byrne, J., Michel, F.M., Pan, Y., Kappler, A., 2015c.

Fractionation of Fe isotopes during Fe(II) oxidation by a marine photoferrotroph is controlled by the formation of organic Fe-complexes and colloidal Fe fractions. Geochim. Cosmochim. Acta 165, 44–61. https://doi.org/10.1016/j.gca.2015.05.024

Tagliabue, A., Bopp, L., Dutay, J.-C., Bowie, A.R., Chever, F., Jean-Baptiste, P., Bucciarelli, E., Lannuzel, D., Remenyi, T., Sarthou, G., Aumont, O., Gehlen, M., Jeandel, C., 2010. Hydrothermal contribution to the oceanic dissolved iron inventory. Nat. Geosci 3, 252–256. https://doi.org/http://www.nature.com/ngeo/journal/v3/n4/suppinfo/ngeo818_S1.html

Takahashi, M., Ichimura, S., 1968. VERTICAL DISTRIBUTION AND ORGANIC MATTER PRODUCTION OF PHOTOSYNTHETIC SULFUR BACTERIA IN JAPANESE LAKES. Limnol. Oceanogr. 13, 644–655. https://doi.org/10.4319/lo.1968.13.4.0644

Taylor, D., Dalstra, H.J., Harding, A.E., Broadbent, G.C., Barley, M.E., 2001. Genesis of High-Grade Hematite Orebodies of the Hamersley Province, Western Australia. Econ. Geol. 96, 837–873. https://doi.org/10.2113/gsecongeo.96.4.837

Taylor, S.R., McLennan, S.M., 1985. The Continental Crust: its Composition and Evolution. Blackwell Scientific, Oxford.

Teutsch, N., Schmid, M., Müller, B., Halliday, A.N., Bürgmann, H., Wehrli, B., 2009. Large iron isotope fractionation at the oxic–anoxic boundary in Lake Nyos. Earth Planet. Sci. Lett. 285, 52–60. https://doi.org/https://doi.org/10.1016/j.epsl.2009.05.044

Thibon, F., Blichert-Toft, J., Tsikos, H., Foden, J., Albalat, E., Albarede, F., 2019. Dynamics of oceanic iron prior to the Great Oxygenation Event. Earth Planet. Sci. Lett. 506, 360–370. https://doi.org/10.1016/j.epsl.2018.11.016

Thompson, K.J., Kenward, P.A., Bauer, K.W., Warchola, T., Gauger, T., Martinez, R., Simister, R.L., Michiels, C.C., Llirós, M., Reinhard, C.T., Kappler, A., Konhauser, K.O., Crowe, S.A., 2019. Photoferrotrophy, deposition of banded iron formations, and methane production in Archean oceans. Sci. Adv. 5, eaav2869. https://doi.org/10.1126/sciadv.aav2869

Tonolla, M., Storelli, N., Danza, F., Ravasi, D., Peduzzi, S., Posth, N.R., Cox, R.P., Jørgensen, M.F., Gregersen, L.H., Daugbjerg, N., Frigaard, N.-U., 2017. Lake Cadagno: Microbial Life in Crenogenic Meromixis, in: Gulati, R.D., Zadereev, E.S., Degermendzhi, A.G. (Eds.), Ecology of Meromictic Lakes. Springer International Publishing, Cham, pp. 155–186. https://doi.org/10.1007/978-3-319-49143-1_7

Tosca, N.J., Guggenheim, S., Pufahl, P.K., 2016. An authigenic origin for Precambrian greenalite: Implications for iron formation and the chemistry of ancient seawater. GSA Bull. 128, 511–530. https://doi.org/10.1130/B31339.1

Tostevin, R., Mills, B.J.W., 2020. Reconciling proxy records and models of Earth's oxygenation during the Neoproterozoic and Palaeozoic. Interface Focus 10, 20190137. https://doi.org/10.1098/rsfs.2019.0137

Tostevin, R., Poulton, S.W., 2019. Suboxic Sediments BT - Encyclopedia of Astrobiology, in: Gargaud, M., Irvine, W.M., Amils, R., Cleaves, H.J., Pinti, D., Cernicharo Quintanilla, J., Viso, M. (Eds.), . Springer Berlin Heidelberg, Berlin, Heidelberg, pp. 1–4. https://doi.org/10.1007/978-3-642-27833-4_5419-1

Tostevin, R., Wood, R.A., Shields, G.A., Poulton, S.W., Guilbaud, R., Bowyer, F., Penny, A.M., He, T., Curtis, A., Hoffmann, K.H., Clarkson, M.O., 2016. Low-oxygen waters limited habitable space for early animals. Nat. Commun. 7, 12818. https://doi.org/10.1038/ncomms12818

https://www.nature.com/articles/ncomms12818#supplementary-information

Tracey, B., Lee, N., Card, V., 1996. Sediment indicators of meromixis: comparison of laminations, diatoms, and sediment chemistry in Brownie Lake, Minneapolis, USA. J. Paleolimnol. 15, 129–132.

Tribovillard, N., Algeo, T.J., Lyons, T., Riboulleau, A., 2006. Trace metals as paleoredox and paleoproductivity proxies: An update. Chem. Geol. 232, 12–32. https://doi.org/10.1016/j.chemgeo.2006.02.012

Tylmann, W., Zolitschka, B., Enters, D., Ohlendorf, Christian, 2013. Laminated lake sediments in northeast Poland: distribution, preconditions for formation and potential for paleoenvironmental investigation. J. Paleolimnol. 50, 487–503. https://doi.org/10.1007/s10933-013-9741-7

Ueno, Y., Yamada, K., Yoshida, N., Maruyama, S., Isozaki, Y., 2006. Evidence from fluid inclusions for microbial methanogenesis in the early Archaean era. Nature 440, 516–519. https://doi.org/10.1038/nature04584

Urban, N.R., Eisenreich, S.J., Gorham, E., 1987. Aluminum, Iron, Zinc, and Lead in Bog Waters of Northeastern North America. Can. J. Fish. Aquat. Sci. 44, 1165–1172.

van Dijk, J., Fernandez, A., Storck, J.C., White, T.S., Lever, M., Müller, I.A., Bishop, S., Seifert, R.F., Driese, S.G., Krylov, A., Ludvigson, G.A., Turchyn, A. V, Lin, C.Y., Wittkop, C., Bernasconi, S.M., 2019. Experimental calibration of clumped isotopes in siderite between 8.5 and 62 °C and its application as paleo-thermometer in paleosols. Geochim. Cosmochim. Acta 254, 1–20. https://doi.org/https://doi.org/10.1016/j.gca.2019.03.018

Veizer, J., Hoefs, J., Lowe, D.R., Thurston, P.C., 1989. Geochemistry of Precambrian carbonates:

3862 II. Archean greenstone belts and Archean sea water. Geochim. Cosmochim. Acta 53, 859–
3863 871. https://doi.org/http://dx.doi.org/10.1016/0016-7037(89)90031-8
3864 Verpoorter, C., Kutser, T., Seekell, D.A., Tranvik, L.J., 2014. A global inventory of lakes based on
3865 high-resolution satellite imagery. Geophys. Res. Lett. 41, 6396–6402.
3866 https://doi.org/10.1002/2014GL060641
3867 Viollier, E., Michard, G., Jézéquel, D., Pèpe, M., Sarazin, G., 1997. Geochemical study of a crater
3868 lake: Lake Pavin, Puy de Dôme, France. Constraints afforded by the particulate matter
3869 distribution in the element cycling within the lake. Chem. Geol. 142, 225–241.
3870 https://doi.org/https://doi.org/10.1016/S0009-2541(97)00093-4
3871 Vorlicek, T.P., Helz, G.R., Chappaz, A., Vue, P., Vezina, A., Hunter, W., 2018. Molybdenum Burial
3872 Mechanism in Sulfidic Sediments: Iron-Sulfide Pathway. ACS Earth Sp. Chem. 2, 565–576.
3873 https://doi.org/10.1021/acsearthspacechem.8b00016
3874 Vuillemin, A., Friese, A., Alawi, M., Henny, C., Nomosatryo, S., Wagner, D., Crowe, S.A.,
3875 Kallmeyer, J., 2016. Geomicrobiological Features of Ferruginous Sediments from Lake
3876 Towuti, Indonesia. Front. Microbiol.
3877 Vuillemin, A., Friese, A., Wirth, R., Schuessler, J.A., Schleicher, A.M., Kemnitz, H., Lücke, A.,
3878 Bauer, K.W., Nomosatryo, S., von Blanckenburg, F., Simister, R., Ordoñez, L.G., Ariztegui,
3879 D., Henny, C., Russell, J.M., Bijaksana, S., Vogel, H., Crowe, S.A., Kallmeyer, J., Team,
3880 T.D.P.S., 2019a. Vivianite formation in ferruginous sediments from Lake Towuti, Indonesia.
3881 Biogeosciences Discuss. 2019, 1–26. https://doi.org/10.5194/bg-2019-426
3882 Vuillemin, A., Horn, F., Friese, A., Winkel, M., Alawi, M., Wagner, D., Henny, C., Orsi, W.D.,
3883 Crowe, S.A., Kallmeyer, J., 2018. Metabolic potential of microbial communities from

ferruginous sediments. Environ. Microbiol. 20, 4297–4313. https://doi.org/10.1111/1462-2920.14343

Vuillemin, A., Wirth, R., Kemnitz, H., Schleicher, A.M., Friese, A., Bauer, K.W., Simister, R., Nomosatryo, S., Ordoñez, L., Ariztegui, D., Henny, C., Crowe, S.A., Benning, L.G., Kallmeyer, J., Russell, J.M., Bijaksana, S., Vogel, H., The Towuti Drilling Project Science Team, 2019b. Formation of diagenetic siderite in modern ferruginous sediments. Geology 47, 540–544. https://doi.org/10.1130/G46100.1

Wagner, M., Chappaz, A., Lyons, T.W., 2017. Molybdenum speciation and burial pathway in weakly sulfidic environments: Insights from XAFS. Geochim. Cosmochim. Acta 206, 18–29. https://doi.org/https://doi.org/10.1016/j.gca.2017.02.018

Walker, K.F., Likens, G.E., 1975. Meromixis and a reconsidered typology of lake circulation patterns. Verh Intern. Verein Limnol 19, 442–458.

Walter, X.A., Picazo, A., Miracle, M.R., Vicente, E., Camacho, A., Aragno, M., Zopfi, J., 2014. Phototrophic Fe(II)-oxidation in the chemocline of a ferruginous meromictic lake. Front. Microbiol. 5. https://doi.org/10.3389/fmicb.2014.00713

Wasylenki, L.E., 2012. Establishing the Basis for Using Stable Isotope Ratios of Metals as Paleoredox Proxies. Isot. Anal., Wiley Online Books. https://doi.org/doi:10.1002/9783527650484.ch11

Wen, H., Carignan, J., Chu, X., Fan, H., Cloquet, C., Huang, J., Zhang, Y., Chang, H., 2014. Selenium isotopes trace anoxic and ferruginous seawater conditions in the Early Cambrian. Chem. Geol. 390, 164–172. https://doi.org/https://doi.org/10.1016/j.chemgeo.2014.10.022

West, W.E., Coloso, J.J., Jones, S.E., 2012. Effects of algal and terrestrial carbon on methane production rates and methanogen community structure in a temperate lake sediment. Freshw. Biol. 57, 949–955. https://doi.org/10.1111/j.1365-2427.2012.02755.x

Wetzel, R.G., 2001. Limnology: Lake and River Ecosystems, Third. ed. Academic Press, San Diego.

Whiticar, M.J., 1999. Carbon and hydrogen isotope systematics of bacterial formation and oxidation of methane. Chem. Geol. 161, 291–314. https://doi.org/https://doi.org/10.1016/S0009-2541(99)00092-3

Whitney, L., 1938. Microstratification of inland lakes. Trans. Wisconsin Acad. Sci. Arts, Lett. 31, 155–173.

Widdel, F., Schnell, S., Heising, S., Ehrenreich, A., Assmus, B., Schink, B., 1993. Ferrous iron oxidation by anoxygenic phototrophic bacteria. Nature 362, 834–836.

Wignall, P.B., Twitchett, R.J., 1996. Oceanic Anoxia and the End Permian Mass Extinction. Science (80-.). 272, 1155 LP – 1158. https://doi.org/10.1126/science.272.5265.1155

Williams, J.J., McLauchlan, K.K., Mueller, J.R., Mellicant, E.M., Myrbo, A.E., Lascu, I., 2015. Ecosystem development following deglaciation: A new sedimentary record from Devils Lake, Wisconsin, USA. Quat. Sci. Rev. 125, 131–143. https://doi.org/https://doi.org/10.1016/j.quascirev.2015.08.009

Wilson, J.P., Fischer, W.W., Johnston, D.T., Knoll, A.H., Grotzinger, J.P., Walter, M.R., McNaughton, N.J., Simon, M., Abelson, J., Schrag, D.P., Summons, R., Allwood, A., Andres, M., Gammon, C., Garvin, J., Rashby, S., Schweizer, M., Watters, W.A., 2010. Geobiology of the late Paleoproterozoic Duck Creek Fromation, Western Australia. Precambrian Res. 179,

135–149.

Winter, B.L., Knauth, L.P., 1992. Stable isotope geochemistry of cherts and carbonates from the 2.0 Ga gunflint iron formation: implications for the depositional setting, and the effects of diagenesis and metamorphism. Precambrian Res. 59, 283–313. https://doi.org/http://dx.doi.org/10.1016/0301-9268(92)90061-R

Wittkop, C., Bartley, J.K., Krueger, R., Bouvier, A., Georg, R.B., Knaeble, A.R., St. Clair, K., Piper, C., Breckenridge, A., 2020a. Influence of provenance and transport process on the geochemistry and radiogenic (Hf, Nd, and Sr) isotopic composition of Pleistocene glacial sediments, Minnesota, USA. Chem. Geol. 532, 119390. https://doi.org/https://doi.org/10.1016/j.chemgeo.2019.119390

Wittkop, C., Swanner, E.D., Grengs, A., Lambrecht, N., Fakhraee, M., Myrbo, A., Bray, A.W., Poulton, S.W., Katsev, S., 2020b. Evaluating a primary carbonate pathway for manganese enrichments in reducing environments. Earth Planet. Sci. Lett. 538, 116201. https://doi.org/https://doi.org/10.1016/j.epsl.2020.116201

Wittkop, C., Teranes, J., Lubenow, B., Dean, W.E., 2014. Carbon- and oxygen-stable isotope signatures of methanogenesis, temperature, and water column stratification in Holocene siderite varves. Chem. Geol. 389, 153–166. https://doi.org/10.1016/j.chemgeo.2014.09.016

Wolfe, J.M., Fournier, G.P., 2018. Horizontal gene transfer constrains the timing of methanogen evolution. Nat. Ecol. Evol. 2, 897–903. https://doi.org/10.1038/s41559-018-0513-7

Wood, R.A., Poulton, S.W., Prave, A.R., Hoffmann, K.H., Clarkson, M.O., Guilbaud, R., Lyne, J.W., Tostevin, R., Bowyer, F., Penny, A.M., Curtis, A., Kasemann, S.A., 2015. Dynamic redox

conditions control late Ediacaran metazoan ecosystems in the Nama Group, Namibia. Precambrian Res. 261, 252–271. https://doi.org/http://dx.doi.org/10.1016/j.precamres.2015.02.004

Wu, W., Swanner, E.D., Hao, L., Zeitvogel, F., Obst, M., Pan, Y., Kappler, A., 2014. Characterization of the physiology and cell-mineral interactions of the marine anoxygenic phototrophic Fe(II) oxidizer Rhodovulum iodosum - implications for Precambrian Fe(II) oxidation. FEMS Microbiol. Ecol. 88, 503–515. https://doi.org/10.1111/1574-6941.12315

Wu, W., Swanner, E.D., Kleinhanns, I.C., Schoenberg, R., Pan, Y., Kappler, A., 2017. Fe isotope fractionation during Fe(II) oxidation by the marine photoferrotroph Rhodovulum iodosum in the presence of Si – Implications for Precambrian iron formation deposition. Geochim. Cosmochim. Acta 211, 307–321. https://doi.org/10.1016/j.gca.2017.05.033

Xiong, Y., Guilbaud, R., Peacock, C.L., Cox, R.P., Canfield, D.E., Krom, M.D., Poulton, S.W., 2019. Phosphorus cycling in Lake Cadagno, Switzerland: A low sulfate euxinic ocean analogue. Geochim. Cosmochim. Acta 251, 116–135. https://doi.org/https://doi.org/10.1016/j.gca.2019.02.011

Yang, J., Junium, C.K., Grassineau, N. V, Nisbet, E.G., Izon, G., Mettam, C., Martin, A., Zerkle, A.L., 2019. Ammonium availability in the Late Archaean nitrogen cycle. Nat. Geosci. 12, 553–557. https://doi.org/10.1038/s41561-019-0371-1

Yang, X.-Q., Zhang, Z.-H., Duan, S.-G., Zhao, X.-M., 2015. Petrological and geochemical features of the Jingtieshan banded iron formation (BIF): A unique type of BIF from the Northern Qilian Orogenic Belt, NW China. J. Asian Earth Sci. 113, 1218–1234. https://doi.org/https://doi.org/10.1016/j.jseaes.2015.03.024

Yang, X., Zhang, Z., Santosh, M., Duan, S., Liang, T., 2018. Anoxic to suboxic Mesoproterozoic ocean: Evidence from iron isotope and geochemistry of siderite in the Banded Iron Formations from North Qilian, NW China. Precambrian Res. 307, 115–124. https://doi.org/https://doi.org/10.1016/j.precamres.2018.01.007

Yoshimura, S., 1937. Abnormal Thermal Stratifications of Inland Lakes. Proc. Imp. Acad. 13.

Yoshimura, S., 1936. Contributions to the Knowledge of Iron Dissolved in the Lake Waters of Japan. Second Report. Japanese J. Geol. Geogr. 13, 39–56.

Yoshimura, S., 1931. Contributions to the knowledge of the stratification of iron and manganese in the lake water of Japan. Japanese J. Geol. Geogr. 9, 61–69.

Yu, W., Algeo, T.J., Du, Y., Maynard, B., Guo, H., Zhou, Q., Peng, T., Wang, P., Yuan, L., 2016. Genesis of Cryogenian Datangpo manganese deposit: Hydrothermal influence and episodic post-glacial ventilation of Nanhua Basin, South China. Palaeogeogr. Palaeoclimatol. Palaeoecol. 459, 321–337. https://doi.org/https://doi.org/10.1016/j.palaeo.2016.05.023

Yurkov, V., Hughes, E., 2013. Chapter Eleven - Genes Associated with the Peculiar Phenotypes of the Aerobic Anoxygenic Phototrophs, in: Beatty, J.T.B.T.-A. in B.R. (Ed.), Genome Evolution of Photosynthetic Bacteria. Academic Press, pp. 327–358. https://doi.org/https://doi.org/10.1016/B978-0-12-397923-0.00011-4

Zadereev, E.S., Boehrer, B., Gulati, R.D., 2017. Introduction: Meromictic Lakes, Their Terminology and Geographic Distribution BT - Ecology of Meromictic Lakes, in: Gulati, R.D., Zadereev, E.S., Degermendzhi, A.G. (Eds.), . Springer International Publishing, Cham, pp. 1–11. https://doi.org/10.1007/978-3-319-49143-1_1

Zeebe, R.E., Wolf-Gladrow, D.B.T., 2001. Chapter 3 Stable isotope fractionation, in: Zeebe, R.E.,

Wolf-Gladrow, D.B.T.-E.O.S. (Eds.), CO in Seawater: Equilibrium, Kinetics, Isotopes. Elsevier, pp. 141–250. https://doi.org/https://doi.org/10.1016/S0422-9894(01)80004-0

Zegeye, A., Bonneville, S., Benning, L.G., Sturm, A., Fowle, D.A., Jones, C., Canfield, D.E., Ruby, C., MacLean, L.C., Nomosatryo, S., Crowe, S.A., Poulton, S.W., 2012. Green rust formation controls nutrient availability in a ferruginous water column. Geology 40, 599–602. https://doi.org/10.1130/g32959.1

Zeikus, J.G., Winfrey, M.R., 1976. Temperature limitation of methanogenesis in aquatic sediments. Appl. Environ. Microbiol. 31, 99–107.

Zerkle, A.L., House, C.H., Cox, R.P., Canfield, D.E., 2006. Metal limitation of cyanobacterial N2 fixation and implications for the Precambrian nitrogen cycle. Geobiology 4, 285–297. https://doi.org/10.1111/j.1472-4669.2006.00082.x

Zerkle, A.L., Poulton, S.W., Newton, R.J., Mettam, C., Claire, M.W., Bekker, A., Junium, C.K., 2017. Onset of the aerobic nitrogen cycle during the Great Oxidation Event. Nature 542, 465.

Zhang, C.L., Horita, J., Cole, D.R., Zhou, J., Lovley, D.R., Phelps, T.J., 2001. Temperature-dependent oxygen and carbon isotope fractionations of biogenic siderite. Geochim. Cosmochim. Acta 65, 2257–2271. https://doi.org/https://doi.org/10.1016/S0016-7037(01)00596-8

Zhang, K., Zhu, X., Wood, R.A., Shi, Y., Gao, Z., Poulton, S.W., 2018. Oxygenation of the Mesoproterozoic ocean and the evolution of complex eukaryotes. Nat. Geosci. 11, 345–350. https://doi.org/10.1038/s41561-018-0111-y

Zhang, S., Wang, X., Wang, H., Bjerrum, C.J., Hammarlund, E.U., Costa, M.M., Connelly, J.N.,

Zhang, B., Su, J., Canfield, D.E., 2016. Sufficient oxygen for animal respiration 1,400 million years ago. Proc. Natl. Acad. Sci. 113, 1731–1736. https://doi.org/10.1073/pnas.1523449113